5-1-2010

Spectrally accurate initial data in numerical relativity

Nicholas Battista

Spectrally Accurate Initial Data in Numerical Relativity

by

Nicholas A. Battista

Submitted to the School of Mathematical Sciences

in partial fulfillment of the requirements for the degree of

Masters of Science

at the

ROCHESTER INSTITUTE OF TECHNOLOGY

May 2010

Author .....

Nicholas A. Battista
School of Mathematical Sciences

Accepted by .....

Anthony A. Harkin
School of Mathematical Sciences

Accepted by .....

David S. Ross
School of Mathematical Sciences

Accepted by .....

Joshua A. Faber
School of Mathematical Sciences

Spectrally Accurate Initial Data in Numerical Relativity

by

Nicholas A. Battista

Submitted to the School of Mathematical Sciences
on May 10, 2010, in partial fulfillment of the
requirements for the degree of
Masters of Science

Abstract

Einstein's theory of general relativity has radically altered the way in which we perceive the universe. His breakthrough was to realize that the fabric of space is deformable in the presence of mass, and that space and time are linked into a continuum. Much evidence has been gathered in support of general relativity over the decades. Some of the indirect evidence for GR includes the phenomenon of gravitational lensing, the anomalous perihelion of mercury, and the gravitational redshift. One of the most striking predictions of GR, that has not yet been confirmed, is the existence of gravitational waves. The primary source of gravitational waves in the universe is thought to be produced during the merger of binary black hole systems, or by binary neutron stars. The starting point for computer simulations of black hole mergers requires highly accurate initial data for the space-time metric and for the curvature. The equations describing the initial space-time around the black hole(s) are non-linear, elliptic partial differential equations (PDE). We will discuss how to use a pseudo-spectral (collocation) method to calculate the initial puncture data corresponding to single black hole and binary black hole systems.

Thesis Supervisor: Anthony A. Harkin, School of Mathematical Sciences
Thesis Supervisor: David S. Ross, School of Mathematical Sciences
Thesis Supervisor: Joshua A. Faber, School of Mathematical Sciences

Acknowledgments

I would like to thank Dr. Anthony Harkin for introducing me to the joys of applied mathematics, scientific computing, and spectral theory early in my undergraduate education. I would like to thank my other advisors, Dr. Joshua Faber and Dr. David Ross, as well, for all the help and guidance they have given me over the past few years, regarding not only this thesis, mathematics, and physics, but also life.

I also wish to thank Dr. Manuela Campanelli and the Center for Computational Relativity and Gravitation (CCRG) for proposing this project to Dr. Harkin and Dr. Ross initially, as well as, for all the useful comments and suggestions they have always provided over the years. I also want to thank NASA and the NASA ROSES ATFP grant 08-ATFP08-0093 for supporting much of this work. I would also like to thank Anna Fiorucci in the Mathematics Student Support Office for always motivating and selflessly going out of her way for us students on a daily basis.

Furthermore, I would like to especially thank my mother, Carol Battista, and my sister, Christina Battista, for all their love, support, and encouragement they always have given me. Without them, I would not be the person I am today, nor would I have accomplished a fraction of what I have.

Contents

List of Figures

Chapter 1

Introduction

The purpose of this project is the numerical computation of solutions to partial differential equations (PDE) that are required for simulations of black hole dynamics in general relativity. Einstein's theory of General Relativity (GR) has radically altered the way in which scientists perceive the universe. Einstein theorized that space is deformable in the presence of mass and that space and time are one intertwined entity, called space-time.

Over the last 90 years there has been much experimental evidence that verifies predictions of GR. Moreover, some of the results of GR are used by many people in their everyday routine, as GR is fundamental in the operation of Global Positioning Systems (GPS). One of the most astonishing predictions, which has not yet been confirmed, is the existence of gravitational radiation, which ripples through the universe like waves on a pond. Gravitational wave astronomy is a new frontier of twenty-first century physics. Once gravitational radiation is successfully detected, scientists will able to better understand some of the dynamics of the universe, such as how stars die, the birth of black holes, and how the universe evolved into what it is today. Most importantly, detecting gravitational waves would be a dramatic confirmation that Einstein's General Theory of Relativity is correct.

The LIGO (Laser Interferometer Gravitational Wave Observatory) project is dedicated to detecting gravitational waves. From ground based instruments, data is

collected and compared to waveforms derived from numerical relativistic simulations. Conclusively matching the observational data to a computationally predicted gravitational waveform would confirm the existence of gravitational waves. It is expected that a primary source of gravitational radiation is from a coalescing black hole binary system [5]. Hence much effort has been expended into solving the equations of GR involving solutions with black hole mergers. The first fully relativistic simulations of a coalescing binary black hole system were performed for the first time in 2005. Calculating the starting point for relativistic simulations is the focus of this thesis.

There is an exceptional amount of computer resources needed to simulate a system that exhibits gravitational radiation. This is due to the field equations of GR, which consist of ten coupled nonlinear PDEs. A necessity for numerical relativity is finding accurate initial data to begin the simulation. Unlike in classical Newtonian physics, where the initial data consists of initial positions and velocities, in GR we need to initially specify the space-time metric and curvature. The equations for initial data, which encompass the space-time metric and curvature at time zero are nonlinear, elliptical PDEs of the form

$$\Delta u = \rho(u), \tag{1.1}$$

whose domain is all of three-space, R^3, omitting the puncture(s) at the position of the black hole(s). Unlike other initial data PDEs in GR, there are many more mathematical and computational challenges that arise in an initial puncture data PDE. In the case of a single black hole with spin and linear momentum, the elliptic equation has a C^2 singularity at the position of the black hole, which can only be resolved through clever coordinate transformations that compactifies R^3 into a single rectangular patch. Solving (1.1) in the case of a binary black hole system is much more arduous, as two punctures need to be resolved. This is accomplished in [1] with the aid of an ingenious coordinate transformation that simultaneously renders the punctures smooth, C^∞, and maps them to the boundary of a single rectangular computational domain. This is a big improvement over previous methods that map the physical domain onto multiple computational domains and then match them with

overlap and compatibility conditions. Using a single-domain numerical method is much more effective in terms of accuracy and cost [2]. In this thesis our focus is using a single-domain spectral method for finding the initial puncture data for black hole systems with linear momentum and spin in vacuum space-times. Since it is critically important to find highly accurate initial data, numerically a spectral scheme is most logical.

Spectral methods have been utilized successfully in numerous areas such as numerical relativity, elasticity, and fluid mechanics [3],[6],[7]. Spectral methods involve a high order expansion of the solution in terms of orthogonal basis functions, and generally yield exponential convergence for smooth solutions ($u \in C^{\infty}$). Finite differences, on the other hand, provide only algebraic convergence at best, and are therefore not appropriate for problems where high accuracy is desired.

Chapter 2

Spectral Methods For Ordinary Differential Equations

We will present the basic framework of Chebyshev and Fourier pseudo-spectral methods for various ordinary differential equations in this section.

2.1 Chebyshev Pseudo-Spectral Method for Linear ODEs

Suppose we wish to solve the following linear ordinary differential equation,

$$a(x)u'' + b(x)u' + c(x)u = f(x), \tag{2.1}$$

with boundary conditions, $u(-1) = \alpha, u(1) = \beta$. In performing a spectral method, we assume a solution in the form of a finite sum over some orthogonal basis functions, ϕ_k, which we call the *trial functions*,

$$u(x) = \sum_{k=0}^{N} \tilde{u}_k \phi_k(x). \tag{2.2}$$

Typically these polynomials are eigenfunctions of a Sturm-Liouville differential operator, such as Legendre Polynomials, Hermite Polynomials, or Chebyshev Polynomials.

The next step is to substitute our spectral solution into the ODE:

$$a(x)\frac{d^2}{dx^2}\left(\sum_{k=0}^{N}\tilde{u}_k\phi_k(x)\right)+b(x)\frac{d}{dx}\left(\sum_{k=0}^{N}\tilde{u}_k\phi_k(x)\right)+c(x)\left(\sum_{k=0}^{N}\tilde{u}_k\phi_k(x)\right)=f(x).$$

Then we multiply both sides of the equation by a function $\chi_m(x)$, which we call the *test function*,

$$\chi_m(x)\left(a(x)\frac{d^2}{dx^2}\left(\sum_{k=0}^{N}\tilde{u}_k\phi_k(x)\right)+b(x)\frac{d}{dx}\left(\sum_{k=0}^{N}\tilde{u}_k\phi_k(x)\right)+c(x)\left(\sum_{k=0}^{N}\tilde{u}_k\phi_k(x)\right)\right)$$
$$=\chi_m(x)f(x).$$

Now we integrate both sides of the above equation over the domain in which the ODE is defined,

$$\int_{-1}^{1}\chi_m(x)\left(a(x)\frac{d^2}{dx^2}\left(\sum_{k=0}^{N}\tilde{u}_k\phi_k(x)\right)+b(x)\frac{d}{dx}\left(\sum_{k=0}^{N}\tilde{u}_k\phi_k(x)\right)\right.$$
$$\left.+c(x)\left(\sum_{k=0}^{N}\tilde{u}_k\phi_k(x)\right)\right)dx=\int_{-1}^{1}\chi_m(x)f(x)dx. \quad (2.3)$$

The choice of test functions, $\chi_m(x)$, and trial functions, $\phi_k(x)$, determines what kind of spectral method is implemented. In a *Galerkin Method* one chooses the test functions to be the same as the trial functions. For self-adjoint differential operators, one can integrate by parts and the Galerkin method gives rise to a symmetric matrix system.

In this thesis we focus on a *Pseudo-spectral Method*, or Collocation Method. In this spectral method, one will choose the test functions to be delta functions centered at collocation points, $\{x_n\}_{n=0}^{N}$:

$$\chi_m(x)=\delta(x-x_m). \quad (2.4)$$

Substituting Eq.(2.4) into Eq.(2.3) yields

$$\sum_{k=0}^{N} \tilde{u}_k \Big(a(x_m) \frac{d^2\phi_k(x_m)}{dx^2} + b(x_m) \frac{d\phi_k(x_m)}{dx} + c(x_m)\phi_k(x_m) \Big) = f(x_m),$$

where $m = 0, 1, \ldots, N$. We have arrived at a system of $N+1$ linear algebraic equations for the $N+1$ unknowns, u_k.

For the Pseudo-spectral method, the way in which one chooses what kind of trial functions to use, depends on the structure of the problem. For periodic problems, it makes sense to use Fourier series as the trial functions, since Fourier series inherently are periodic functions. For problems that are not periodic, Chebyshev polynomials are often a suitable choice of trial functions,

$$\phi_k(x) = T_k(x). \tag{2.5}$$

The properties of the Chebyshev Polynomials are given in Appendix A. We choose the collocation points to be the critical points of the n^{th} degree Chebyshev polynomial with the endpoints of the domain:

$$x_m = \cos\left[\frac{\pi}{N} \left(m + \frac{1}{2} \right) \right], \qquad m = 0, 1, \ldots, N \tag{2.6}$$

Therefore since we assume a spectral solution over the Chebyshev bases,

$$u(x) = \sum_{k=0}^{N} \tilde{u_k} T_k(x),$$

the spectral coefficients can be obtained by solving the following matrix equation:

$$\begin{bmatrix} (-1)^0 & (-1)^1 & (-1)^2 & \cdots & (-1)^N \\ A_{10} & A_{11} & A_{12} & \cdots & A_{1N} \\ A_{20} & A_{21} & A_{22} & \cdots & A_{2N} \\ \vdots & & & \cdots & \\ AN-1,0 & A_{N-1,1} & A_{N-1,2} & \cdots & A_{N-1,N} \\ 1 & 1 & 1 & \cdots & 1 \end{bmatrix} \begin{bmatrix} \tilde{u}_0 \\ \tilde{u}_1 \\ \tilde{u}_2 \\ \vdots \\ \tilde{u_N} \\ 0 \end{bmatrix} = \begin{bmatrix} \alpha \\ f(x_1) \\ f(x_2) \\ \vdots \\ f(x_{N-1}) \\ \beta \end{bmatrix}.$$

The entries of the matrix A are

$$A_{mk} = a(x_m)\frac{d^2T_k(x_m)}{dx^2} + b(x_m)\frac{dT_k(x_m)}{dx} + c(x_m)T_k(x_m),$$

for all $m \neq 0, N$ and $k = 0, 1, \ldots N$. The first and last rows of A account for the boundary conditions of the ODE, $u(-1) = \alpha$ and $u(1) = \beta$.

2.1.1 Example: $u'' = f(x)$

Consider the following ordinary differential equation

$$u'' = \sin x + \cos x,$$

with the following boundary conditions,

$$u(-1) = 0,$$
$$u(1) = 0,$$

By solving the above ODE analytically we find that the solution is

$$u(x) = -\sin x - \cos x + x \sin x + \cos(1).$$

Numerically solving this linear ordinary differential equation using our Chebyshev pseudo-spectral method, we find that it does in fact show exponential convergence.

This is seen in Figure(B-1). Note the error calculated is the L^2 Norm between the spectral solution and the exact solution. Also when using only 10 grid points, we achieve high accuracy, with an L^2 error of roughly 10^{-10}.

2.2 Chebyshev Pseudo-Spectral Method for Non-linear ODEs

In this section we will show what the procedure for implementing a pseudo-spectral method for solving a non-linear ordinary differential equation. To illustrate method we will assume the non-linear ODE is of the form

$$a(x)u'' + b(x)u' + u^2 = r(x),$$

where $u = u(x)$, and with boundary conditions $u(-1) = b_0$ and $u(1) = b_1$.

As in the linear ODE case, we first construct a vector of the collocation points, $\{x_k\}_{k=0}^{N}$ where each is a zero of the k^{th} Chebyshev polynomial, as seen from Eq.(2.6).

Similarly to the linear ODE case once again, we assume the solution u(x) can be written as a finite sum over the Chebyshev basis,

$$u(x) = \sum_{i=0}^{N} \tilde{u_i} T_i(x).$$

By discretizing the ODE, we obtain

$$\sum_{i=0}^{N} \tilde{u_i} \Big(a(x_k) \frac{d^2 T_i(x_k)}{dx^2} + b(x_k) \frac{dT_i(x_k)}{dx} \Big) + \left(\sum_{i=0}^{N} \tilde{u_i} T_i(x_k) \right)^2 = r(x_k),$$

for $k = 0, 1, \ldots, N$. However, in this case of a non-linear ODE we cannot write a linear equation such as $A\vec{\tilde{u}} = \vec{b}$, to solve for the coefficients $\{\tilde{u_i}\}_{i=0}^{N}$. Instead we will

implement the Multivariate Newton's Method:

$$\begin{pmatrix} \tilde{u}_0 \\ \tilde{u}_1 \\ \tilde{u}_2 \\ \vdots \\ \tilde{u}_N \end{pmatrix}^{n+1} = \begin{pmatrix} \tilde{u}_0 \\ \tilde{u}_1 \\ \tilde{u}_2 \\ \vdots \\ \tilde{u}_N \end{pmatrix}^{n} - J^{-1}F_k^n, \tag{2.7}$$

where $\tilde{u}_{i,n}$ is the n^{th} iterated coefficient $\tilde{u}_i$, J^{-1} is the inverse of a Jacobian matrix, and F_k^n is an n^{th} iterated vector of functions set equal to zero.

We must build the vector F_k^n This vector is comprised of N+1 functions of the coefficients $\left\{\tilde{u}_{i,n}\right\}_{i=0}^{i=N}$. Each component of F_k^n will have the following form,

$$F_k^n(\tilde{u}_{0,n}, \tilde{u}_{1,n}, \ldots, \tilde{u}_{N,n}) = 0, \tag{2.8}$$

where $k = 0, 1, \ldots, N$ and corresponds to each collocation point.To fill in this vector, we first look at the collocation points $x_0 = b_0$, and $x_N = b_1$, corresponding to the boundary. We will implement the boundary conditions as follows:

$$F_0^n = \sum_{i=0}^{N} \tilde{u}_{i,n} T_i(x_0) - b_0,$$
$$F_N^n = \sum_{i=0}^{N} \tilde{u}_{i,n} T_i(x_N) - b_1.$$

Note that F_0^n and F_N^n have the form of Eq.(2.8). To fill in the remaining components of F_k^n, for $k = 1, 2, \ldots, N-1$, we substitute our spectral solution into the functional described in Eq.(2.8) and set it equal to zero. Then we evaluate it at every collocation point within the boundary, or more explicitly,

$$F_k^n(\tilde{u}_0, \tilde{u}_1, \ldots, \tilde{u}_N) = \sum_{i=0}^{N} \tilde{u}_{i,n}\Big(a(x_k)\frac{d^2T_i(x_k)}{dx^2} + b(x_k)\frac{dT_i(x_k)}{dx}\Big) + \left(\sum_{i=0}^{N} \tilde{u}_{i,n} T_i(x_k)\right)^2 - r(x_k),$$

for $k = 1, 2, \ldots, N-1$.

We must now construct the Jacobian matrix $J_n = J_n(k,i)$. The Jacobian J_n will be of size (N+1)×(N+1). It will have the form:

$$J_n = \begin{bmatrix} \frac{\partial F_0}{\partial \tilde{u}_0} & \frac{\partial F_0}{\partial \tilde{u}_1} & \cdots & \frac{\partial F_0}{\partial \tilde{u}_N} \\ \frac{\partial F_1}{\partial \tilde{u}_0} & \frac{\partial F_1}{\partial \tilde{u}_1} & \cdots & \frac{\partial F_1}{\partial \tilde{u}_N} \\ \vdots & & \ddots & \\ \frac{\partial F_N}{\partial \tilde{u}_0} & \frac{\partial F_N}{\partial \tilde{u}_1} & \cdots & \frac{\partial F_N}{\partial \tilde{u}_N} \end{bmatrix}.$$

The top row of the matrix corresponds to the collocation point $x_0 = -1$ and the bottom row corresponds to the collocation point $x_N = 1$. Explicitly writing out the components of those rows we see

$$J_n(0,i) = \frac{\partial F_0^n}{\partial \tilde{u}_i} = T_i(x_0),$$

$$J_n(N,i) = \frac{\partial F_N^n}{\partial \tilde{u}_i} = T_i(x_N),$$

recalling the definitions of F_k^n. The rest of the matrix components will fill in similarly, as follows

$$J_n(k,i) = \frac{\partial F_k}{\partial \tilde{u}_i} = a(x_k)\frac{d^2T_i(x_k)}{dx^2} + b(x_j)\frac{dT_i(x_k)}{dx} + 2\ T_i(x_k)\left(\sum_{i=0}^{N} \tilde{u_{i,n}}\ T_i(x_k)\right).$$

Finally, to find the coefficients $\tilde{u_i}$, we must first give an initial guess for the coffi-cients, $\left\{\tilde{u_i}\right\}_{i=0}^{N}$. This will allow us to begin the iterations. By using the Multivariate Newton's Method algorithm,

$$\vec{\tilde{u}}_{n+1} = \vec{\tilde{u}}_n - J_n^{-1}F_k^n,$$

we can find the coefficients $\left\{\tilde{u}_{i,n}\right\}_{i=0}^{N}$ to complete our numerical solution.

Let the chosen error tolerance be ϵ when using the Newton's method. The algo-rithm stops iterating when the L^2 norm between the coefficient vector of two successive

iterations is smaller than ϵ. Explicitly, the Newton's algorithm stops iterating when the following condition is satisfied

$$|\vec{\tilde{u}}_{n+1} - \vec{\tilde{u}}_n|_2 < \epsilon.$$

Hence, we will have the coefficients $\left\{\tilde{u}_{i,n}\right\}_{i=0}^{N}$ and then can use the solution as

$$u(x) = \sum_{i=0}^{N} \tilde{u}_{i,n}\ T_i(x),$$

within the given error tolerance ϵ for the coefficients.

2.2.1 Example: $u'' + u^2 = f(x)$

Consider the following nonlinear ordinary differential equation

$$u'' + u^2 = e^x + e^{2x},$$

with the following boundary conditions,

$$u(-1) = e^{-1},$$
$$u(1) = e^1.$$

By solving the above equation analytically, we find the solution is

$$u(x) = e^x.$$

Numerically solving this nonlinear ordinary differential equation using our Chebyshev pseudo-spectral method, we find that it does in fact exhibit exponential convergence. The convergence plot can be seen in Figure(B-2) Note the error calculated is the L^2 Norm between the spectral solution and the exact solution. .

The error when $N \geq 15$ is due to the error tolerance on our Multivariate Newton's Method, which was set at $\epsilon = 10^{-12}$.

2.3 Fourier Pseudo-Spectral Method for Linear ODEs

In this section we will show the procedure for implementing a pseudo-spectral method for solving an equation of the form:

$$a(x)u'' + b(x)u' + c(x)u = f(x),$$

with periodic boundary conditions $u(0) = u(2\pi)$ and $u'(0) = u'(2\pi)$.

Since this problem has periodic boundary conditions, it alludes to using the Fourier basis functions, which are inherently periodic. Recall the Fourier modes are periodic on some interval [a,b]. They can be written in exponential form as the following,

$$\phi_n = e^{\frac{i2\pi nx}{b-a}}. \tag{2.9}$$

First we must create a vector of the collocation points. Since we are working in the Fourier basis, our collocation points will be the zeros of the N^{th} Fourier sine functions. Because the ODE is defined on $[0, 2\pi]$, we note that the Fourier basis functions are of the form: e^{inx}. Therefore we easily find that the set of collocation points $\{x_k\}$, are found as

$$x_k = \frac{2\pi k}{N}, \tag{2.10}$$

where N is the number of Fourier Collocation points.

We assume the spectral solution, u(x), has the form of a finite sum over the Fourier basis,

$$u(x) = \sum_{n=-\frac{N}{2}+1}^{n=\frac{N}{2}-1} \tilde{u}_n e^{inx}.$$

We then discretize the ODE to the following form:

$$\sum_{n=-\frac{N}{2}+1}^{n=\frac{N}{2}-1} \tilde{u_n}\Big(- a(x_k)n^2 + ib(x_k) + c(x_k)\Big)e^{inx_k} = f(x_k), \qquad k = 0, 1, \ldots, N,$$

where each function of x is evaluated at each collocation point,x_k.

It is important to note that in the case $-a(x_k)n^2 + ib(x_k) + c(x_k) = 0$ the spectral method may not converge to the solution. For example, consider the equation $y'' + y = f(x)$ on the interval $0 < x < 2\pi$ with periodic boundary conditions. We wish to solve this ODE using a Fourier Psuedo-Spectral method.

Proceeding with the numerical scheme, we assume our solution is of the form,

$$u(x) = \sum_{n=-\frac{N}{2}+1}^{n=\frac{N}{2}-1} a_n e^{inx},$$

we then discretize the ODE. Upon discretizing the ODE as well as the right hand side of the equation give:

$$\sum_{n=-\frac{N}{2}+1}^{n=\frac{N}{2}-1} a_n \Big(1 - n^2\Big) e^{inx_k} = \sum_{n=-\frac{N}{2}+1}^{n=\frac{N}{2}-1} \tilde{c_n} e^{inx_k}.$$

Analytically, we then see that

$$a_n(1 - n^2) = c_n,$$

and hence if we know the right hand side's coefficients, $\{c_n\}$, we can deduce that our solution's coefficients will be

$$a_n = \frac{c_n}{1 - n^2}.$$

It is clear that when $n = -1, 1$ there is a potential problem with the solution's coefficients, especially if $c_{-1} \neq 0$ and/or $c_1 \neq 0$. In these cases where $c_{-1} = 1$ or $c_1 = 1$ we will have resonance in the solution, causing the solution not to be periodic. Therefore we will not be able to achieve a numerical solution that is converging to the true solution. Hence, implementing a Fourier Pseudo-Spectral method will not work for this ODE.

In the event that if we had a different non-homogenous term that when expressed as a Fourier series, did not have $c_{-1} = c_1 = 0$, we would see convergence to the correct

solution from the Fourier pseudo-spectral method.

Pseudo-spectral theory allows us to find the coefficients $\tilde{u_n}$ by solving the following linear equation

$$A\vec{\tilde{u}} = \vec{b},$$

where A is a $(N-1) \times (N-1)$ matrix, $\vec{\tilde{u}}$ is the coefficient vector, and $\vec{b}$ is a vector describing the nonhomogenous term of the ODE.

To construct the vector $\vec{b} = [b_0\ b_1 \dots b_N]$, we first consider the boundary conditions. Since we are enforcing periodicity of the solution and its first derivative at the boundary, unlike Chebyshev Pseudo-Spectral methods, and because the Fourier modes are periodic themselves, we do not explicitly have to state boundary conditions. The choice of Fourier basis functions will enforce periodicity automatically. We will only evaluate the ODE on the interior points within the boundaries. To do that we will implement for all $b_k,\ k = 1, 2, \dots, N-1$ that $b_k = f(x_k)$. Note that we obtain this result because we are using delta functions as our test functions in spectral theory, hence

$$b_i = \int_a^b f(x)\delta(x - x_k)dx = f(x_k).$$

So the vector b will have the following form:

$$\vec{b} = \begin{bmatrix} f(x_1) \\ f(x_2) \\ f(x_3) \\ \vdots \\ f(x_{N-1}) \end{bmatrix}$$

Now we will construct the matrix $A = A_{kn}$ using two for loops, where the outer for loop runs over the interior collocation points, $k = 1 : N-1$, and nested for loop runs over the interval, $n = 1 : N-1$. We then use the transformation

$$n = j - N/2$$

to include the correct Fourier modes. For all interior points, the matrix will take on the value

$$A_{kn} = \Big(-a(x_k)n^2 + ib(x_k) + c(x_k) \Big) e^{inx_k}, \text{ for all } k \neq 1, N-1 \text{ and } n = 1, 1, \ldots N-1.$$

We obtain this result similarly to the way we obtained the values of $\vec{b}$, ie-

$$A_{kn} = \int_a^b \Big(-a(x)n^2 + ib(x) + c(x) \Big) e^{inx} \delta(x - x_k) dx = \Big(-a(x_k)n^2 + ib(x_k) + c(x_k) \Big) e^{inx_k}.$$

We then have the following matrix equation to solve:

$$\begin{bmatrix} A_{11} & A_{12} & A_{13} & \cdots & A_{1,N-1} \\ A_{21} & A_{22} & A_{23} & \cdots & A_{2,N-1} \\ A_{31} & A_{32} & A_{33} & \cdots & A_{3,N-1} \\ \vdots & & & \cdots & \\ A_{N-2,1} & A_{N-2,2} & A_{N-2,3} & \cdots & A_{N-2,N-1} \\ A_{N-1,1} & A_{N-1,2} & A_{N-1,3} & \cdots & A_{N-1,N-1} \end{bmatrix} \begin{bmatrix} \tilde{u}_1 \\ \tilde{u}_2 \\ \tilde{u}_3 \\ \vdots \\ \tilde{u}_{N-2} \\ \tilde{u}_{N-1} \end{bmatrix} = \begin{bmatrix} f(x_1) \\ f(x_2) \\ f(x_3) \\ \vdots \\ f(x_{N-2}) \\ f(x_{N-1}) \end{bmatrix}.$$

Hence, by inverting the matrix A, we will be able to attain the coefficients in the vector $\vec{\tilde{u}}$. We then need to create a method to interpolate each Fourier mode with its respective coefficient.

Note that there are two ways we could have implemented the Fourier basis functions, ie-

$$y = \sum_{n=-\frac{N}{2}+1}^{n=\frac{N}{2}-1} c_n e^{inx} \quad \text{or} \quad y = \sum_{n=0}^{\frac{N}{2}-1} \Big(a_n \cos(nx) + b_n \sin(nx) \Big).$$

Since we do not want to carry our final solution as a summation with imaginary parts. We will convert our solution into the second form of the finite Fourier series.

To do this, we realize that

$$c_n = \begin{cases} a_0 & \text{if } n = 0 \\ \frac{a_n - ib_n}{2} & \text{if } n < 0 \\ \frac{a_n + ib_n}{2} & \text{if } n > 0 \end{cases} \tag{2.11}$$

These relations can be derived using the identity $e^{i\theta} = \cos\theta + i\sin\theta$. We then can solve for the $\{a_n\}_{n=0}^{N}$ and $\{b_n\}_{n=0}^{N}$ coefficients using Eq.(2.11). Therefore our final numerical solution will be of the form

$$y(x) = a_0 + a_1\cos(x) + b_1\sin(x) + a_2\cos(2x) + b_2\sin(2x) + \ldots = \sum_{n=0}^{\frac{N}{2}-1} \Big(a_n\cos(nx) + b_n\sin(nx) \Big).$$

Please note it is only because of numerical error that we must break apart the complex coefficients c_n into its real and imaginary parts rather than simply call our final solution,

$$u(x) = \sum_{n=-\frac{N}{2}+1}^{n=\frac{N}{2}-1} \tilde{u}_n e^{inx}.$$

2.3.1 Example: $u'' + u' + u = f(x)$

Consider the following ordinary differential equation

$$u'' + u' + u = e^{\cos x}\Big(1 - \sin x - \cos x + \sin^2 x\Big),$$

with the following boundary conditions,

$$u(-\pi) = u(\pi), \text{ and}$$
$$u'(-\pi) = u'(\pi).$$

By solving the above ODE analytically we find that the solution is

$$u(x) = e^{\cos x}.$$

Upon solving this linear ordinary differential equation using our Fourier pseudo-spectral method, we find that our numerical scheme does in fact exhibit exponential convergence. Note that the error calculated is the L^2 Norm between the spectral solution and the exact solution. This can be seen in Figure(B-3).

2.4 Fourier Pseudo-Spectral Method for Non-Linear ODEs

In this section we will describe the procedure for implementing a pseudo-spectral method for solving an equation of the form:

$$a(x)u'' + b(x)u' + c(x)u^2 = r(x),$$

with periodic boundary conditions $u(0) = u(2\pi)$ and $u'(0) = u'(2\pi)$.

As in the linear ODE case, we first construct a vector of the collocation points, $\{x_n\}_{k=0}^{N}$ where each is a zero of the n^{th} Fourier sine function, as given by Eq.(2.10). Since the ODE is defined on $[0, 2\pi]$, we note that the Fourier modes are of the form: e^{inx}.

Similarly to the linear ODE case once again, we assume a spectral solution over the Fourier basis,

$$u(x) = \sum_{n=-\frac{N}{2}+1}^{n=\frac{N}{2}-1} \tilde{u}_n e^{inx},$$

because we are considering only solutions that are periodic.

We then discretize the ODE to the following form:

$$\sum_{n=-\frac{N}{2}+1}^{n=\frac{N}{2}-1} \tilde{u}_n\Big(-a(x_k)n^2 + ib(x_k) + c(x_k)\Big)e^{inx_k} + \Big(\sum_{n=-\frac{N}{2}+1}^{n=\frac{N}{2}-1} \tilde{u_n}e^{inx}\Big)^2 = r(x_k),$$

where every function of x is evaluated at each collocation point x_k. It is also important to note that in the case $-a(x_k)n^2 + ib(x_k) + c(x_k) = 0$ the spectral method may not converge to the solution.

However, in this case of a non-linear ODE we cannot write a linear equation such as $A\vec{\tilde{u}} = \vec{b}$, to solve for the spectral coefficients $\left\{\tilde{u}_i\right\}_{i=0}^{N}$. Instead we will implement the Multivariate Newton's Method. For our problem, our algorithm will look like the following:

$$\begin{pmatrix} \tilde{u}_1 \\ \tilde{u}_2 \\ \tilde{u}_3 \\ \vdots \\ \tilde{u}_{N-1} \end{pmatrix}^{n+1} = \begin{pmatrix} \tilde{u}_1 \\ \tilde{u}_2 \\ \tilde{u}_3 \\ \vdots \\ \tilde{u}_{N-1} \end{pmatrix}^{n} - J^{-1}F_k^n, \tag{2.12}$$

where $\tilde{u}_{i,n}$ is the n^{th} iterated coefficient $\tilde{u}_i$, J^{-1} is the inverse of a Jacobian matrix, and F_k^n is the n^{th} iterated vector of functions set equal to zero.

We must build the vector F_k^n This vector is comprised of N-1 functions of the coefficients $\left\{\tilde{u}_i\right\}_{i=0}^{i=N}$. Each component of F_k^n will have the following form

$$F_k^n(\tilde{u}_1, \tilde{u}_2 \ldots, \tilde{u}_{N-1}) = 0, \tag{2.13}$$

where the index $k = 1, \ldots, N-1$ and corresponds to each collocation point. We now define the following functional, To fill in the components of F_k^n, we substitute our spectral solution into the functional described in Eq.(2.13) and set it equal to zero. Then we evaluate it at every collocation point within the boundary, or more

explicitly,

$$F_k^n = \sum_{n=-\frac{N}{2}+1}^{n=\frac{N}{2}-1} \tilde{u_n}\Big(-a(x_k)n^2 + ib(x_k) + c(x_k)\Big)e^{inx_k} + \left(\sum_{n=-\frac{N}{2}+1}^{n=\frac{N}{2}-1} \tilde{u_n} e^{inx} \right)^2 - r(x_k) = 0.$$

for $k = 1, 2, \ldots, N-1$. Note that we still do not have to specify boundary conditions when using the Fourier basis because of the Fourier modes' inherent periodicity.

We must now construct the Jacobian matrix $J_n = J_n(k, j)$. The Jacobian J_n will be of size (N+1)×(N+1). It will have the form:

$$J_n = \begin{bmatrix} \frac{\partial F_0}{\partial \tilde{u}_0} & \frac{\partial F_0}{\partial \tilde{u}_1} & \cdots & \frac{\partial F_0}{\partial \tilde{u}_N} \\ \frac{\partial F_1}{\partial \tilde{u}_0} & \frac{\partial F_1}{\partial \tilde{u}_1} & \cdots & \frac{\partial F_1}{\partial \tilde{u}_N} \\ \vdots & & \ddots & \\ \frac{\partial F_N}{\partial \tilde{u}_0} & \frac{\partial F_N}{\partial \tilde{u}_1} & \cdots & \frac{\partial F_N}{\partial \tilde{u}_N} \end{bmatrix}$$

Explicitly writing out the components of those rows we see

$$J_n(k, j) = \frac{\partial F_k}{\partial \tilde{u}_i} = \Big(-a(x_k)n^2 + ib(x_k) + c(x_k)\Big)e^{inx_k} + 2\left(\sum_{n=-\frac{N}{2}+1}^{n=\frac{N}{2}-1} \tilde{u_n} e^{inx} \right) e^{inx_k},$$

recalling the definitions of F_k^n.

Finally, to find the coefficients $\tilde{u_i}$, we must first give an initial guess for the coffi-cients, $\left\{\tilde{u}_{i,0}\right\}_{i=0}^{N}$. This will allow us to begin the iterations. By using the Multivariate Newton's Method algorithm,

$$\tilde{u}_{n+1} = u_n - J_n^{-1} f_n,$$

we can find the coefficients $\left\{\tilde{u}_{i,n}\right\}_{i=0}^{N}$ to complete our numerical solution.

Let the chosen error tolerance be ϵ when using the Newton's method. The algo-rithm stops iterating when the L^2 norm between the coefficient vector of two successive iterations is smaller than ϵ. Explicitly, the Newton's algorithm stops iterating when

the following condition is satisfied

$$\left(\sum_{i=0}^{N} (u_{i,n+1} - u_{i,n})^2 \right)^{1/2} < \epsilon.$$

Hence, we will have the coefficients $\left\{ \tilde{u}_{i,n} \right\}_{i=0}^{N}$ and then can use the solution as

$$y(x) = \sum_{n=-\frac{N}{2}+1}^{n=\frac{N}{2}-1} \tilde{u_n} e^{inx},$$

within the given error tolerance ϵ for the coefficients.

Chapter 3

Poisson's Equation on a Bounded Domain

We will present the basic framework of Chebyshev and Fourier pseudo-spectral methods for solving the Poisson-type Equations and Nonlinear Poisson-type Equations in this chapter.

3.1 Poisson's Equation on a Rectangle

In this section we will show the procedure for solving a Poission problem with a pseudo-spectral method. We consider an equation of the form,

$$u_{xx} + u_{yy} = f(x, y),$$

where $u = (x, y)$, and with boundary conditions $u(-1, y) = u(1, y) = 0$ and $u(x, -1) = u(x, 1) = 0$. Note that we are considering the domain as $[-1, 1] \times [-1, 1]$ namely because we will use the Chebyshev basis functions in our numerical solution and they are only defined between $[-1, 1]$.

The numerical setup of this problem will be much like the numerical setup of a Pseudo-Spectral Method for Linear ODEs; however, now we consider a 2 dimensional problem. Not only will we have collocation points in the x direction, but we will also

have them in the y direction as well. These collocation points will now define a 2 dimensional computational grid.

Since we are still using the Chebyshev polynomials as our basis functions, our collocation points will be the zeros of k^{th} degree Chebyshev polynomials, so we will use Eq.(2.6) to determine them. We will call the collocation points in the x direction, $\{x_k\}_{k=0}^{N}$, and the collocation points in the y direction, $\{y_l\}_{l=0}^{N}$.

Since we now are considering a 2 dimensional region, we define our computational domain at the grid points (x_k, y_l) for $k, l = 0, 1, \ldots, N$. For example, when $N = 6$ the region is seen below. We see that the Chebyshev collocation points are not evenly spaced along the interval, as the Fourier collocation points are. They are more dense along the boundary of the domain. This is illustrated in Figure(B-4).

We then assume the solution $u(x, y)$ has the form of a double finite sum using Chebyshev functions as the basis functions,

$$u(x, y) = \sum_{i=0}^{N} \sum_{j=0}^{N} \tilde{u}_{ij} T_i(x) T_j(y).$$

Upon discretizing the PDE, we see:

$$\sum_{i=0}^{N} \sum_{j=0}^{N} \tilde{u}_{ij} \left[\frac{d^2 T_i(x_k)}{dx^2} \; T_j(y_l) + \; T_i(x_k) \; \frac{d^2 T_j(y_l)}{dx^2} \right] = f(x_k, y_l).$$

Recall that Pseudo-Spectral theory allows us to find the coefficients $\tilde{u}_i$ in the ODE case by solving the following linear equation

$$A\vec{\tilde{u}} = \vec{b},$$

where A is a $(N+1)^2 \times (N+1)^2$ matrix, $\vec{\tilde{u}}$ is the coefficient vector, and $\vec{b}$ is a vector describing the non-homogeneous term of the equation. We are able to use the same approach in the PDE case; however, we must "flatten" out matrices to vectors.

For example, it appears that instead of having a vector of coefficients, we will have

a matrix, such as

$$\vec{\tilde{u}} = \begin{bmatrix} \tilde{u}_{00} & \tilde{u}_{01} & \cdots & \tilde{u}_{0N} \\ \tilde{u}_{10} & \tilde{u}_{11} & \cdots & \tilde{u}_{1N} \\ \vdots & & \cdots & \\ \tilde{u}_{20} & \tilde{u}_{21} & \cdots & \tilde{u}_{NN} \end{bmatrix}.$$

However since we wish to only have a vector of coefficients rather than a matrix, we need to transform the (N+1)×(N+1) matrix above into an $(N+1)^2 \times 1$ vector. More explicitly we need

$$\begin{bmatrix} \tilde{u}_{00} & \tilde{u}_{01} & \cdots & \tilde{u}_{0N} \\ \tilde{u}_{10} & \tilde{u}_{11} & \cdots & \tilde{u}_{1N} \\ \vdots & & \cdots & \\ \tilde{u}_{20} & \tilde{u}_{21} & \cdots & \tilde{u}_{NN} \end{bmatrix} \rightarrow \begin{bmatrix} \tilde{u}_{00} \\ \tilde{u}_{01} \\ \tilde{u}_{02} \\ \vdots \\ \tilde{u}_{ij} \\ \vdots \\ \tilde{u}_{NN} \end{bmatrix}.$$

In order to flatten the matrix into the vector above, we will define a quantity called r that will determine where each component $\tilde{u}_{ij}$ will go in the vector. We can see that r can be defined as

$$r = i(N+1) + (j+1). \tag{3.1}$$

So in our vector $\vec{\tilde{u}}$, we see

$$\tilde{u}_r = \tilde{u}_{ij}.$$

We will use this idea for all Pseudo-Spectral Methods used to solve PDEs. Now we will construct the vector $\vec{b} = [b_{00}\ b_{01} \ldots b_{ij} \ldots b_{NN}]$, we consider the following. At the boundary points, we want $u(-1, y) = y(1, y) = u(x, -1) = u(x, 1) = 0$, so at the collocation points $x_0 = -1$,$x_N = 1$,$y_0 = -1$, and $y_N = 1$ we enforce that those corresponding components of $\vec{b}$ are zero.(Note that whenever $k = 0, N$ or $l = 0, N$ that

$b_{kl} = 0$). Next, since we are solving the PDE on the interior of 2D grid, we need that for all $b_{kl},\ k, l = 1, 2, \ldots, N-1$ that $b_{kl} = f(x_k, y_l)$. Note we obtain this result in an analogous way to those is Section(2.2); however, now we must perform a double integral and use two trial functions. Since we are still implementing a pseudo-spectral method, we again will use delta functions, ie- $\chi_k = \delta(x - x_k)$ and $\chi_l = \delta(y - y_l)$. By performing the integrations we see,

$$b_{kl} = \int_{-1}^{1}\int_{-1}^{1} f(x,y)\delta(x - x_k)\delta(y - y_l)dxdy = f(x_k, y_l).$$

So the vector $\vec{b}$ will have the following form:

$$b = \begin{bmatrix} b_{00} \\ b_{01} \\ \vdots \\ b_{10} \\ b_{11} \\ b_{12} \\ \vdots \\ b_{kl} \\ \vdots \\ b_{NN} \end{bmatrix} = \begin{bmatrix} 0 \\ 0 \\ \vdots \\ 0 \\ f(x_1, y_1) \\ f(x_1, y_2) \\ \vdots \\ f(x_k, y_l) \\ \vdots \\ 0 \end{bmatrix}$$

Now we will construct the matrix A using four for loops, where the outer two for loop runs over the collocation points, $k = 0 : N$ and then $l = 0 : N$, and the two innermost for loops run over the i^{th} and j^{th} Chebyshev polynomials from $i, j = 0, 1, \ldots N$. The matrix A will be of size $(\mathrm{N}+1)^2 \times (\mathrm{N}+1)^2$. Recalling Eq.(3.1), we will construct another index, call it c, that has the exact same form as r. That is,

$$c = i(N+1) + (j+1) = r.$$

Since we can think of r as an index running over rows of a matrix, we can think

of c as the index running over the columns of a matrix. Hence, the matrix A's components will be filled in as $A = A(r, c)$. Similarly to how we constructed the vector $\vec{b}$, whenever our for loops running over an index of $k = 0, N$ or $l = 0, N$, we want to fill in those corresponding components of A as

$$A(r, c) = T_i(x_k)\ T_j(y_l).$$

To fill in the remaining components of A, that is for all $k, l = 1, 2, \ldots, N-1$ we wish that the corresponding components of A to be

$$A(r, c) = \frac{d^2T_i(x_k)}{dx^2}\ T_j(y_l) + \ T_i(x_k)\ \frac{d^2T_j(y_l)}{dx^2},$$

which we obtain from performing all the integrations analogous to (2.3), ie-

$$\int_{-1}^{1}\int_{-1}^{1}\Big[\frac{d^2T_i(x)}{dx^2}\ T_j(y) + \ T_i(x)\ \frac{d^2T_j(y)}{dx^2}\Big]\ \delta(x - x_k)\delta(y - y_l)dxdy$$
$$= \frac{d^2T_i(x_k)}{dx^2}\ T_j(y_l) + \ T_i(x_k)\ \frac{d^2T_j(y_l)}{dx^2}. \quad (3.2)$$

We then have the following matrix equation to solve:

$$A\vec{\tilde{u}} = \vec{b}.$$

Hence, by inverting the matrix A, we will be able to attain the coefficients in the vector $\vec{\tilde{u}}$, thereby creating a method to interpolate each Chebyshev polynomial with its respective coefficient will give the final numerical solution. So finally, the numerical solution is

$$u(x, y) = \tilde{u_{00}}T_0(x)T_0(y) + \tilde{u_{01}}T_0(x)T_1(y) + \ldots + \tilde{u_{NN}}T_N(x)T_N(y) = \sum_{i=0}^{N}\sum_{j=0}^{N}\tilde{u_{ij}}T_i(x)T_j(y).$$

3.1.1 Example: $u_{xx} + u_{yy} = f(x, y)$

Consider the following Poisson problem,

$$u_{xx} + u_{yy} = -\pi^2 \sin(\pi y)\big[2\cos(\pi x) + 1\big]$$

with the following boundary conditions,

$$u(-1, y) = u(1, y) = 0,$$
$$u(x, -1) = u(x, 1) = 0.$$

By solving the above equation analytically, we find the solution is

$$u(x, y) = \sin(\pi y)\big(\cos(\pi x) + 1\big).$$

By solving this linear partial differential equation using our Chebyshev pseudo-spectral method, we find that it does in fact show exponential convergence. Note the error calculated is the L^2 Norm between the interpolated solution and the exact solution. The convergence plot can be seen in Figure(B-5).

A plot comparing the interpolated solution and exact solution is found in Figure(B-6).

3.2 Nonlinear Poisson Equation on a Rectangle

In this section we will show the procedure for solving a nonlinear Poisson-type problem on a rectangle using a pseudo-spectral method. To illustrate the algorithm we will consider the following nonlinear PDE,

$$u_{xx} + u_{yy} + u^2 = r(x, y),$$

where $u = (x, y)$, and with boundary conditions $u(-1, y) = b_1, u(1, y) = b_2, u(x, -1) = b_3$, and $u(x, 1) = b_4$.

The numerical setup of this problem will be much like the numerical setup of a Pseudo-Spectral Method for Linear ODEs; however, now we must consider a 2 dimensional problem. Not only will we have collocation points in the x direction, but we will also have them in the y direction as well. These collocation points will now define a 2 dimensional computational region.

Since we are still using the Chebyshev polynomials as our basis functions, our collocation points will be the zeros of k^{th} degree Chebyshev polynomials, so we use Eq.(2.6) to determine them. We will call the collocation points in the x direction, $\{x_k\}_{k=0}^{N}$, and the collocation points in the y direction, $\{y_l\}_0^N$. Since we now are considering a 2 dimensional region, we will define our computational domain at the grid points (x_k, y_l) for $k, l = 0, 1, \ldots, N$. For $N = 6$, the region is seen in Figure(B-4).

We then assume the solution u(x,y) has the following form,

$$u(x,y) = \sum_{i=0}^{N}\sum_{j=0}^{N} \tilde{u}_{ij} T_i(x) T_j(y).$$

Upon discretizing the PDE, we see:

$$\sum_{i=0}^{N}\sum_{j=0}^{N} \tilde{u}_{ij}\left[\frac{d^2T_i(x_k)}{dx^2}\,T_j(y_l) + T_i(x_k)\,\frac{d^2T_j(y_l)}{dx^2}\right] + \left(\sum_{i=0}^{N}\sum_{j=0}^{N} \tilde{u}_{ij} T_i(x_k) T_j(y_l)\right)^2 = r(x_k, y_l).$$

However, in this case of a nonlinear ODE we cannot write a linear equation such as $A\vec{\tilde{u}} = \vec{b}$, to solve for the coefficients $\left\{\tilde{u_i}\right\}_{i=0}^{N}$. Instead we will implement the Multivariate Newton's Method, as in the Nonlinear ODE case. For our problem, our algorithm will look like the following:

$$\begin{pmatrix} \tilde{u}_{00,n+1} \\ \tilde{u}_{01,n+1} \\ \vdots \\ \tilde{u}_{N(N-1),n+1} \\ \tilde{u}_{NN,n+1} \end{pmatrix} = \begin{pmatrix} \tilde{u}_{00,n} \\ \tilde{u}_{01,n} \\ \vdots \\ \tilde{u}_{N(N-1),n} \\ \tilde{u}_{NN,n} \end{pmatrix} - \; J^{-1} f_{ij,n}, \tag{3.3}$$

where $\tilde{u}_{ij,n}$ is the n^{th} iterated coefficient $\tilde{u}_{ij}$, J^{-1} is the inverse of a Jacobian matrix, and $f_{kl,n}$ is an n^{th} iterated vector of functions set equal to zero corresponding to $k, l = 1, 2, \ldots, N$. We must build the vector $f_{kl,n}$ This vector is comprised of (N+1)^2 functions of the coefficients $\left\{\tilde{u}_{ij}\right\}_{i=0,j=0}^{i=N,j=N}$. Each component of $f_{kl,n}$ will have the following form

$$f_{kl,n} = F_{kl}(\tilde{u}_{00}, \tilde{u}_{01}, \ldots, \tilde{u}_{0N}, \tilde{u}_{10}, \ldots, \tilde{u}_{NN}) = 0, \tag{3.4}$$

where the indices $k, l = 0, 1, \ldots, N$ and correspond to each collocation point (x_k, y_l). To fill in this vector, we first look at the collocation points $x_{k=0} = -1$,$x_{k=N} = 1$, $y_{l=0} = -1$, and $y_{l=N} = 1$ corresponding to the boundary. We will implement the boundary conditions as follows.

$$\begin{aligned}
f_{0l,n} &= \sum_{i=0}^{N}\sum_{j=0}^{N} \tilde{u}_{ij,n}\ T_i(x_0)\ T_j(y_l) - b_1, \\
f_{Nl,n} &= \sum_{i=0}^{N}\sum_{j=0}^{N} \tilde{u}_{ij,n}\ T_i(x_N)\ T_j(y_l) - b_2, \\
f_{k0,n} &= \sum_{i=0}^{N}\sum_{j=0}^{N} \tilde{u}_{ij,n}\ T_i(x_k)\ T_j(y_0) - b_3, \\
f_{kN,n} &= \sum_{i=0}^{N}\sum_{j=0}^{N} \tilde{u}_{ij,n}\ T_i(x_k)\ T_j(y_N) - b_4.
\end{aligned}$$

Note that $f_{0l,n}, f_{Nl,n}, f_{k0,n}$ and $f_{kN,n}$ have the form of Eq.(3.4). To fill in the remaining components of $f_{kl,n}$, we set the differential equation equal to zero and then evaluate it at every collocation point within the boundary, or more explicitly,

$$\begin{aligned}
f_{kl,n} = F_{kl} = \sum_{i=0}^{N}\sum_{j=0}^{N} \tilde{u}_{ij} \left[\frac{d^2T_i(x_k)}{dx^2}\ T_j(y_l) + \ T_i(x_k)\ \frac{d^2T_j(y_l)}{dx^2} \right] \\
+ \left(\sum_{i=0}^{N}\sum_{j=0}^{N} \tilde{u}_{ij} T_i(x_k) T_j(y_l) \right)^2 - r(x_k, y_l),
\end{aligned} \tag{3.5}$$

To obtain the above result, consider the following function, where we are substituting our assumed solution into the PDE,

$$G(x,y,\vec{\tilde{u}}) = \sum_{i=0}^{N}\sum_{j=0}^{N}\tilde{u}_{ij}\left[\frac{d^2T_i(x)}{dx^2}\ T_j(y) + \ T_i(x)\ \frac{d^2T_j(y)}{dx^2}\right] + \left(\sum_{i=0}^{N}\sum_{j=0}^{N}\tilde{u}_{ij}T_i(x)T_j(y)\right)^2 - r(x,y) = 0. \quad (3.6)$$

As we did in deriving Eq.(2.3), we will multiply (3.6) by the delta test functions, $\chi_k = \delta(x - x_k)$ and$\chi_l = \delta(y - y_l)$, and integrate over the domain we obtain,

$$\int_{-1}^{1}\int_{-1}^{1} G(x,y,\vec{\tilde{u}})\delta(x-x_k)\delta(y-y_l)dxdy = \sum_{i=0}^{N}\sum_{j=0}^{N}\tilde{u}_{ij}\left[\frac{d^2T_i(x_k)}{dx^2}\ T_j(y_l) + \ T_i(x_k)\ \frac{d^2T_j(y_l)}{dx^2}\right] + \left(\sum_{i=0}^{N}\sum_{j=0}^{N}\tilde{u}_{ij}T_i(x_k)T_j(y_l)\right)^2 - r(x_k,y_l). \quad (3.7)$$

for $k, l = 1, 2, \ldots, N-1$.

We must now construct the Jacobian matrix $J_n = J_n(k,i)$. The Jacobian J_n will be of size (N+1)$^2\times$(N+1)^2. It will have the form:

$$J_n = \begin{bmatrix} \frac{\partial F_{00}}{\partial \tilde{u}_{00}} & \frac{\partial F_{00}}{\partial \tilde{u}_{01}} & \dots & \frac{\partial F_{00}}{\partial \tilde{u}_{0N}} & \frac{\partial F_{00}}{\partial \tilde{u}_{10}} & \dots & \frac{\partial F_{00}}{\partial \tilde{u}_{NN}} \\ \frac{\partial F_{01}}{\partial \tilde{u}_{00}} & \frac{\partial F_{01}}{\partial \tilde{u}_{01}} & \dots & \frac{\partial F_{01}}{\partial \tilde{u}_{0N}} & \frac{\partial F_{01}}{\partial \tilde{u}_{10}} & \dots & \frac{\partial F_{01}}{\partial \tilde{u}_{NN}} \\ \vdots & \vdots & & \vdots & \vdots & & \vdots \\ \frac{\partial F_{0N}}{\partial \tilde{u}_{00}} & \frac{\partial F_{0N}}{\partial \tilde{u}_{01}} & \dots & \frac{\partial F_{0N}}{\partial \tilde{u}_{0N}} & \frac{\partial F_{0N}}{\partial \tilde{u}_{10}} & \dots & \frac{\partial F_{0N}}{\partial \tilde{u}_{NN}} \\ \frac{\partial F_{10}}{\partial \tilde{u}_{00}} & \frac{\partial F_{10}}{\partial \tilde{u}_{01}} & \dots & \frac{\partial F_{10}}{\partial \tilde{u}_{0N}} & \frac{\partial F_{10}}{\partial \tilde{u}_{10}} & \dots & \frac{\partial F_{10}}{\partial \tilde{u}_{NN}} \\ \vdots & \vdots & & \vdots & \vdots & & \vdots \\ \frac{\partial F_{NN}}{\partial \tilde{u}_{00}} & \frac{\partial F_{NN}}{\partial \tilde{u}_{01}} & \dots & \frac{\partial F_{NN}}{\partial \tilde{u}_{0N}} & \frac{\partial F_{NN}}{\partial \tilde{u}_{10}} & \dots & \frac{\partial F_{NN}}{\partial \tilde{u}_{NN}} \end{bmatrix}$$

From our definitions of the functions F_{kl}, we see that at the collocation points corresponding to either $k = 0, N$ or $l = 0, N$, the values in the Jacobian will be vastly different from the others. We illustrate them below.

$$J_n(0l, ij) = \frac{\partial F_{0l}}{\partial \tilde{u}_{ij}} = T_i(x_0)T_j(y_l),$$

$$J_n(Nl, ij) = \frac{\partial F_{Nl}}{\partial \tilde{u}_{ij}} = T_i(x_N)T_j(y_l),$$

$$J_n(k0, ij) = \frac{\partial F_{k0}}{\partial \tilde{u}_{ij}} = T_i(x_k)T_j(y_0),$$

$$J_n(kN, ij) = \frac{\partial F_{kN}}{\partial \tilde{u}_{ij}} = T_i(x_k)T_j(y_N).$$

The rest of the matrix components will fill in similarly, as follows

$$J_n(kl,ij) = \frac{\partial F_{kl}}{\partial \tilde{u}_{ij}} = \frac{d^2T_i(x_k)}{dx^2}\ T_j(y_l) + \ T_i(x_k)\ \frac{d^2T_j(y_l)}{dx^2} + 2\ T_i(x_k)\ T_j(y_l)\ \left(\sum_{i=0}^{N}\sum_{j=0}^{N}\tilde{u}_{ij}T_i(x_k)T_j(y_l)\right). \quad (3.8)$$

Finally, to find the coefficients $\tilde{u}_{ij}$, we must first provide an initial guess for the coefficients, $\left\{\tilde{u}_{ij,0}\right\}_{i,j=0}^{i,j=N}$. This will allow us to begin the iterations. By using the Multivariate Newton's Method algorithm,

$$\vec{\tilde{u}}_{n+1} = \vec{\tilde{u}}_n - J_n^{-1}\vec{f}_{kl,n},$$

we can find the coefficients $\left\{\tilde{u}_{ij,n}\right\}_{i,j=0}^{i,j=N}$ to interpolate the solution. Let the chosen error tolerance be ϵ when using the Newton's method. The algorithm stops iterating when the L^2 norm between the coefficient vector of two successive iterations is smaller than ϵ. Explicitly, the Newton's algorithm stops iterating when the following condition is satisfied

$$\left(\sum_{i=0}^{N}\sum_{j=0}^{N}(u_{ij,n+1} - u_{ij,n})^2\right)^{1/2} < \epsilon.$$

Hence, we will have the coefficients $\left\{\tilde{u}_{ij,n}\right\}_{i,j=0}^{i,j=N}$ and then we will have our full numerical solution as

$$u(x,y) = \sum_{i=0}^{N}\sum_{j=0}^{N}\tilde{u}_{ij,n}\ T_i(x)\ T_j(y),$$

within the given error tolerance ϵ for the coefficients.

3.2.1 Example: $u_{xx} + u_{yy} + u^2 = f(x,y)$

Consider the following nonlinear Poisson problem,

$$u_{xx} + u_{yy} + u^2 = -\pi^2\sin(\pi y)\big[2\cos(\pi x) + 1\big] + \Big(\sin(\pi y)\big(\cos(\pi x) + 1\big)\Big)^2$$

with the following boundary conditions,

$$u(-1, y) = u(1, y) = 0,$$
$$u(x, -1) = u(x, 1) = 0.$$

By solving the above equation analytically, we find the solution is

$$u(x, y) = \sin(\pi y)\big(\cos(\pi x) + 1\big).$$

By solving this nonlinear partial differential equation using our Chebyshev pseudo-spectral method, we find that it does in fact show exponential convergence. Note the error calculated is the L^2 Norm between the interpolated solution and the exact solution. This exponential convergence is illustrated in Figure(B-7).

A plot comparing the interpolated solution and exact solution is found in Figure(B-8).

3.3 Nonlinear Poisson Equation on a Disk

In this section we will show the procedure for implementing a pseudo-spectral method for solving a nonlinear Poisson-like problem in polar coordinates. The equation we wish to solve is:

$$u_{rr} + \frac{1}{r}u_r + \frac{1}{r^2}u_{\phi\phi} + u^2 = d(r, \phi),$$

with boundary conditions

$$\begin{aligned} &u(0, \phi) = 0, \\ &u(1, \phi) = 0, \\ &u(r, 0) = u(r, 2\pi), \text{ and} \\ &\frac{\partial u}{\partial \phi}(r, 0) = \frac{\partial u}{\partial \phi}(r, 2\pi). \end{aligned}$$

We will use a Chebyshev scheme to solve in the radial coordinate and a Fourier Spectral Scheme to solve in the angular coordinate. However, since the Chebyshev

polynomials are defined between [-1,1] and not [0,1], we have the option to either transform the polynomials to be defined between [0,1] ,or we can perform a coordinate transformation to define the PDE itself on [-1,1]×[0,2π] rather than [0,1]×[0,2π]. We will do the latter.

We will use the following coordinate transformation to transform the PDE into the appropriate domain,

$$A = 2r - 1 \tag{3.9}$$

By applying the chain rule, we see

$$\frac{\partial u}{\partial r} = \frac{\partial u}{\partial A}\frac{\partial A}{\partial r} = 2\frac{\partial u}{\partial A},$$

$$\frac{\partial^2 u}{\partial r^2} = \frac{\partial A}{\partial r}\frac{\partial}{\partial A}(\frac{\partial u}{\partial A}) = 4\frac{\partial^2 u}{\partial A^2}.$$

By using the above relation and Eq.(3.9), we see the PDE transforms to

$$4u_{AA} + \frac{2}{\frac{A+1}{2}}u_A + \frac{1}{\left(\frac{A+1}{2}\right)^2}u_{\phi\phi} + u^2 = d(\frac{A+1}{2}, \phi),$$

or more simplified as

$$4u_{AA} + \frac{4}{A+1}u_A + \frac{4}{(A+1)^2}u_{\phi\phi} + u^2 = d(A, \phi).$$

The numerical setup of this problem will be much like the numerical setup of a Pseudo-Spectral Method for Nonlinear ODEs; however, now we must consider a 2 dimensional problem. Not only will we have collocation points in the A direction, but we will also have them in the ϕ direction as well. These collocation points will now define a 2 dimensional computational region.

Since we are still using the Chebyshev polynomials as our basis functions for the A coordinate, our collocation points will be the zeros of k^{th} degree Chebyshev polynomials, so we will use Eq.(2.6) to determine them. We will call the collocation points in the A direction, $\{A_k\}_{k=0}^{N_A}$. The collocation points in the ϕ direction will

be the zeros of the l^{th} 2π periodic Fourier basis function, so we will use Eq.(2.10) to determine them. We will call them $\{\phi_l\}_0^{N_{phi}}$. We will define our computational domain at the grid points (A_k, ϕ_l) for $k = 0, 1, \ldots, N_A$ and $l = 1, 2, \ldots, N_{phi} - 1$. For $N_A = N_\phi = 7$, the region is seen in Figure(B-9). Note that we need to define on our computational domain on an odd number of Fourier Collocation points.

We then assume the solution u(x,y) has the following form,

$$u(A, \phi) = \sum_{m=0}^{N_A} \sum_{n=\frac{N_{phi}}{2}+1}^{n=\frac{N_{phi}}{2}-1} \tilde{u}_{mn} T_m(A) e^{in\phi}.$$

By discretizing the PDE, we see:

$$\sum_{m=0}^{N_A} \sum_{n=\frac{N_{phi}}{2}+1}^{n=\frac{N_{phi}}{2}-1} \tilde{u}_{mn} \left[4\frac{d^2 T_m(A_k)}{dx^2} + \frac{4}{A+1}\frac{dT_m(A_k)}{dx} - \frac{4n^2}{(A+1)^2} T_m(A_k) \right] e^{in\phi_l}$$
$$+ \left(\sum_{m=0}^{N_A} \sum_{n=\frac{N_{phi}}{2}+1}^{n=\frac{N_{phi}}{2}-1} \tilde{u}_{mn} T_m(A_k)) e^{in\phi_l} \right)^2 = r(A_k, \phi_l).$$

However, in this case of a nonlinear ODE we cannot write a linear equation such as $A\vec{\tilde{u}} = \vec{b}$, to solve for the coefficients $\left\{\tilde{u_{mn}}\right\}$. Instead we will implement the Multivariate Newton's Method, as in the nonlinear ODE case. For our problem, our algorithm will look like the following:

$$\begin{pmatrix} \tilde{u}_{01,j+1} \\ \tilde{u}_{02,j+1} \\ \vdots \\ \tilde{u}_{N(N-2),j+1} \\ \tilde{u}_{N(N-1),j+1} \end{pmatrix} = \begin{pmatrix} \tilde{u}_{01,j} \\ \tilde{u}_{02,j} \\ \vdots \\ \tilde{u}_{N(N-2),j} \\ \tilde{u}_{N(N-1),j} \end{pmatrix} - \; J^{-1} f_{mn,j}, \tag{3.10}$$

where $\tilde{u}_{mn,j}$ is the j^{th} iterated coefficient $\tilde{u}_{mn}$, J^{-1} is the inverse of a Jacobian matrix, and $f_{mn,j}$ is an j^{th} iterated vector of functions set equal to zero corresponding to $m = 0, 1, 2, \ldots, N$ and $n = \frac{-N_\phi}{2} + 1, \frac{-N_\phi}{2} + 2, \ldots, 0, \ldots, \frac{N_\phi}{2} - 1$.

We must build the vector $f_{mn,j}$ This vector is comprised of (N_A+1)(N_{phi}-1) functions of the coefficients $\left\{\tilde{u}_{mn}\right\}$. Each component of $f_{mn,j}$ will have the following form

$$f_{mn,j} = F_{kl}\left(\tilde{u}_{01}, \tilde{u}_{02}, \ldots, \tilde{u}_{0\ N_{phi}-1}, \tilde{u}_{11}, \ldots, \tilde{u}_{N_A N_{phi}-1}\right) = 0, \tag{3.11}$$

where the indices $k, = 0, 1, \ldots, N_A$ and $l = 1, 2, \ldots, N_{phi} - 1$ correspond to each collocation point (A_k, ϕ_l). To fill in this vector, we first look at the collocation points $x_{k=0} = -1$ and $x_{k=N} = 1$ corresponding to the A-boundary. We will implement the boundary conditions as follows.

$$f_{0l,n} = \sum_{m=0}^{N_A} \sum_{n=\frac{N_{phi}}{2}+1}^{n=\frac{N_{phi}}{2}-1} \tilde{u}_{mn,j}\ \frac{dT_m(A_0)}{dA} e^{in\phi_l},$$
$$f_{Nl,n} = \sum_{m=0}^{N_A} \sum_{n=\frac{N_{phi}}{2}+1}^{n=\frac{N_{phi}}{2}-1} \tilde{u}_{mn,j}\ T_m(A_0) e^{in\phi_l}.$$

Note that $f_{0l,n}$ and $f_{Nl,n}$ have the form of Eq.(3.11). To fill in the remaining components of $f_{mn,j}$, we set the differential equation equal to zero and then evaluate it at every collocation point within the boundary, or more explicitly,

$$f_{mn,j} = F_{mn} = \sum_{m=0}^{N_A} \sum_{n=\frac{N_{phi}}{2}+1}^{n=\frac{N_{phi}}{2}-1} \tilde{u}_{mn} \left[4\frac{d^2 T_m(A_k)}{dx^2} + \frac{4}{A_k + 1}\frac{dT_m(A_k)}{dx} - \frac{4n^2}{(A_k+1)^2} T_m(A_k) \right] e^{in\phi_l}$$
$$+ \left(\sum_{m=0}^{N_A} \sum_{n=\frac{N_{phi}}{2}+1}^{n=\frac{N_{phi}}{2}-1} \tilde{u}_{mn} T_m(A_k) e^{in\phi_l} \right)^2 - r(A_k, \phi_l) = 0.$$

for $k = 1, 2, \ldots, N_A - 1$ and $l = 1, 2, \ldots, N_{phi} - 1$.

To obtain the above result, consider the following function, where we are substi-

tuting our assumed solution into the PDE,

$$G(A,\phi,\vec{\tilde{u}}) = \sum_{m=0}^{N_A} \sum_{n=\frac{N_{phi}}{2}+1}^{n=\frac{N_{phi}}{2}-1} \tilde{u}_{mn} \left[4\frac{d^2T_m(A)}{dx^2} \quad + \quad \frac{4}{A+1}\frac{dT_m(A)}{dx} - \frac{4n^2}{(A+1)^2}T_m(A) \right] e^{in\phi}$$
$$+ \quad \left(\sum_{m=0}^{N_A} \sum_{n=\frac{N_{phi}}{2}+1}^{n=\frac{N_{phi}}{2}-1} \tilde{u}_{mn} T_m(A) e^{in\phi} \right)^2 - r(A,\phi) = 0. \tag{3.12}$$

Analogously to (2.3), we will multiply (3.12) by the delta test functions, $\chi_k = \delta(A - A_k)$ and$\chi_l = \delta(\phi - \phi_l)$, and integrate over the domain we obtain,

$$\int_{-1}^{1}\int_{-1}^{1} G(A,\phi,\vec{\tilde{u}})\delta(A-A_k)\delta(\phi - phi_l)dxdy$$
$$= \sum_{m=0}^{N_A} \sum_{n=\frac{N_{phi}}{2}+1}^{n=\frac{N_{phi}}{2}-1} \tilde{u}_{mn} \left[4\frac{d^2T_m(A_k)}{dx^2} + \frac{4}{A_k+1}\frac{dT_m(A_k)}{dx} - \frac{4n^2}{(A_k+1)^2}T_m(A_k) \right] e^{in\phi_l}$$
$$+ \left(\sum_{m=0}^{N_A} \sum_{n=\frac{N_{phi}}{2}+1}^{n=\frac{N_{phi}}{2}-1} \tilde{u}_{mn} T_m(A_k) e^{in\phi_l} \right)^2 - r(A_k,\phi_l) \tag{3.13}$$

for $k, l = 1, 2, \ldots, N-1$.

We must now construct the Jacobian matrix $J_n = J_n(k,j)$. The Jacobian J_n will

be of size $(N_A{+}1)(N_{phi}\text{-}1){\times}(N_{phi}\text{-}1)(N_A{+}1)$. It will have the form:

$$J_n = \begin{bmatrix} \frac{\partial F_{01}}{\partial \tilde{u}_{01}} & \frac{\partial F_{01}}{\partial \tilde{u}_{02}} & \cdots & \frac{\partial F_{01}}{\partial \tilde{u}_{0(N_{phi}-1)}} & \frac{\partial F_{01}}{\partial \tilde{u}_{11}} & \cdots & \frac{\partial F_{01}}{\partial \tilde{u}_{N_A(N_{phi}-1)}} \\ \frac{\partial F_{02}}{\partial \tilde{u}_{01}} & \frac{\partial F_{02}}{\partial \tilde{u}_{02}} & \cdots & \frac{\partial F_{02}}{\partial \tilde{u}_{0(N_{phi}-1)}} & \frac{\partial F_{02}}{\partial \tilde{u}_{11}} & \cdots & \frac{\partial F_{02}}{\partial \tilde{u}_{N_A(N_{phi}-1)}} \\ \vdots & \vdots & & \vdots & \vdots & & \vdots \\ \frac{\partial F_{0(N_{Phi}-1)}}{\partial \tilde{u}_{01}} & \frac{\partial F_{0(N_{Phi}-1)}}{\partial \tilde{u}_{02}} & \cdots & \frac{\partial F_{0(N_{Phi}-1)}}{\partial \tilde{u}_{0(N_{Phi}-1)}} & \frac{\partial F_{0(N_{Phi}-1)}}{\partial \tilde{u}_{11}} & \cdots & \frac{\partial F_{0(N_{phi}-1)}}{\partial \tilde{u}_{N_A(N_{phi}-1)}} \\ \frac{\partial F_{11}}{\partial \tilde{u}_{01}} & \frac{\partial F_{11}}{\partial \tilde{u}_{02}} & \cdots & \frac{\partial F_{11}}{\partial \tilde{u}_{0(N_{Phi}-1)}} & \frac{\partial F_{11}}{\partial \tilde{u}_{11}} & \cdots & \frac{\partial F_{11}}{\partial \tilde{u}_{N_A(N_{phi}-1)}} \\ \vdots & \vdots & & \vdots & \vdots & & \vdots \\ \frac{\partial F_{N_A(N_{Phi}-1)}}{\partial \tilde{u}_{01}} & \frac{\partial F_{N_A(N_{Phi}-1)}}{\partial \tilde{u}_{02}} & \cdots & \frac{\partial F_{N_A(N_{Phi}-1)}}{\partial \tilde{u}_{0(N_{Phi}-1)}} & \frac{\partial F_{N_A(N_{Phi}-1)}}{\partial \tilde{u}_{11}} & \cdots & \frac{\partial F_{N_A(N_{Phi}-1)}}{\partial \tilde{u}_{N_A(N_{Phi}-1)}} \end{bmatrix}$$

From our definitions of the functions F_{mn}, we see that at the collocation points corresponding to either $k = 0$ or $k = N_A$, the values in the Jacobian will be vastly different from the others. We illustrate them below.

$$J_n(0l, mn) = \frac{\partial F_{0l}}{\partial \tilde{u}_{mn}} = T_m(A_0)\ e^{in\phi_l},$$

$$J_n(N_A l, mn) = \frac{\partial F_{N_A l}}{\partial \tilde{u}_{mn}} = T_m(A_{N_A})\ e^{in\phi_l}.$$

The rest of the matrix components will fill in similarly, as follows

$$J_n(mn, kl) = \frac{\partial F_{mn}}{\partial \tilde{u}_{kl}} = \left[4\frac{d^2 T_m(A_k)}{dx^2} \quad + \quad \frac{4}{A+1}\frac{dT_m(A_k)}{dx} - \frac{4n^2}{(A+1)^2} T_m(A_k) \right] e^{in\phi_l}$$
$$+ \quad 2\left(\sum_{m=0}^{N_A} \sum_{n=\frac{N_{phi}}{2}+1}^{n=\frac{N_{phi}}{2}-1} \tilde{u}_{mn} T_m(A_k)) e^{in\phi_l} \right) T_m(A_k) e^{in\phi_l}.$$

Finally, to find the coefficients $\tilde{u}_{mn}$, we must first give an initial guess for the coffi-cients, $\left\{\tilde{u}_{mn,0}\right\}$. This will allow us to begin the iterations. By using the Multivariate Newton's Method algorithm,

$$\vec{\tilde{u}}_{j+1} = \vec{\tilde{u}}_j - J_n^{-1}\vec{f}_{mn,j},$$

we can find the coefficients $\left\{\tilde{u}_{mn,j}\right\}$ to interpolate the solution.

Let the chosen error tolerance be ϵ when using the Newton's method. The algorithm stops iterating when the L^2 norm between the coefficient vector of two successive iterations is smaller than ϵ. Explicitly, the Newton's algorithm stops iterating when the following condition is satisfied

$$\left(\sum_{i=0}^{N_A}\sum_{n=\frac{N_{phi}}{2}+1}^{n=\frac{N_{phi}}{2}-1}\left(u_{mn,j+1}-u_{mn,j}\right)^2\right)^{1/2} < \epsilon.$$

Hence, we will have the coefficients $\left\{\tilde{u}_{ij,n}\right\}$and then can write our final numeric solution as

$$u(A,\phi) = \sum_{m=0}^{N_A}\sum_{n=\frac{N_{phi}}{2}+1}^{n=\frac{N_{phi}}{2}-1}\tilde{u}_{mn}T_m(A)e^{in\phi},$$

within the given error tolerance ϵ.

Note: Recall that the original problem was in terms of r and not A. We simply had to do a coordinate transformation from r to A in order to ensure we could use the Chebyshev polynomials, which are defined on $[-1,1]$. If we wish to transform our solution back into terms of $u(r,\phi)$, then in our numerical solution, wherever there is an A, we can then substitute $A \to (2r-1)$ so that you may enter values of r rather than values of A.

3.3.1 Example: $u_{rr} + \frac{1}{r}u_r + \frac{1}{r^2}u_{\phi\phi} + u^2 = f(r,\phi)$

Consider the following Poisson problem,

$$\begin{aligned} u_{rr} + \frac{1}{r}u_r + \frac{1}{r^2}u_{\phi\phi} + u^2 \\ = \left[-4\pi^2\cos[(2r-1)\pi] - \frac{2\pi}{r}\sin[(2r-1)\pi] + \frac{1}{r^2}\left(\sin^2\phi - \cos\phi\right)\right]e^{\cos\phi} \\ + \left(\Big[\cos[(2r-1)\pi] + 1\Big]e^{\cos\phi}\right)^2, \end{aligned}$$

with the following boundary conditions,

$$\begin{aligned} &u(0,\phi) = u(1,\phi) = 0, \\ &u(r,-\pi) = u(r,\pi), \text{ and} \\ &\frac{\partial u}{\partial\phi}(r,-\pi) = \frac{\partial u}{\partial\phi}(r,\pi). \end{aligned}$$

By solving the above equation analytically, we find the solution is

$$u(r,\phi) = \Big[\cos[(2r-1)\pi] + 1\Big]e^{\cos\phi}.$$

By solving this nonlinear partial differential equation using our Fourier pseudo-spectral method, we find that it does in fact show exponential convergence. Note the error calculated is the Sup Norm between the interpolated solution and the exact solution. The convergence plot is found in Figure(B-10).

A plot comparing the interpolated solution and exact solution is found in Figure(B-11) for $N_r = N_\phi = 10$.

Chapter 4

Poisson's Equation on an Unbounded Domain

In this Section we will present the basic framework of using Chebyshev and Fourier pseudo-spectral methods in solving problems whose domain is all of R^3.

4.1 Compactification of R^3

In this section we will introduce the change of variables that will inherently compactify all of R^3 into a finite box. Upon doing so, we will present the spherical Laplacian in compactified coordinates. Recall in spherical coordinates, (r, θ, ϕ), we consider,

$$r \in [0, \infty)$$

$$\theta \in [0, \pi]$$

$$\phi \in [0, 2\pi)$$

We will use the following transformations to compactify all of R^3 into the box, $[-1, 1] \times [-1, 1] \times [0, 2\pi)$,

$$\tilde{A} = 2\left[1 + \frac{m}{2r}\right]^{-1} - 1,$$

$$\tilde{B} = \frac{2}{\pi}\theta - 1,$$

$$\tilde{\phi} = \phi.$$

where $\tilde{A} \in [-1, 1]$, $\tilde{B} \in [-1, 1]$, and $\tilde{\phi} \in [0, 2\pi)$. The above transformations will compactify the domain $[0, \infty] \times [0, \pi] \times [0, 2\pi) \to [-1, 1] \times [-1, 1] \times [0, 2\pi)$.

Now we wish to transform the Laplacian in spherical coordinates into the comactified coordinates. Recall the Laplacian in spherical coordinates is,

$$\Delta u = u_{rr} + \frac{2}{r}u_r + \frac{1}{r^2 \sin^2\theta}u_{\phi\phi} + \frac{1}{r^2 \sin\theta}\left[\frac{d}{d\theta}\left(\sin\theta u_\theta\right)\right]. \tag{4.1}$$

To perform the change of variables we must compute all the necessary chain rules. Upon doing so, we see

$$\frac{\partial u}{\partial r} = \frac{1}{m}(1 - \tilde{A})^2 \frac{\partial u}{\partial \tilde{A}},$$

$$\frac{\partial^2 u}{\partial r^2} = \frac{1}{m^2}(1 - \tilde{A})^4 \frac{\partial^2 u}{\partial \tilde{A}^2} - \frac{2}{m^2}(1 - \tilde{A})^3 \frac{\partial u}{\partial \tilde{A}},$$

$$\frac{\partial u}{\partial \theta} = \frac{2}{\pi}\frac{\partial u}{\partial \tilde{B}},$$

$$\frac{\partial^2 u}{\partial \theta^2} = \frac{4}{\pi^2}\frac{\partial^2 u}{\partial \tilde{B}^2}.$$

Substituting the coordinate transformations and the above relations into the Laplacian in spherical coordinates, we find the Laplacian in compactified coordinates

takes the following form,

$$\Delta u = \frac{1}{m^2}\left(1-\tilde{A}\right)^4 u_{\tilde{A}\tilde{A}} + \frac{2}{m^2}\frac{(1-\tilde{A})^4}{1+\tilde{A}}u_{\tilde{A}} + \frac{4}{m^2}\left(\frac{1-\tilde{A}}{1+\tilde{A}}\right)^2\left[\frac{4}{\pi^2}u_{\tilde{B}\tilde{B}} + \frac{2}{\pi}\cos\left[\frac{2}{\pi}(\tilde{B}+1)\right]u_{\tilde{B}} + \frac{u_{\phi\phi}}{\sin^2\left[\frac{2}{\pi}(\tilde{B}+1)\right]}\right]. \quad (4.2)$$

4.2 Radially Symmetric Problems

4.2.1 Example of slow convergence: $u_{rr} + \frac{2}{r}u_r = f(r)$

Consider the following ordinary differential equation

$$u_{rr} + \frac{2}{r}u_r = (r^2-6)e^{-r^2}$$

with the following boundary conditions,

$$\left.\frac{du}{dr}\right|_{r=0} = 0, \text{ and}$$
$$u(r\to\infty) = 0.$$

Upon solving the above ODE analytically we find that the solution is

$$u(r) = e^{-r^2}.$$

By solving this linear ordinary differential equation using our Chebyshev pseudo-spectral method, we find that it does in fact show exponential convergence; however, the convergence rate is slow.The plot in Figure(B-12) compares the interpolated solution versus the exact solution. The plot in Figure(B-13) illustrates the exponential convergence achieved by the pseudo-spectral method. Note the error that was calculated is the sup norm of the difference between the interpolated and exact solution.

4.2.2 Example of fast convergence: $u_{rr} + \frac{2}{r}u_r = f(r)$

Consider the following ordinary differential equation

$$u_{rr} + \frac{2}{r}u_r = \frac{8r^2}{(1+r^2)^3} - \frac{6}{(1+r^2)^2}$$

with the following boundary conditions,

$$u(0) = 1, \text{ and}$$
$$u(r \to \infty) = 0.$$

Upon solving the above ODE analytically we find that the solution is

$$u(r) = \frac{1}{1+r^2}.$$

By solving this linear ordinary differential equation using our Chebyshev pseudo-spectral method, we find that it does in fact show exponential convergence. The plot in Figure(B-14) compares the interpolated solution and the exact solution.

The plot in Figure(B-15) illustrates the exponential convergence achieved by the pseudo-spectral method.Note the error that was calculated is the sup norm of the difference between the interpolated and exact solution.

In comparison with the previous example we note that the convergence rate is much faster in this case. This is because when compactifying the domain from $(0, \infty) \Rightarrow (-1, 1)$, we find that Chebyshev polynomials will be better for converging to the solution if the true solution algebraically goes to zero. In the first example, we find the solution decays exponentially whereas in the second example the true solution decays algebraically.

4.2.3 Example: $u_{rr} + \frac{2}{r}u_r + \frac{1}{1+u} = f(r)$

Consider the following ordinary differential equation

$$u_{rr} + \frac{2}{r}u_r + \frac{1}{1+u} = \frac{8r^2}{(1+r^2)^3} - \frac{6}{(1+r^2)^2} + \frac{1+r^2}{2+r^2}$$

with the following boundary condition,

$$u(r \to \infty) = 0.$$

Note that we will not explicitly impose a boundary condition at $r = 0$. Upon solving the above ODE analytically we find that the solution is

$$u(r) = \frac{1}{1 + r^2}.$$

By solving this nonlinear ordinary differential equation using our Chebyshev pseudo-spectral method, we find that it does in fact show exponential convergence. The plot in Figure(**??**) compares the interpolated solution versus the exact solution.

The plot in Figure(B-17) illustrates the exponential convergence achieved by the pseudo-spectral method. Note the error that was calculated is the sup norm of the difference between the interpolated and exact solution.

4.3 Axisymmetric Problems

4.3.1 Example of slow convergence: $u_{rr} + \frac{2}{r}u_r + \frac{1}{r^2}u_\theta + \frac{\cot\theta}{r^2}u_\theta = f(r, \theta)$

Consider the following ordinary differential equation

$$u_{rr} + \frac{2}{r}u_r + \frac{1}{r^2}u_\theta + \frac{\cot\theta}{r^2}u_\theta = 2e^{-r^2}r(2r^2 - 5)\cos\theta$$

with the following boundary conditions,

$$\begin{aligned} u(0, \theta) &= 0, \\ u(r \to \infty, \theta) &= 0, \\ u(r, 0) &= re^{-r^2}, \\ u(r, \pi) &= -re^{-r^2}. \end{aligned}$$

Upon solving the above PDE analytically we find that the solution is

$$u(r,\theta) = r\cos\theta e^{-r^2}.$$

By solving this linear partial differential equation using our Chebyshev pseudo-spectral method, we find that it does in fact show exponential convergence. The plot in Figure(B-18) compares the interpolated solution versus the exact solution.

The plot in Figure(B-19) illustrates the exponential convergence achieved by the pseudo-spectral method. Note the error that was calculated is the sup norm of the difference between the interpolated and exact solution.

4.3.2 Example of fast convergence: $u_{rr} + \frac{2}{r}u_r + \frac{1}{r^2}u_\theta + \frac{\cot\theta}{r^2}u_\theta = f(r,\theta)$

Consider the following ordinary differential equation

$$u_{rr} + \frac{2}{r}u_r + \frac{1}{r^2}u_\theta + \frac{\cot\theta}{r^2}u_\theta = \frac{-2r(r^2+5)\cos(\theta)\sin(\theta)}{(1+r^2)^3}$$

with the following boundary conditions,

$$\begin{aligned} &u(0,\theta) = 0,\\ &u(r\to\infty,\theta) = 0,\\ &\frac{\partial u}{\partial\theta}\Big|_{(r,0)} = 0,\\ &\frac{\partial u}{\partial\theta}\Big|_{(r,\pi)} = 0. \end{aligned}$$

The computational domain we consider is illustrated in Figure(B-20), where we enforce the appropriate boundary conditions.

Upon solving the above PDE analytically we find that the solution is

$$u(r,\theta) = \frac{r\cos\theta}{1+r^2}.$$

By solving this linear partial differential equation using our Chebyshev pseudo-spectral method, we find that it does in fact show exponential convergence. The plot found in Figure(B-21) compares the interpolated solution versus the exact solution.

The plot in Figure(B-22) illustrates the exponential convergence achieved by the pseudo-spectral method. Note the error that was calculated is the sup norm of the difference between the interpolated and exact solution.

In comparison with the previous example we note that the convergence rate is much faster in this case. This is because when compactifying the domain from $(0, \infty) \Rightarrow (-1, 1)$, we find that Chebyshev polynomials will be better for converging to the solution if the true solution algebraically goes to zero. In the first example, we find the solution decays exponentially whereas in the second example the true solution decays algebraically.

We can also choose to omit one of the boundary conditions in the r-direction, either at $r = 0$ or $r \to \infty$. We will show examples of doing so, specifically what boundary conditions we enforce, the computational grids, and the exponential convergence plots associated with each trial.

Omitting the Boundary Condition at $r = 0$.

If we omit the boundary condition at the origin, then the only boundary conditions we are enforcing are

$$u(r \to \infty, \theta) = 0.$$
$$\frac{\partial u}{\partial \theta}\Big|_{(r,0)} = 0,$$
$$\frac{\partial u}{\partial \theta}\Big|_{(r,\pi)} = 0.$$

The collocation grid is found in Figure(B-23). We find the exponential convergence to be the 2-cycle shown in Figure(B-24)

Omitting the Boundary Condition at $r \to \infty$.

If we omit the boundary condition at infinity, the only boundary conditions we enforce are

$$\begin{aligned} u(0,\theta) &= 0. \\ \left.\frac{\partial u}{\partial \theta}\right|_{(r,0)} &= 0, \\ \left.\frac{\partial u}{\partial \theta}\right|_{(r,\pi)} &= 0. \end{aligned}$$

The collocation grid is found in Figure(B-25).

We find the exponential convergence to be the 2-cycle shown in Figure(B-26).

4.3.3 Example: $u_{rr} + \frac{2}{r}u_r + \frac{1}{r^2}u_\theta + \frac{\cot\theta}{r^2}u_\theta + \frac{1}{1+u} = f(r,\theta)$

Consider the following partial differential equation

$$u_{rr} + \frac{2}{r}u_r + \frac{1}{r^2}u_\theta + \frac{\cot\theta}{r^2}u_\theta = \frac{-2r(r^2+5)\cos(\theta)\sin(\theta)}{(1+r^2)^3} + \frac{1+r^2}{1+r\cos\theta+r^2}$$

with the following boundary conditions,

$$\begin{aligned} u(r\to\infty,\theta) &= 0. \\ u(r,0) &= \frac{1}{1+r^2}, \\ u(r,\pi) &= \frac{-1}{1+r^2}. \end{aligned}$$

Note we do not explicitly impose a boundary condition at $r = 0$. The computational domain we consider is illustrated in Figure(B-27), where we enforce the appropriate boundary conditions.

Upon solving the above PDE analytically we find that the solution is

$$u(r,\theta) = \frac{r\cos\theta}{1+r^2}.$$

By solving this linear partial differential equation using our Chebyshev pseudo-spectral method, we find that it does in fact show exponential convergence. The plot in Figure(B-28) compares the interpolated solution versus the exact solution.

The plot found in Figure(B-29) illustrates the exponential convergence achieved by the pseudo-spectral method. Note the error that was calculated is the sup norm of the difference between the interpolated and exact solution.

Chapter 5

Initial Data for a Single Puncture

In this chapter we will discuss the initial data problem in numerical relativity for single black holes. First we will introduce the governing equations, then we will solve them using a pseudo-spectral method.

5.1 The Hamiltonian Constraint and The Momentum Constraint

The Hamiltonian constraint in Numerical Relativity is an elliptic equation for the scalar field, ψ,

$$\Delta\psi + \frac{1}{8}K^{ab}K_{ab}\psi^{-7} = 0. \tag{5.1}$$

The Momentum constraint in Numerical Relativity is an equation in terms of the extrinsic curvature, K_{ab},

$$\nabla_a K^{ab} = 0. \tag{5.2}$$

There are explicit solutions of Eq.(5.2) that characterize a single black hole with a given momentum, P^a, and spin, S^a. By letting n^a be the radial normal vector, ie-

$$n^a = \frac{x^a}{r},$$

the solution for K^{ab} is found to be:

$$K^{ab} = \frac{3}{r^2}\left(P^a n^b + P^b n^a - (g^{ab} - n^a n^b)P^c n_c\right) + \frac{3}{r^3}\left((\vec{S}\times\vec{n})^a n^b + (\vec{S}\times\vec{n})^b n^a\right), \quad (5.3)$$

where $g^{ab} = \delta_{ab}$, the Kronecker delta.

We will now examine two cases- one where there is spin aligning in only the x-direction with no momentum and one where there is only momentum in the x-direction but no spin. Note that in the following discussion we will use the following spherical coordinates:

$$\begin{aligned} x &= r\cos\theta, \\ y &= r\sin\theta\cos\phi, \\ z &= r\sin\theta\sin\phi. \end{aligned} \quad (5.4)$$

These coordinates are illustrated in Figure(B-30).

5.1.1 Single Puncture with Spin

In this section we will use equations Eq.(5.1) and Eq.(5.3) to derive the equation governing the initial puncture data for a black hole with spin, but no linear momentum. We let

$$\vec{S} = (S_x, 0, 0),$$

$$\vec{P} = (0, 0, 0),$$

$$\vec{n} = \left(\frac{x}{r}, \frac{y}{r}, \frac{z}{r}\right).$$

By using Eq.(5.3) we find that

$$K_{S_x} = \frac{3S_x}{r^5} \begin{pmatrix} 0 & -xz & xy \\ -xz & -2yz & y^2 - z^2 \\ xy & y^2 - z^2 & 2yz \end{pmatrix} \tag{5.5}$$

Now performing the contraction on the extrinsic curvature K_{S_x}, we find

$$K^{ab}_{S_x} K_{S_x ab} = \frac{18 S_x^2}{r^6} \sin^2 \theta. \tag{5.6}$$

Substituting Eq.(5.6) into Eq.(5.1) we find

$$\Delta \psi + \frac{9 S_x^2}{4 r^6} \sin^2 \theta \psi^{-7} = 0. \tag{5.7}$$

5.1.2 Single Puncture with Linear Momentum

In this section we will use equations Eq.(5.1) and Eq.(5.3) to derive the equation governing the initial puncture data for a black hole with linear momentum, but no spin. We let

$$\vec{S} = (0, 0, 0),$$

$$\vec{P} = (P_x, 0, 0),$$

$$\vec{n} = \left(\frac{x}{r}, \frac{y}{r}, \frac{z}{r} \right).$$

By using Eq.(5.3) we find that

$$K_{P_x} = \frac{3P_x}{2r^3} \begin{pmatrix} x + \frac{x^3}{r^2} & y + \frac{x^2 y}{r^2} & z + \frac{x^2 z}{r^2} \\ y + \frac{x^2 y}{r^2} & \frac{xy^2}{r^2} - x & \frac{xyz}{r^2} \\ z + \frac{x^2 z}{r^2} & \frac{xyz}{r^2} & \frac{xz^2}{r^2} - x \end{pmatrix} \tag{5.8}$$

Now performing the contraction on the extrinsic curvature K_{P_x}, we find

$$K_{P_x}^{ab} K_{P_x ab} = \frac{9P_x^2}{2r^4}\left(1 + 2\cos^2\theta\right). \tag{5.9}$$

Substituting Eq.(5.9) into Eq.(5.1) we find

$$\Delta\psi + \frac{9P_x^2}{16r^4}\left(1 + 2\cos^2\theta\right)\psi^{-7} = 0. \tag{5.10}$$

5.2 Computation for Single Puncture with Spin

We will start with the following equation,

$$\Delta\Psi + \frac{9S_x^2}{4r^6}\Psi^{-7}\sin^2\theta = 0, \tag{5.11}$$

which is in terms of the spherical coordinates defined in Eq.(5.4).

The solution for Ψ is known to be singular at the location of the black holes. To ensure that our numerical scheme will exhibit the proper convergence to the solution, we will break the solution into its singular part and an auxillary function, u. We proceed in doing so by re-defining the function Ψ,

$$\Psi = 1 + \frac{m}{2r} + u. \tag{5.12}$$

We can then substitute this definition of Ψ into Eq.(5.11) to obtain an equation in terms of u,

$$\Delta(1 + \frac{m}{2r} + u) = \Delta 1 + \Delta(\frac{m}{2r}) + \Delta u = \Delta u. \tag{5.13}$$

Note that $\Delta(\frac{m}{2r}) = 0$ because $\frac{1}{r}$ is an exact solution of the laplacian in spherical coordinates. We then are left to solve the following non-linear, elliptic PDE in terms of u,

$$\Delta u + \frac{9S_x^2}{4r^6}\frac{\sin^2\theta}{(1 + \frac{m}{2r} + u)^7} = 0. \tag{5.14}$$

Simplifying further we obtain,

$$\Delta u + \frac{9S_x^2}{4r^6}\frac{128\ r^7 \sin^2\theta}{(2r+m+2ru)^7} = 0, \tag{5.15}$$

and then

$$\Delta u + 288\ S_x^2\ r\ \ \sin^2\theta\ (2r+m+2ru)^{-7} = 0. \tag{5.16}$$

5.2.1 Comfactification: $(r,\theta,\phi) \rightarrow (\tilde{A},\tilde{B},\phi)$

In this section we will transform Eq.(5.14) from (r,θ,ϕ) to (A,θ,ϕ). The case when we consider a single puncture with linear momentum follows analogously.

First we use the Laplacian in the compactified coordinates, as described in Section(4.1). This transformation is necessary for two reasons. In the numerical sense, we must compactify R^3 into a computational box for our pseudo-spectral method to perform accurately.

The other reason is more profound because the solution for u is found to be C^2 at the puncture, the location of the black hole. This is illustrated in Appendix(5.2.4). To achieve exponential convergence to the solution from our spectral method, we need the solution to be C^∞ everywhere in the computational domain. We will use the following coordinate transformation render the puncture smooth,

$$\tilde{A} = 2\left[1+\frac{m}{2r}\right]^{-1} - 1, \tag{5.17}$$

which is the compactification transformation we used in Section(4.1). By solving for r, we find

$$r = \frac{m}{2}\left(\frac{1+\tilde{A}}{1-\tilde{A}}\right). \tag{5.18}$$

Hence, by substituting Eq.(5.18) into Eq.(5.14), we obtain

$$\Delta u = -\frac{9S_x^2}{4\left(\frac{m}{2}\left(\frac{1+\tilde{A}}{1-\tilde{A}}\right)\right)^6}\left(1+\left(\frac{1-\tilde{A}}{1+\tilde{A}}\right)+u\right)^{-7}\sin^2\theta = 0. \tag{5.19}$$

Simplifying the above expression further we see

$$\Delta u = -\frac{144S_x^2}{m^6}\,\frac{(1+\tilde{A})(1-\tilde{A})^6}{[(1-\tilde{A})+(1+\tilde{A})(1+u)]^7}\sin^2\theta \tag{5.20}$$

Now recall the Laplacian in the compactified coordinates of Section(4.1),

$$\begin{aligned}\Delta u = {} & \frac{1}{m^2}\left(1-\tilde{A}\right)^4 u_{\tilde{A}\tilde{A}} + \frac{2}{m^2}\frac{(1-\tilde{A})^4}{1+\tilde{A}}u_{\tilde{A}} \\ & + \frac{4}{m^2}\left(\frac{1-\tilde{A}}{1+\tilde{A}}\right)^2\left[\frac{4}{\pi^2}u_{\tilde{B}\tilde{B}} + \frac{2}{\pi}\cos\left[\frac{2}{\pi}(\tilde{B}+1)\right]u_{\tilde{B}} + \frac{u_{\phi\phi}}{\sin^2\left[\frac{2}{\pi}(\tilde{B}+1)\right]}\right].\end{aligned} \tag{5.21}$$

By putting Eq.(5.20) and Eq.(5.21) together, we see the equation we will be solving with our spectral scheme will be

$$\begin{aligned}&\left(1-\tilde{A}^2\right)^2 u_{\tilde{A}\tilde{A}} + 2(1-\tilde{A})^2(1+\tilde{A})u_{\tilde{A}} \\ &\qquad + 2\left[\frac{4}{\pi^2}u_{\tilde{B}\tilde{B}} + \frac{2}{\pi}\cos\left[\frac{2}{\pi}(\tilde{B}+1)\right]u_{\tilde{B}} + \frac{u_{\phi\phi}}{\sin^2\left[\frac{2}{\pi}(\tilde{B}+1)\right]}\right] \\ &\qquad\qquad = -144w^2\,\frac{(1+\tilde{A})^3(1-\tilde{A})^4}{[(1-\tilde{A})+(1+\tilde{A})(1+u)]^7}\sin^2\theta,\end{aligned} \tag{5.22}$$

where $w = \frac{S_x}{m^2}$.

5.2.2 Test Example: $\Delta u + \frac{9}{16r^6}\frac{\sin^2\theta}{\left(1+\frac{1}{r}+u\right)^7} = f(r,\theta,\phi)$

Before we solve the Single Puncture with Spin Initial Data PDE, we will consider the following partial differential equation, which takes a similar form to the Single

Puncture Initial data PDE but with a non-homogeneous term,

$$\Delta u + \frac{9}{16r^6}\frac{\sin^2\theta}{\left(1+\frac{1}{r}+u\right)^7} = -\frac{2r(r^2+5)\sin\theta\cos\phi}{(1+r^2)^3} + \frac{9\sin^2\theta}{16r^6\left(1+\frac{1}{r}+\frac{r\sin\theta\cos\phi}{1+r^2}\right)^7}$$

which we want to satisfy the following boundary condition,

$$u(r\to\infty,\theta) = 0.$$

Note that we do not explicitly impose boundary conditions at $r = 0, \theta = 0$, or $\theta = \pi$. In the ϕ direction we note periodicity is enforced by our choice of periodic basis functions. By solving the above PDE analytically we find that the solution is

$$u(r,\theta) = \frac{r\sin\theta\cos\phi}{1+r^2}.$$

Also, this PDE has the same non-linear term as the Single Puncture Initial Data PDE; however, it has been constructed so we know an exact solution to the problem. In solving this problem with our psuedo-spectral method, we assume a spectral solution of the form,

$$u(\tilde{A},\tilde{B},\phi) = \sum_{l=0}^{N_A}\sum_{m=0}^{N_B}\sum_{n=\frac{N_{phi}}{2}+1}^{n=\frac{N_{phi}}{2}-1}\tilde{u}_{lmn}T_l(\tilde{A})T_m(\tilde{B})e^{in\phi}.$$

Also we use the same compactification procedure as in Section(4.1). Note for this example, we consider the case when $m = 2$ and $S_x = 1$.

The plot in Figure(B-31) illustrates the exponential convergence achieved by the pseudo-spectral method. Note the error that was calculated is the absolute error of the Sup-Norm between the interpolated solution and the exact solution.

5.2.3 The Physical Problem: $\Delta u = -\frac{9}{4r^6}\frac{\sin^2\theta}{\left(1+\frac{m}{2r}+u\right)^7}$

Consider the following non-linear, elliptic PDE,

$$\Delta u = -\frac{9}{4r^6}\frac{\sin^2\theta}{\left(1+\frac{m}{2r}+u\right)^7},$$

with the following boundary condition,

$$u(r\to\infty,\theta)=0.$$

We will solve this using a pseudo-spectral method, assuming a spectral solution of the form,

$$u(\tilde{A},\tilde{B},\phi)=\sum_{l=0}^{N_A}\sum_{m=0}^{N_B}\sum_{n=\frac{N_{phi}}{2}+1}^{n=\frac{N_{phi}}{2}-1}\tilde{u}_{lmn}T_l(\tilde{A})T_m(\tilde{B})e^{in\phi}.$$

We then solved this PDE for the case when $w=\frac{S_x}{m^2}=0.2$. First we numerically solved this problem on a computational grid with $N=N_{\tilde{A}}=N_{\tilde{B}}=30$ points and $N_\phi=4$ points. Then we compared other cases in which we vary N. Upon doing so we obtain the convergence plot in Figure(B-32), which illustrates exponential convergence to the solution.

Hence, we find that our pseudo-spectral code can successfully solve the single puncture with spin initial data PDE.

5.2.4 Differentiability of u at $r=0$.

Recall Eq.(5.16):

$$\Delta u + 72\ S_x^2\ r\ sin^2\theta\ (2r+m+2ru)^{-7}=0.$$

Expanding the $\frac{r}{(2r+m+2ru)^{-7}}$ in a Machlaurin Series, we see

$$\Delta u + \frac{72\ S_x^2}{m^7}\ r\ sin^2\theta\ [1-\frac{14}{m}\ r\ (1+u)]+O(r^3)=0, \tag{5.23}$$

Hence, we see that the leading order term is

$$\Delta u + \beta r \sin^2\theta = 0, \tag{5.24}$$

where

$$\beta = \frac{72\ S_x^2}{m^7}.$$

We are interested in finding the leading term behavior of Eq.(5.24). Note: $r\sin^2\theta$ is continuous but not differentiable at $x = 0$. Therefore Δu is continuous but not differentiable and hence is C^2. Recall in spherical polar coordinates:

$$r\sin^2\theta = \frac{y^2+z^2}{\sqrt{x^2+y^2+z^2}}.$$

Therefore we have an equation of the form

$$\Delta u = r\sin^2\theta = \frac{y^2+z^2}{\sqrt{x^2+y^2+z^2}}.$$

By setting $x = 0$ we see that

$$\Delta u = \frac{y^2+z^2}{\sqrt{y^2+z^2}} = \sqrt{y^2+z^2}.$$

Hence, we verified that the above expression is differentiable but not continuous and hence $u \in C^2$.

5.3 Computation for Single Puncture with Linear Momentum

We will start with the following equation,

$$\Delta\Psi + \frac{9P_x^2}{16r^4}\Psi^{-7}\left(1 + 2\cos^2\theta\right) = 0, \tag{5.25}$$

in terms of the spherical coordinates defined in Eq.(5.4). The solution for Ψ is known to be singular at the location of the black holes. To ensure that our numerical scheme will exhibit the proper convergence to the solution, we will break the solution into a singular part. We proceed in doing so by re-defining the function Ψ,

$$\Psi = 1 + \frac{m}{2r} + u. \tag{5.26}$$

We can then substitute this definition of Ψ into Eq.(5.11) to obtain an equation in terms of u,

$$\Delta(1 + \frac{m}{2r} + u) = \Delta 1 + \Delta(\frac{m}{2r}) + \Delta u = \Delta u. \tag{5.27}$$

Note that $\Delta(\frac{m}{2r}) = 0$ because $\frac{1}{r}$ is an exact solution of the laplacian in spherical coordinates. We then are left to solve the following non-linear, elliptic PDE in terms of u,

$$\Delta u + \frac{9P_x^2}{16r^4}\frac{1 + 2\cos^2\theta}{(1 + \frac{m}{2r} + u)^7} = 0. \tag{5.28}$$

5.3.1 Comfactification: $(r, \theta, \phi) \rightarrow (\tilde{A}, \tilde{B}, \phi)$

In this section we will transform Eq.(5.28) from (r,θ,ϕ) to (A,θ,ϕ). First we use the Laplacian in the compactified coordinates, as described in Section(4.1). This transformation is necessary for two reasons. In the numerical sense, we must compactify R^3 into a computational box for our pseudo-spectral method to perform accurately.

The other reason is more profound because the solution for u is found to be C^2 at the puncture, the location of the black hole. To achieve exponential convergence to the solution from our spectral method, we need the solution to be C^∞ everywhere in the computational domain. The same coordinate transformation, Eq.(5.17), from Section(5.2.1) will be used to render the puncture smooth.

Hence, by substituting Eq.(5.18) into Eq.(5.28), we obtain

$$\Delta u = -\frac{9P_x^2}{16\left(\frac{m}{2}\left(\frac{1+\tilde{A}}{1-\tilde{A}}\right)\right)^4}\left(1 + \left(\frac{1-\tilde{A}}{1+\tilde{A}}\right) + u\right)^{-7}\left(1 + 2\cos^2\theta\right) = 0. \tag{5.29}$$

Simplifying the above expression further we see

$$\Delta u = -\frac{9P_x^2}{m^4}\ \frac{(1+\tilde{A})^3(1-\tilde{A})^4}{[(1-\tilde{A})+(1+\tilde{A})(1+u)]^7}\left(1+2\cos^2\theta\right). \tag{5.30}$$

Now recall the Laplacian in the compactified coordinates of Section(4.1),

$$\begin{aligned}\Delta u = &\frac{1}{m^2}\left(1-\tilde{A}\right)^4 u_{\tilde{A}\tilde{A}} + \frac{2}{m^2}\frac{(1-\tilde{A})^4}{1+\tilde{A}}u_{\tilde{A}} \\ &+ \frac{4}{m^2}\left(\frac{1-\tilde{A}}{1+\tilde{A}}\right)^2\left[\frac{4}{\pi^2}u_{\tilde{B}\tilde{B}} + \frac{2}{\pi}\cos\left[\frac{2}{\pi}(\tilde{B}+1)\right]u_{\tilde{B}} + \frac{u_{\phi\phi}}{\sin^2\left[\frac{2}{\pi}(\tilde{B}+1)\right]}\right].\end{aligned} \tag{5.31}$$

By putting Eq.(5.30) and Eq.(5.31) together, we see the equation we will be solving with our spectral scheme will be

$$\begin{aligned}&\left(1-\tilde{A}^2\right)^2 u_{\tilde{A}\tilde{A}} + 2(1-\tilde{A})^2(1+\tilde{A})u_{\tilde{A}} \\ &\qquad + 2\left[\frac{4}{\pi^2}u_{\tilde{B}\tilde{B}} + \frac{2}{\pi}\cos\left[\frac{2}{\pi}(\tilde{B}+1)\right]u_{\tilde{B}} + \frac{u_{\phi\phi}}{\sin^2\left[\frac{2}{\pi}(\tilde{B}+1)\right]}\right] \\ &\qquad\qquad = -9w^2\ \frac{(1+\tilde{A})^5(1-\tilde{A})^3}{[(1-\tilde{A})+(1+\tilde{A})(1+u)]^7}\left(1+2\cos^2\theta\right),\end{aligned} \tag{5.32}$$

where $w = \frac{P_x}{m}$.

5.3.2 The Physical Problem: $\Delta u = -\frac{9}{16r^4}\frac{1+2\cos^2\theta}{\left(1+\frac{m}{2r}+u\right)^7}$

Consider the following non-linear, elliptic PDE,

$$\Delta u = -\frac{9}{16r^4}\frac{1+2\cos^2\theta}{\left(1+\frac{m}{2r}+u\right)^7},$$

with the following boundary condition,

$$u(r\to\infty,\theta) = 0.$$

We will solve this using a pseudo-spectral method, assuming a spectral solution of the form,

$$u(\tilde{A},\tilde{B},\phi)=\sum_{l=0}^{N_A}\sum_{m=0}^{N_B}\sum_{n=\frac{N_{phi}}{2}+1}^{n=\frac{N_{phi}}{2}-1}\tilde{u}_{lmn}T_l(\tilde{A})T_m(\tilde{B})e^{in\phi}.$$

We then solved this PDE for the case when $w=\frac{P_x}{m}=0.2$. First we numerically solved this problem on a computational grid with $N=N_{\tilde{A}}=N_{\tilde{B}}=40$ points and $N_\phi=4$ points. Then we compared other cases in which we vary N. Upon doing so we obtain the convergence plot in Figure(B-33), which illustrates exponential convergence to the solution.

Chapter 6

Initial Data For Two Punctures

In this chapter we will discuss the initial data problem in numerical relativity for binary black hole systems. First we will introduce the governing equations. Next we will explain the compactification scheme and then will solve the initial data PDEs using a pseudo-spectral method.

6.1 The Hamiltonian Constraint and The Momentum Constraint

Unlike the single black hole initial data problem, we now have two singularities located at $x = \pm b$, instead of one singular point at the origin. However, the governing equation for the initial space-time still takes the form of the elliptic equation described in, Eq.(5.1),

$$\Delta\psi + \frac{1}{8}K^{ab}K_{ab}\psi^{-7} = 0.$$

By using the Momentum Constraint, which is expressed in Eq.(5.2), we find that the explicit solutions, K^{ab}, that characterize a binary black hole system are given in terms of the momentums, P_1^a and P_2^a, and spins, S_1^a and S_2^a, where the subscript differentiates the black hole's and the superscript denotes which respective component of linear momentum or spin. By letting n_1^a and n_2^a be the radial normal vectors of

each black hole, ie-

$$n_1^a = \frac{x_1^a}{r_1} \qquad \text{and} \qquad n_2^a = \frac{x_2^a}{r_2},$$

the solution is found to be:

$$K^{ab} = \frac{3}{r_1^2}\left(P_1^a n_1^b + P_1^b n_1^a - (g^{ab} - n_1^a n_1^b)P_1^c n_c^1\right) + \frac{3}{r_1^3}\left((\vec{S_1} \times \vec{n_1})^a n_1^b + (\vec{S_1} \times \vec{n_1})^b n_1^a\right) + \frac{3}{r_2^2}\left(P_2^a n_2^b + P_2^b n_2^a - (g^{ab} - n_2^a n_2^b)P_2^c n_c^2\right) + \frac{3}{r_2^3}\left((\vec{S_2} \times \vec{n_2})^a n_2^b + (\vec{S_2} \times \vec{n_2})^b n_2^a\right) \quad (6.1)$$

where $g^{ab} = \delta_{ab}$, the Kronecker delta.

We examine multiple cases, where there is spin and momentum in only the x-direction for each black hole, giving rise to axisymmetric systems, as well as various combinations of other spins and momentums for each black hole.

Before we introduce each initial puncture data PDE, we will give a detailed description of the compactification scheme we will use for our pseudo-spectral method. As in the singular case, each black hole will give rise to another singular point in the domain; however, rather than only having to work with one singular point, there are two in the binary case. We will assume that the black holes are located at $x = \pm b$.

The distances to each puncture will be described as,

$$r_1 = \sqrt{(x+b)^2 + y^2 + z^2} \qquad \text{and} \qquad r_2 = \sqrt{(x-b)^2 + y^2 + z^2}. \quad (6.2)$$

6.2 Compactification and Numerical Setup

In this section we will discuss the numerical setup of the initial puncture data problem for two black holes. We will see that rather than numerically solving for the scalar field,ψ, we will solve the PDE in terms of a function u. Also we will discuss an elaborate series of coordinate transformations used to compactify R^3 into a rectangular box, in hopes of rendering the punctures smooth to achieve exponential convergence to the correct solution.

6.2.1 The Auxiliary Function u

We will start with the general form of an elliptic equation,

$$\Delta\psi = f(\psi), \tag{6.3}$$

where we will assume the potentially nonlinear term, $f(\psi)$, takes on a form corresponding to an initial puncture equation for two black holes. As in the single puncture case, the solution for ψ is known to be singular at the location of each black hole. To ensure that our numerical scheme achieves the maximum convergence rate possible to the solution, we will deconstruct ψ into its singular part and nonsingular counterpart. We do this by defining ψ to be

$$\psi = 1 + \frac{m_1}{2r_1} + \frac{m_2}{2r_2} + u, \tag{6.4}$$

where the terms $\frac{m_i}{2r_i}$ take care of the singular part. Substituting this definition of ψ into Eq.(6.3), we obtain an equation in terms of the auxiliary function u, ie-

$$\Delta\psi\Delta\left(1 + \frac{m_1}{2r_1} + \frac{m_2}{2r_2} + u\right) = \Delta 1 + \Delta\left(\frac{m_1}{2r_1}\right) + \Delta\left(\frac{m_2}{2r_2}\right) + \Delta u = \Delta u.$$

Hence, we will be left to solve the nonlinear, elliptic initial puncture data PDEs in terms of the auxiliary function u.

6.2.2 Compactification for Binary Black Holes

In this section we will describe the compacfication scheme for the initial data problem of binary black holes. Compared to the compactification for the single puncture case, it is much less self-explanatory. Recall that for the single black hole system, the compactification consisted of going from spherical coordinates describing all of R^3 to a compact box by use of the single coordinate transformation,

$$\tilde{A} = 2\left[1 + \frac{m}{2r}\right]^{-1} - 1.$$

We will follow the same compactification approach as in [1]. In their approach, they use multiple transformations to get from the cartesian coordinates, x,y and z, to the compactified coordinates, $A, \tilde{B}$, and ϕ, where

$$\begin{aligned} A &\in [0,1], \\ \tilde{B} &\in [-1,1], \\ \phi &\in [-\pi,\pi) \end{aligned}$$

To obtain to the compactified coordinates, we will perform the following series of transformations:

$$(x,y,z) \to (x,\rho,\phi) \to (X,R,\phi) \to (\xi,\eta,\phi) \to (A,\tilde{B},\phi).$$

These coordinate transformations will allow us to achieve regularity at both of the punctures as well as compactifying R^3 into a compact rectangular domain. Regularity at both of the punctures in the compactified coordinates will allow our pseudo-spectral method to exhibit exponential convergence to the solution.

First we consider the following cylindrical coordinates, (x,ρ,ϕ),

$$y = \rho\cos\phi, \quad z = \rho\sin\phi, \quad \text{where} \quad \phi \in [-\pi,\pi).$$

Now we will form the complex variable c,

$$c = x + i\rho. \tag{6.5}$$

Now consider the Joukowsky mapping,

$$c = \frac{b}{2}\left(C + C^{-1}\right), \tag{6.6}$$

where $C = X + iR$. Note that the punctures are located at $C = \pm 1$, or $c = \pm b$. The key idea behind the Joukowsky transformation is that it will map lines to circles.

In our case, it will map the line between the two punctures, from $c = x = -b$ to $c = x = b$, to a unit circle in the coordinates (X, R).

Before we compactify into a rectangular box, we consider the following polar transformation,

$$C = e^{\zeta}, \quad \text{where} \;\; \zeta = \xi + \eta, \tag{6.7}$$

and $\xi \in [0, \infty)$ and $\eta \in [0, \pi]$. This transformation yields an infinite strip with respect to positive ξ -values. Now if we write c in terms of this polar transformation we find that

$$c = \frac{b}{2}\left(C + C^{-1}\right) = b\left[\frac{e^{\zeta} + e^{-\zeta}}{2}\right] = b\cosh\zeta. \tag{6.8}$$

By using Eq.(6.8) above we can recover the transformation from our original cylindrical coordinates,

$$\begin{aligned} x &= Re\left[\cosh\left(\xi + i\eta\right)\right] \\ &= b\; Re\left[\cosh(\xi)\cosh(i\eta) + i\sinh(\xi)\sinh(i\eta)\right] \\ &= b\cosh(\xi)\cos(\eta). \end{aligned} \tag{6.9}$$

Similarly we obtain the following definition of ρ,

$$\begin{aligned} \rho &= Im\left[\cosh\left(\xi + i\eta\right)\right] \\ &= b\; Im\left[\cosh(\xi)\cosh(i\eta) + i\sinh(\xi)\sinh(i\eta)\right] \\ &= b\sinh(\xi)\sin(\eta). \end{aligned} \tag{6.10}$$

The definitions listed above for x and ρ, in Eq.(6.9) and Eq.(6.10) respectively, map the prolate spheroidal coordinates (ξ, η) onto the cylindrical coordinates (x, ρ). Note that constant values of ξ correspond to confocal ellipses, and constant $\eta-$values correspond to confocal hyperbolas in the (x, ρ) plane. The focal points are located at the two punctures, at $(0, 0)$ and $(0, \pi)$. Now we need to compactify to a rectangular box in order to use our single-domain pseudo-spectral method to solve the PDE. The

compacfication scheme we will use is

$$\xi = 2\,\mathrm{arctanh} A, \tag{6.11}$$

$$\eta = \frac{\pi}{2} + 2\arctan\tilde{B}. \tag{6.12}$$

Note that the inverse hyperbolic tangent is defined between $[-1,1]$ and is unbounded. By using Eq.(6.11), we will be able to compactify $\xi \in [0,\infty)$ to $A \in [0,1]$. By using Eq.(6.12) we are able to compactify $\eta \in [0,\pi]$ to $\tilde{B} \in [-1,1]$.

In these coordinates the two black holes get mapped to corners of a rectangle in the $(A,\tilde{B})$ compactified coordinates. By using Eq.(6.7), we find the black hole located at $C=1$ gets mapped to $(\xi,\eta)=(0,0)$. Then using the transformations Eq.(6.11) and Eq.(6.12), we see that black hole gets mapped to $(A,\tilde{B},\phi)=(0,-1,\phi)$. Similarly we find the other black hole at $C=-1$ gets mapped to $(A,\tilde{B},\phi)=(0,1,\phi)$. Moreover the line connecting the black holes gets mapped to the $A=0$ face. Note that because of this, the numerical solution we obtain must obey the following symmetry relation,

$$u(A=0,\tilde{B},\phi) = u(A=0,\tilde{B}).$$

By putting all these transformations together, we recover the following mappings from the compactified coordinates $(A,\tilde{B},\phi)$ to the cartesian coordinates (x,y,z),

$$x = b\,\frac{A^2+1}{A^2-1}\,\frac{2\tilde{B}}{1+\tilde{B}^2}, \tag{6.13}$$

$$y = b\,\frac{2A}{1-A^2}\,\frac{1-\tilde{B}^2}{1+\tilde{B}^2}\cos\phi, \tag{6.14}$$

$$z = b\,\frac{2A}{1-A^2}\,\frac{1-\tilde{B}^2}{1+\tilde{B}^2}\sin\phi. \tag{6.15}$$

By using this compactification scheme, we will be able to use a single-domain pseudo-spectral method. Note that in the actual code we perform one more linear transformation on A to compactify from $A \in [0,1]$ to $\tilde{A} \in [-1,1]$. We do this for simplicity in that the Chebyshev polynomials are defined on $[-1,1]$.

We will now find the Laplacian in these compactified coordinates, $(A,\tilde{B},\phi)$.

6.2.3 Laplacian in Compactified Coordinates

By using Eqs.(6.13), (6.14), and (6.15), we will find the Laplacian in the compactified coordinates. Because the coordinates x,y, and z are not functions themselves of any single coordinate, A, $\tilde{B}$, or ϕ, we will use a Jacobian matrix approach to find the necessary partial derivatives in formulating the Laplacian.

Recall that the Laplacian in cartesian coordinates is

$$\Delta u = \frac{\partial^2 u}{\partial x^2} + \frac{\partial^2 u}{\partial y^2} + \frac{\partial^2 u}{\partial z^2}.$$

Before we can compute the 2^{nd} derivative of u in these coordinates, we will have to find its 1^{st} derivatives, ie-

$$u_x(A, \tilde{B}, \phi) = \frac{\partial u}{\partial x} = \frac{\partial u}{\partial A}\frac{\partial A}{\partial x} + \frac{\partial u}{\partial \tilde{B}}\frac{\partial \tilde{B}}{\partial x} + \frac{\partial u}{\partial \phi}\frac{\partial \phi}{\partial x}. \tag{6.16}$$

However, we do not have any explicit formulas at this point to compute these partial derivatives. The equations for $\frac{\partial u}{\partial y}$ and $\frac{\partial u}{\partial z}$ are similar. We will find all these partial derivatives now.

First we begin by considering a differential change in x,

$$dx = \frac{\partial x}{\partial A}dA + \frac{\partial x}{\partial \tilde{B}}d\tilde{B} + \frac{\partial x}{\partial \phi}d\phi. \tag{6.17}$$

The above equation allows us to see how x changes infinitesimally with any infinitesimal changes to $A, \tilde{B}$, or ϕ. Analogously, we obtain the following equations when considering infinitesimal changes to y and z,

$$dy = \frac{\partial y}{\partial A}dA + \frac{\partial y}{\partial \tilde{B}}d\tilde{B} + \frac{\partial y}{\partial \phi}d\phi, \tag{6.18}$$

$$dz = \frac{\partial z}{\partial A}dA + \frac{\partial z}{\partial \tilde{B}}d\tilde{B} + \frac{\partial z}{\partial \phi}d\phi. \tag{6.19}$$

We can write Eqs.(6.17), (6.18), and (6.19) more compactly in the following matrix

system:

$$\begin{bmatrix} \mathrm{dx} \\ \mathrm{dy} \\ \mathrm{dz} \end{bmatrix} = \begin{bmatrix} x_A & x_{\tilde{B}} & x_\phi \\ y_A & y_{\tilde{B}} & y_\phi \\ z_A & z_{\tilde{B}} & z_\phi \end{bmatrix} \begin{bmatrix} \mathrm{dA} \\ d\tilde{B} \\ \mathrm{d}\phi \end{bmatrix} \tag{6.20}$$

The matrix in the above system is the Jacobian matrix for the coordinates x,y, and z. Now we can use Cramer's Rule to find $\frac{\partial A}{\partial x}$, $\frac{\partial A}{\partial y}$, and $\frac{\partial A}{\partial z}$, as well as all other necessary partial derivatives, ie-

$$\begin{aligned} \frac{\partial A}{\partial x} &= \frac{y_{\tilde{B}} z_\phi - z_{\tilde{B}} y_\phi}{|J|}, \\ \frac{\partial A}{\partial y} &= \frac{x_{\tilde{B}} z_\phi - z_{\tilde{B}} x_\phi}{|J|}, \\ \frac{\partial A}{\partial z} &= \frac{x_{\tilde{B}} y_\phi - y_{\tilde{B}} x_\phi}{|J|}, \end{aligned}$$

where $|J|$ is the determinant of the Jacobian matrix from Eq.(6.20). By substituting the above partial derivatives into *Eq.*(6.16), we now we have $\frac{\partial u}{\partial x}$. We also find $\frac{\partial u}{\partial y}$ and $\frac{\partial u}{\partial z}$ in a completely analogous way.

To find the second partial derivatives, we note that the partial derivative operators in these coordinates are defined as

$$\begin{aligned} \frac{\partial}{\partial x} &= A_x \frac{\partial}{\partial A} + \tilde{B}_x \frac{\partial}{\partial \tilde{B}} + \phi_x \frac{\partial}{\partial \phi} \\ \frac{\partial}{\partial y} &= A_y \frac{\partial}{\partial A} + \tilde{B}_y \frac{\partial}{\partial \tilde{B}} + \phi_y \frac{\partial}{\partial \phi} \\ \frac{\partial}{\partial z} &= A_z \frac{\partial}{\partial A} + \tilde{B}_z \frac{\partial}{\partial \tilde{B}} + \phi_z \frac{\partial}{\partial \phi} \end{aligned} \tag{6.21}$$

Now we can find the second partials needed for the Laplacian, using Eq.(6.21), ie-

$$\frac{\partial^2 u}{\partial x^2} = \frac{\partial}{\partial x} u_x(A, \tilde{B}, \phi) = \left(A_x \, \frac{\partial}{\partial A} + \tilde{B}_x \, \frac{\partial}{\partial \tilde{B}} + \phi_x \, \frac{\partial}{\partial \phi} \right) u_x(A, \tilde{B}, \phi),$$

$$\frac{\partial^2 u}{\partial y^2} = \frac{\partial}{\partial y} u_y(A, \tilde{B}, \phi) = \left(A_y \, \frac{\partial}{\partial A} + \tilde{B}_y \, \frac{\partial}{\partial \tilde{B}} + \phi_y \, \frac{\partial}{\partial \phi} \right) u_y(A, \tilde{B}, \phi), \tag{6.22}$$

$$\frac{\partial^2 u}{\partial z^2} = \frac{\partial}{\partial z} u_z(A, \tilde{B}, \phi) = \left(A_z \, \frac{\partial}{\partial A} + \tilde{B}_z \, \frac{\partial}{\partial \tilde{B}} + \phi_z \, \frac{\partial}{\partial \phi} \right) u_z(A, \tilde{B}, \phi),$$

Upon simplifying Eq.(6.22), we find the Laplacian can be written in the following form:

$$\Delta u = \frac{\partial^2 u}{\partial x^2} + \frac{\partial^2 u}{\partial y^2} + \frac{\partial^2 u}{\partial z^2} = \gamma^{AA} \, u_{AA} + \gamma^{A} \, u_A + \gamma^{\tilde{B}\tilde{B}} \, u_{\tilde{B}\tilde{B}} + \gamma^{\tilde{B}} \, u_{\tilde{B}} + \gamma^{\phi\phi} \, u_{\phi\phi}, \tag{6.23}$$

where the coefficients are found to be:

$$\gamma^{AA} = \frac{(-1 + A^2)^4 \, (1 + \tilde{B}^2)^2}{4b^2 \, \left[(1 + A^4)(-1 + \tilde{B}^2)^2 + 2A^2(1 + 6\tilde{B}^2 + \tilde{B}^4) \right]}, \tag{6.24}$$

$$\gamma^{A} = \frac{(-1 + A^2)^4 \, (1 + \tilde{B}^2)^2}{4Ab^2 \, \left[(1 + A^4)(-1 + \tilde{B}^2)^2 + 2A^2(1 + 6\tilde{B}^2 + \tilde{B}^4) \right]}, \tag{6.25}$$

$$\gamma^{\tilde{B}\tilde{B}} = \frac{(-1 + A^2)^2 \, (1 + \tilde{B}^2)^4}{4b^2 \, \left[(1 + A^4)(-1 + \tilde{B}^2)^2 + 2A^2(1 + 6\tilde{B}^2 + \tilde{B}^4) \right]}, \tag{6.26}$$

$$\gamma^{\tilde{B}} = \frac{(-1 + A^2)^2 \, \tilde{B} \, (1 + \tilde{B}^2)^4}{2b^2(-1 + \tilde{B}^2) \left[(1 + A^4)(-1 + \tilde{B}^2)^2 + 2A^2(1 + 6\tilde{B}^2 + \tilde{B}^4) \right]}, \tag{6.27}$$

$$\gamma^{\phi\phi} = \frac{(-1 + A^2)^2 \, (1 + \tilde{B}^2)^2}{4A^2 b^2 \, (-1 + \tilde{B}^2)^2}. \tag{6.28}$$

6.3 Binary Punctures with S_{1_x} and S_{2_x}

In this section we will use Eqs.(5.1) and (6.1) to derive the governing initial puncture data equation for two black holes with spins only in the x-direction. This leads to an axisymmetric system. We let

$$\begin{aligned} \vec{S}_1 &= (S_{1_x}, 0, 0) \qquad \text{and} \qquad \vec{P}_1 = (0, 0, 0), \\ \vec{S}_2 &= (S_{2_x}, 0, 0) \qquad \text{and} \qquad \vec{P}_2 = (0, 0, 0). \end{aligned}$$

By using Eq.(6.1) we find that

$$K_{ab} = \begin{pmatrix} 0 & \left(-\frac{3\mathrm{Sx}_1 x_1 z}{r_1^5} - \frac{3\mathrm{Sx}_2 x_2 z}{r_2^5}\right)^2 & \left(\frac{3\mathrm{Sx}_1 x_1 y}{r_1^5} + \frac{3\mathrm{Sx}_2 x_2 y}{r_2^5}\right)^2 \\ \left(-\frac{3\mathrm{Sx}_1 x_1 z}{r_1^5} - \frac{3\mathrm{Sx}_2 x_2 z}{r_2^5}\right)^2 & \left(-\frac{6\mathrm{Sx}_1 yz}{r_1^5} - \frac{6\mathrm{Sx}_2 yz}{r_2^5}\right)^2 & \left(\frac{3Sx_1(y^2-z^2)}{r_1^5} + \frac{3Sx_2(y^2-z^2)}{r_2^5}\right)^2 \\ \left(\frac{3\mathrm{Sx}_1 x_1 y}{r_1^5} + \frac{3\mathrm{Sx}_2 x_2 y}{r_2^5}\right)^2 & \left(\frac{3Sx_1(y^2-z^2)}{r_1^5} + \frac{3Sx_2(y^2-z^2)}{r_2^5}\right)^2 & \left(\frac{6\mathrm{Sx}_1 yz}{r_1^5} + \frac{6\mathrm{Sx}_2 yz}{r_2^5}\right)^2 \end{pmatrix} \tag{6.29}$$

Now performing the contraction on the extrinsic curavture, K_{ab}, we obtain

$$\begin{aligned} K^{ab}K_{ab} = \frac{18}{r_1^{10} r_2^{10}} \Big[& r_2^{10}\mathrm{Sx}_1^2 \left(y_1^2 + z_1^2\right)\left(x_1^2 + y_1^2 + z_1^2\right) + r_1^{10}\mathrm{Sx}_2^2 \left(y_2^2 + z_2^2\right)\left(x_2^2 + y_2^2 + z_2^2\right) \\ & + 2r_1^5 r_2^5 \mathrm{Sx}_1 \mathrm{Sx}_2 \left(4y_1 y_2 z_1 z_2 + x_1 x_2 \left(y_1 y_2 + z_1 z_2\right) + y_1^2\left(y_2^2 - z_2^2\right) + z_1^2\left(-y_2^2 + z_2^2\right)\right) \Big], \end{aligned} \tag{6.30}$$

where x,y, and z are the coordinates definitions derived in Section(6.2.2). Note that $x_1 = x + b,\ x_2 = x - b,\ y_1 = y_2$, and $z_1 = z_2$ because both black holes are located at $x = \pm b$.

Upon substituting Eq.(6.30) into Eq.(5.1), we find

$$\Delta\psi = \frac{9}{4\psi^7 r_1^{10} r_2^{10}}\Bigg[\left(r_2^{10} r_1^2 \mathrm{Sx}_1^2 + r_1^{10} r_2^2 \mathrm{Sx}_2^2\right)\left(y^2+z^2\right) + 2r_1^5 r_2^5 \mathrm{Sx}_1\mathrm{Sx}_2\left(y^4+2y^2z^2+z^4+x_1x_2\left(y^2+z^2\right)\right)\Bigg]. \quad (6.31)$$

Finally, substituting Eq.(6.4) into Eq.(6.31), we obtain

$$\Delta u = \frac{9}{4r_1^{10} r_2^{10}\left(1+\frac{m_1}{2r_1}+\frac{m_2}{2r_2}+u\right)^7}\Bigg[\left(r_2^{10} r_1^2 \mathrm{Sx}_1^2 + r_1^{10} r_2^2 \mathrm{Sx}_2^2\right)\left(y^2+z^2\right) + 2r_1^5 r_2^5 \mathrm{Sx}_1\mathrm{Sx}_2\left(y^4+2y^2z^2+z^4+x_1x_2\left(y^2+z^2\right)\right)\Bigg], \quad (6.32)$$

which is the equation we will numerically solve using our pseudo-spectral scheme. Note that in Eq.(6.32), we use the Laplacian operator derived in Section(6.2.3).

6.3.1 Computation of Binary Punctures with S_{1_x} and S_{2_x}

Consider the following non-linear, elliptic PDE,

$$\Delta u = \frac{9}{4r_1^{10} r_2^{10}\left(1+\frac{m_1}{2r_1}+\frac{m_2}{2r_2}+u\right)^7}\Bigg[\left(r_2^{10} r_1^2 \mathrm{Sx}_1^2 + r_1^{10} r_2^2 \mathrm{Sx}_2^2\right)\left(y^2+z^2\right) + 2r_1^5 r_2^5 \mathrm{Sx}_1\mathrm{Sx}_2\left(y^4+2y^2z^2+z^4+x_1x_2\left(y^2+z^2\right)\right)\Bigg],$$

with the following bounary condition

$$u(r\to\infty,\theta,\phi) = 0.$$

We will solve this using a pseudo-spectral method, assuming a spectral solution

with the following form,

$$u(\tilde{A},\tilde{B},\phi)=\sum_{l=0}^{N_A}\sum_{m=0}^{N_B}\sum_{n=\frac{N_{phi}}{2}+1}^{n=\frac{N_{phi}}{2}-1}\tilde{u}_{lmn}T_l(\tilde{A})T_m(\tilde{B})e^{in\phi}.$$

We will solve this equation in the cases when $b=0.5$ and

1. $S_{1_x}=S_{2_x}=1$
2. $S_{1_x}=1, S_{2_x}=0.5$
3. $S_{1_x}=1, S_{2_x}=0.05$

These cases will illustrate the flexibility of the numerical method for black holes with spins of different magnitude.

In each case we show it's respective convergence plot, where we assume the exact solution is a numerical spectral solution with $N=N_{\tilde{A}}=N_{\tilde{B}}=60$ and $N_\phi=4$. We then compare cases for $N<60$ to that spectral solution.

Also to illustrate that this solution obeys the constraints imposed by the compactification, we show plots of the $\tilde{A}=-1$ face, the line connecting the black holes. For our numerical solution to remain plausible, we need to see symmetry in the ϕ coordinate. That is, the numerical spectral solution for u must satisfy the following relation on the $\tilde{A}=-1$ face,

$$u(-1,\tilde{B},\phi)=u(-1,\tilde{B}).$$

The plots associated with the first case of $S_{x_1}=S_{x_2}=1$ are found in Figures(B-34) and (B-35).

The plots associated with the case of $S_{x_1}=1, S_{x_2}=0.5$ are found in Figures(B-36) and (B-37).

The plots associated with the case of $S_{x_1}=1, S_{x_2}=0.05$ are found in Figures(B-38) and (B-39).

6.4 Binary Punctures with P_{1_x} and P_{2_x}

In this section we will use Eqs.(5.1) and (6.1) to derive the governing initial puncture data equation for two black holes with linear momentum only in the x-direction. This leads to an axisymmetric system. We let

$$\begin{aligned} \vec{S}_1 &= (0,0,0) \qquad \text{and} \qquad \vec{P}_1 = (P_{1_x},0,0), \\ \vec{S}_2 &= (0,0,0) \qquad \text{and} \qquad \vec{P}_2 = (P_{2_x},0,0). \end{aligned}$$

By using Eq.(6.1) we can find the extrinsic curvature, K_{ab}. Now performing the contraction on the extrinsic curavture, K_{ab}, we obtain

$$\begin{aligned} K^{ab}K_{ab} = \frac{9}{4}\Bigg[& \frac{\left(\mathrm{Px_1} r_2^5 x_1 \left(r_1^2 + x_1^2\right) + \mathrm{Px_2} r_1^5 x_2 \left(r_2^2 + x_2^2\right)\right)^2}{r_1^{10} r_2^{10}} \\ & + \frac{2(y^2+z^2)\left(\mathrm{Px_1} r_2^5 \left(r_1^2 + x_1^2\right) + \mathrm{Px_2} r_1^5 \left(r_2^2 + x_2^2\right)\right)^2}{r_1^{10} r_2^{10}} \\ & + \left(\frac{\mathrm{Px_1} x_1 \left(r_1^2 - y^2\right)}{r_1^5} + \frac{\mathrm{Px_2} x_2 \left(r_2^2 - y^2\right)}{r_2^5}\right)^2 \\ & + \left(\frac{\mathrm{Px_1} x_1 \left(r_1^2 - z^2\right)}{r_1^5} + \frac{\mathrm{Px_2} x_2 \left(r_2^2 - z^2\right)}{r_2^5}\right)^2 \\ & + 2\left(\frac{\mathrm{Px_1} x_1 yz}{r_1^5} + \frac{\mathrm{Px_2} x_2 yz}{r_2^5}\right)^2 \Bigg], \end{aligned} \tag{6.33}$$

where x,y, and z are the coordinates definitions derived in Section(6.2.2), and $x_1 = x + b,\ x_2 = x - b,\ y = y_1 = y_2$, and $z = z_1 = z_2$ because both black holes are located at $x = \pm b$.

Upon substituting Eq.(6.33) into Eq.(5.1), we find

$$\Delta\psi = \frac{9}{32\psi^7}\Bigg[\frac{\left(\mathrm{Px}_1 r_2^5 x_1\left(r_1^2+x_1^2\right)+\mathrm{Px}_2 r_1^5 x_2\left(r_2^2+x_2^2\right)\right)^2}{r_1^{10}r_2^{10}} + \frac{2(y^2+z^2)\left(\mathrm{Px}_1 r_2^5\left(r_1^2+x_1^2\right)+\mathrm{Px}_2 r_1^5\left(r_2^2+x_2^2\right)\right)^2}{r_1^{10}r_2^{10}} + \left(\frac{\mathrm{Px}_1 x_1\left(r_1^2-y^2\right)}{r_1^5}+\frac{\mathrm{Px}_2 x_2\left(r_2^2-y^2\right)}{r_2^5}\right)^2 + \left(\frac{\mathrm{Px}_1 x_1\left(r_1^2-z^2\right)}{r_1^5}+\frac{\mathrm{Px}_2 x_2\left(r_2^2-z^2\right)}{r_2^5}\right)^2 + 2\left(\frac{\mathrm{Px}_1 x_1 yz}{r_1^5}+\frac{\mathrm{Px}_2 x_2 yz}{r_2^5}\right)^2\Bigg]. \quad (6.34)$$

Finally, substituting Eq.(6.4) into Eq.(6.34), we obtain

$$\Delta u = \frac{9}{32\left(1+\frac{m_1}{2r_1}+\frac{m_2}{2r_2}+u\right)^7}\Bigg[\frac{\left(\mathrm{Px}_1 r_2^5 x_1\left(r_1^2+x_1^2\right)+\mathrm{Px}_2 r_1^5 x_2\left(r_2^2+x_2^2\right)\right)^2}{r_1^{10}r_2^{10}} + \frac{2(y^2+z^2)\left(\mathrm{Px}_1 r_2^5\left(r_1^2+x_1^2\right)+\mathrm{Px}_2 r_1^5\left(r_2^2+x_2^2\right)\right)^2}{r_1^{10}r_2^{10}} + \left(\frac{\mathrm{Px}_1 x_1\left(r_1^2-y^2\right)}{r_1^5}+\frac{\mathrm{Px}_2 x_2\left(r_2^2-y^2\right)}{r_2^5}\right)^2 + \left(\frac{\mathrm{Px}_1 x_1\left(r_1^2-z^2\right)}{r_1^5}+\frac{\mathrm{Px}_2 x_2\left(r_2^2-z^2\right)}{r_2^5}\right)^2 + 2\left(\frac{\mathrm{Px}_1 x_1 yz}{r_1^5}+\frac{\mathrm{Px}_2 x_2 yz}{r_2^5}\right)^2\Bigg], \quad (6.35)$$

which is the equation we will numerically solve using our pseudo-spectral scheme. Note that in Eq.(6.35), we use the Laplacian operator derived in Section(6.2.3).

6.4.1 Computation of Binary Punctures with P_{1_x} and P_{2_x}

Consider the following non-linear, elliptic PDE,

$$\Delta u = \frac{9}{32\left(1+\frac{m_1}{2r_1}+\frac{m_2}{2r_2}+u\right)^7}\Bigg[\frac{\left(\mathrm{Px}_1 r_2^5 x_1\left(r_1^2+x_1^2\right)+\mathrm{Px}_2 r_1^5 x_2\left(r_2^2+x_2^2\right)\right)^2}{r_1^{10}r_2^{10}} + \frac{2(y^2+z^2)\left(\mathrm{Px}_1 r_2^5\left(r_1^2+x_1^2\right)+\mathrm{Px}_2 r_1^5\left(r_2^2+x_2^2\right)\right)^2}{r_1^{10}r_2^{10}} + \left(\frac{\mathrm{Px}_1 x_1\left(r_1^2-y^2\right)}{r_1^5}+\frac{\mathrm{Px}_2 x_2\left(r_2^2-y^2\right)}{r_2^5}\right)^2 + \left(\frac{\mathrm{Px}_1 x_1\left(r_1^2-z^2\right)}{r_1^5}+\frac{\mathrm{Px}_2 x_2\left(r_2^2-z^2\right)}{r_2^5}\right)^2 + 2\left(\frac{\mathrm{Px}_1 x_1 yz}{r_1^5}+\frac{\mathrm{Px}_2 x_2 yz}{r_2^5}\right)^2\Bigg],$$

with the following bounary condition

$$u(r\to\infty,\theta,\phi)=0.$$

We will solve this using a pseudo-spectral method, assuming a spectral solution with the following form,

$$u(\tilde{A},\tilde{B},\phi)=\sum_{l=0}^{N_A}\sum_{m=0}^{N_B}\sum_{n=\frac{N_{phi}}{2}+1}^{n=\frac{N_{phi}}{2}-1}\tilde{u}_{lmn}T_l(\tilde{A})T_m(\tilde{B})e^{in\phi}.$$

We will solve this equation in the cases when $b=0.5$ and

1. $P_{1_x}=P_{2_x}=1$
2. $P_{1_x}=1, P_{2_x}=-1$
3. $P_{1_x}=0.05, P_{2_x}=-1$

These cases will illustrate the flexibility of the numerical method for black holes with linear momenta of different magnitudes and direction.

In each case we show it's respective convergence plot, where we assume the exact

solution is a numerical spectral solution with $N = N_{\tilde{A}} = N_{\tilde{B}} = 60$ and $N_\phi = 4$. We then compare cases for $N < 60$ to that spectral solution.

Also to illustrate that this solution obeys the constraints imposed by the compactification, we show plots of the $\tilde{A} = -1$ face, the line connecting the black holes. For our numerical solution to remain plausible, we need to see symmetry in the ϕ coordinate. That is, the numerical spectral solution for u must satisfy the following relation on the $\tilde{A} = -1$ face,

$$u(-1, \tilde{B}, \phi) = u(-1, \tilde{B}).$$

The plots associated with the first case of $P_{x_1} = P_{x_2} = 1$ are found in Figures(B-40) and (B-41).

The plots associated with the first case of $P_{x_1} = 1, P_{x_2} = -1$ are found in Figures(B-42) and (B-43).

The plots associated with the first case of $P_{x_1} = 0.05, P_{x_2} = -1$ are found in Figures(B-44) and (B-45).

6.5 Binary Punctures with S_{1_x} and P_{2_z}

In this section we will use Eqs.(5.1) and (6.1) to derive the governing initial puncture data equation for two black holes, one with spin only in the x-direction and the other with linear momentum only in the z-direction. We let

$$\begin{aligned} \vec{S}_1 &= (S_{1_x}, 0, 0) \quad \text{and} \quad \vec{P}_1 = (0, 0, 0), \\ \vec{S}_2 &= (0, 0, 0) \quad \text{and} \quad \vec{P}_2 = (0, 0, P_{2_z}). \end{aligned}$$

By using Eq.(6.1) we can find the extrinsic curvature, K_{ab}. By performing the

contraction on the extrinsic curavture, K_{ab}, we obtain

$$K^{ab}K_{ab} = \frac{9}{4r_1^{10}r_2^{10}}\Big[8r_2^{10}r_1^2\mathrm{Sx}_1^2\left(y^2+z^2\right) + 8\mathrm{Pz}_2 r_1^5 r_2^5 \mathrm{Sx}_1\left(r_2^2\left(x_1x_2y+y^3+yz^2\right)\right) + \mathrm{Pz}_2^2 r_1^{10}\left(3r_2^4z^2 + r_2^4\left(2x_2^2+2y^2+3z^2\right)\right)\Big], \quad (6.36)$$

where x,y, and z are the coordinates definitions derived in Section(6.2.2), and $x_1 = x+b,\ x_2 = x-b,\ y = y_1 = y_2$, and $z = z_1 = z_2$ because both black holes are located at $x = \pm b$.

Upon substituting Eq.(6.36) into Eq.(5.1), we find

$$\Delta\psi = \frac{9}{32\psi^7 r_1^{10}r_2^{10}}9\Big[8r_2^{10}r_1^2\mathrm{Sx}_1^2\left(y^2+z^2\right) + 8\mathrm{Pz}_2 r_1^5 r_2^5 \mathrm{Sx}_1\left(r_2^2\left(x_1x_2y+y^3+yz^2\right)\right) + \mathrm{Pz}_2^2 r_1^{10}\left(3r_2^4z^2 + r_2^4\left(2x_2^2+2y^2+3z^2\right)\right)\Big]. \quad (6.37)$$

Finally, substituting Eq.(6.4) into Eq.(6.37), we obtain

$$\Delta u = \frac{9}{32\left(1+\frac{m_1}{2r_1}+\frac{m_2}{2r_2}+u\right)^7 r_1^{10}r_2^{10}}9\Big[8r_2^{10}r_1^2\mathrm{Sx}_1^2\left(y^2+z^2\right) + 8\mathrm{Pz}_2 r_1^5 r_2^5 \mathrm{Sx}_1\left(r_2^2\left(x_1x_2y+y^3+yz^2\right)\right) + \mathrm{Pz}_2^2 r_1^{10}\left(3r_2^4z^2 + r_2^4\left(2x_2^2+2y^2+3z^2\right)\right)\Big], \quad (6.38)$$

which is the equation we will numerically solve using our pseudo-spectral scheme. Note that in Eq.(6.38), we use the Laplacian operator derived in Section(6.2.3).

6.5.1 Computation of Binary Punctures with S_{1_x} and P_{2_z}

Consider the following non-linear, elliptic PDE,

$$\Delta u = \frac{9}{32\left(1+\frac{m_1}{2r_1}+\frac{m_2}{2r_2}+u\right)^7 r_1^{10} r_2^{10}} 9\Bigg[8r_2^{10}r_1^2\mathrm{Sx}_1^2\left(y^2+z^2\right)$$

$$+ 8\mathrm{Pz}_2 r_1^5 r_2^5 \mathrm{Sx}_1\left(r_2^2\left(x_1x_2y+y^3+yz^2\right)\right)+\mathrm{Pz}_2^2 r_1^{10}\left(3r_2^4z^2+r_2^4\left(2x_2^2+2y^2+3z^2\right)\right)\Bigg],$$

with the following bounary condition

$$u(r\to\infty,\theta,\phi)=0.$$

We will solve this using a pseudo-spectral method, assuming a spectral solution with the following form,

$$u(\tilde{A},\tilde{B},\phi)=\sum_{l=0}^{N_A}\sum_{m=0}^{N_B}\sum_{n=\frac{N_{phi}}{2}+1}^{n=\frac{N_{phi}}{2}-1}\tilde{u}_{lmn}T_l(\tilde{A})T_m(\tilde{B})e^{in\phi}.$$

We will solve this equation in the cases when $b=0.5$ and

1. $S_{1_x}=P_{2_z}=1$
2. $S_{1_x}=1, P_{2_z}=-1$
3. $S_{1_x}=0.05, P_{2_x}=1$
4. $S_{1_x}=1, P_{2_x}=0.05$

These cases will illustrate the flexibility of the numerical method for a black hole system in which one black hole has spin and the other has linear momentum.

In each case we show it's respective convergence plot, where we assume the exact solution is a numerical spectral solution with $N=N_{\tilde{A}}=N_{\tilde{B}}=40$ and $N_\phi=10$. We then compare cases for $N<40$ to that spectral solution. However, in the case of $S_{x_1}=P_{z_2}=1$, we assume a solution with $N=N_{\tilde{A}}=N_{\tilde{B}}=50$ and $N_\phi=10$ to

illustrate greater accuracy in the convergence plot.

Also to illustrate that this solution obeys the constraints imposed by the compactification, we show plots of the $\tilde{A} = -1$ face, the line connecting the black holes. For our numerical solution to remain plausible, we need to see symmetry in the ϕ coordinate. That is, the numerical spectral solution for u must satisfy the following relation on the $\tilde{A} = -1$ face,

$$u(-1, \tilde{B}, \phi) = u(-1, \tilde{B}).$$

The plots associated with the first case of $S_{x_1} = P_{z_2} = 1$ are found in Figures(B-46) and (B-47).

The plots associated with the second case of $S_{x_1} = 1, P_{z_2} = -1$ are found in Figures(B-48) and (B-49).

The plots associated with the first case of $S_{x_1} = 0.05, P_{z_2} = 1$ are found in Figures(B-50) and (B-51).

The plots associated with the second case of $S_{x_1} = 1, P_{z_2} = 0.05$ are found in Figures(B-52) and (B-53).

Bibliography

[1] M. Ansorg, B. Brugmann and W. Tichy, A single-domain spectral method for black hole puncture data, *Phys. Rev D* **70**(6), 2004.

[2] M. Ansorg, A multi-domain spectral method for initial data of arbitrary binaries in general relativity, *Class. Quantum Grav.* **24**, S1-S14, 2007.

[3] J.P. Boyd, Chebyshev and Fourier Spectral Methods, *Dover Publications*, 668 pages, 2001.

[4] S. Brandt and B. Brugmann, A simple construction of initial data for multiple black holes, *Phys. Rev Letters* **78**(19), 3606-3609, 1997.

[5] E. Flanagan and S. Hughes, The basis of gravitational wave theory, *arxiv:0501.0501041v3 [gr-qc]* 12 Jan 2005.

[6] P. Grandclement and J. Novak, Spectral Methods for Numerical Relativity, *arXiv:0706.228v1 [gr-qc]*, 15 Jun 2007.

[7] L. Kidder and L.S. Finn, Spectral methods for numerical relativity: The initial data problem, *Phys. Rev D* **62**(8), 2000.

Appendix A

Chebyshev Theory

The Sturm-Liouville Chebyshev ODE of the 1st Kind:

$$(1-x^2)y'' - xy' + n^2 y = 0.$$

We define the solutions to be $T_n(x)$. They are defined through the trigonometric relation:

$$T_n(x) = \cos(n \arccos x),$$

on the interval $[-1, 1]$. Note: when $x = \cos\theta$, we have solutions of the form:

$$T_n(\cos\theta) = \cos(n\theta).$$

The Sturm-Liouville Chebyshev ODE of the 2nd Kind:

$$(1-x^2)y'' - 3xy' + n(n+2)y = 0.$$

We define the solutions to be $U_n(x)$. They are defined through the trigonometric relation when $x = \cos\theta$:

$$U_n(\cos\theta) = \frac{\sin((n+1)\theta)}{\sin\theta},$$

on the interval $[-1, 1]$.

Recurrence Relations:

$$T_{n+1}(x) = 2xT_n(x) - T_{n-1}(x),$$

$$U_{n+1}(x) = 2xU_n(x) - U_{n-1}(x).$$

Differentiation Relation:

$$\frac{dT_n}{dx} = nU_{n-1},$$

$$\frac{d^2T_n}{dx^2} = n\frac{nT_n - xU_{n-1}}{x^2-1} = n\frac{(n+1)T_n - U_n}{x^2-1}.$$

Orthogonality:

Both T_n and U_n form a sequence of orthogonal polynomials. The polynomials of the first kind are orthogonal with respect to the weight function, $w_1(x) = \frac{1}{\sqrt{1-x^2}}$, while the polynomials of the second are orthogonal with respect to the weight function $w_2(x) = \sqrt{1-x^2}$.

On the interval $[-1, 1]$ we have the following relations:

$$\int_{-1}^{1} T_n(x)T_m(x)w_1(x)dx = \begin{cases} 0 & \text{if } n \neq m \\ \pi & \text{if } n = m = 0 \\ \frac{\pi}{2} & \text{if } n = m \neq 0 \end{cases},$$

and

$$\int_{-1}^{1} U_n(x)U_m(x)w_2(x)dx = \begin{cases} 0 & \text{if } n \neq m \\ \frac{\pi}{2} & \text{if } n = m \end{cases}.$$

Extrema at Endpoints:

$$T_n(1) = 1,$$

$$T_n(-1) = (-1)^n.$$

$$U_n(1) = n + 1,$$

$$U_n(-1) = (n + 1)(-1)^n.$$

First Few Polynomials of the First Kind:

$$\begin{aligned}
T_0(x) &= 1, \\
T_1(x) &= x. \\
T_2(x) &= 2x^2 - 1, \\
T_3(x) &= 4x^3 - 3x, \\
T_4(x) &= 8x^4 - 8x^2 + 1, \\
T_5(x) &= 16x^5 - 20x^3 + 5x, \\
T_6(x) &= 32x^6 - 48x^4 + 18x^2 - 1, \\
T_7(x) &= 64x^7 - 112x^5 + 56x^3 - 7x,
\end{aligned}$$

Now we will expand two functions in the Chebyshev basis. We consider $f(x) = \frac{1}{1+x^2}$ and $g(x) = e^{-x^2}$ for $0 \leq x \leq \infty$. Note that $f(x)$ goes to 0 algebraically as $x \to \infty$ and that $g(x)$ goes to 0 exponentially as $x \to \infty$. We will show that the Chebyshev polynomials will be able to better approximate $f(x)$ than $g(x)$, as Chebyshev polynomials are better for approximating functions that go to zero algebraically.

Before we expand either function in the Chebyshev basis, we will compactify the domain from $[0, \infty) \to [-1, 1]$. We do this because the Chebyshev polynomials are defined between $[1, 1]$. Using the following coordinate transformation,

$$A = 2\left(1 + \frac{1}{x}\right)^{-1} - 1,$$

we find the functions become

$$f(A) = \frac{1}{1 + \left(\frac{1+A}{1-A}\right)^2} \qquad \text{and} \qquad g(A) = e^{-\left(\frac{1+A}{1-A}\right)^2}.$$

First we will expand $f(A)$ in the Chebyshev basis,

$$f(A) = \frac{1}{1 + \left(\frac{1+A}{1-A}\right)^2} = \sum_{j=0}^{N} c_n^f T_n(A).$$

We find the first 21 coefficients are:

$$c_n^f = \begin{pmatrix} 1/2 \\ -0.5857864376269049 \\ 0 \\ 0.10050506308641538 \\ 0 \\ -0.01724394270310834 \\ 0 \\ 0.002958592830277995 \\ 0 \\ -0.0005076142786067245 \\ 0 \\ 0.00008709284132776829 \\ 0 \\ -0.000014942769289455482 \\ 0 \\ 2.5637733918684735 * 10^{-6} \\ 0 - 4.3958425521850586 * 10^{-7} \\ 0 \\ 7.450580596923828 * 10^{-8} \\ 0 \\ -1.4901161193847656 * 10^{-8} \end{pmatrix}$$

Now we will expand $g(A)$ in the Chebyshev basis,

$$g(A) = e^{-\left(\frac{1+A}{1-A}\right)^2} = \sum_{j=0}^{N} c_n^g T_n(A).$$

We find the first 21 coefficients are:

$$c_n^g = \begin{pmatrix} 0.4576214719981695 \\ -0.6049508714432735 \\ 0.06447710413504479 \\ 0.13911719569350045 \\ -0.02771317319720939 \\ -0.04768674673861184 \\ 0.005355469928721216 \\ 0.01892679043487716 \\ 0.0018286112131115854 \\ -0.007221763902819989 \\ -0.0028690061546408907 \\ 0.0021332622938663587 \\ 0.002008155684506298 \\ -0.00016116484455153818 \\ -0.0009638411127716323 \\ -0.0003494268883310891 5 \\ 0.0002803853894068356 \\ 0.0002967858481988696 \\ 0.00001768189033368727 8 \\ -0.0001308141723563444 \\ -0.00007862613725924741 \\ 0.00001924200561773115 \end{pmatrix}$$

Plotting the logarithm of the n^{th} coefficient versus n, it is clear that the coefficients in $f(A)$ decay much faster than those of $g(A)$. This illustrates that Chebyshev functions are better at approximating functions that decay algebraically than those that decay exponentially. The plot is found in Figure(B-54).

Appendix B

Figures

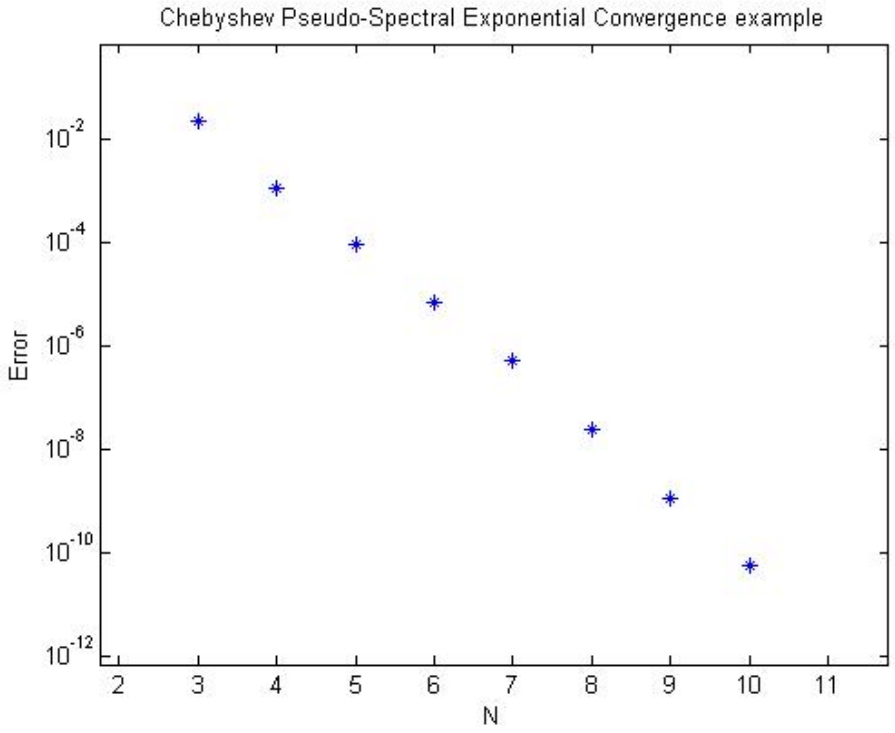

Figure B-1: Exponential convergence to the exact solution of the linear ODE, $u_{xx} = \sin(x) + \cos(x)$, with Dirichlet boundary conditions on the interval [-1,1]. The error is the norm of the difference between the computed solution and exact solution.

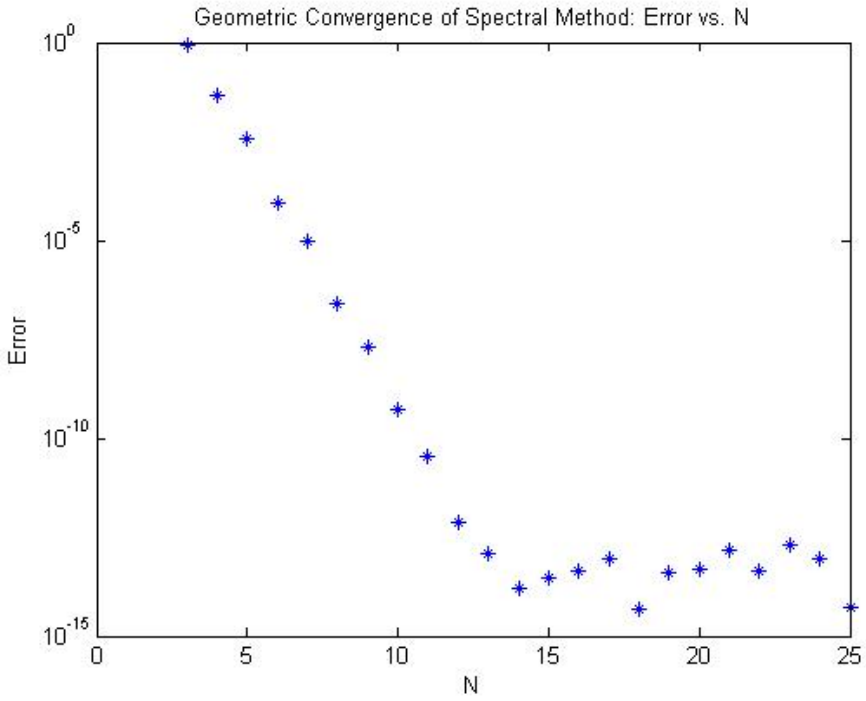

Figure B-2: Exponential convergence to the exact solution of the nonlinear ODE, $u_{xx} + u^2 = e^x + e^{2x}$, with boundary conditions $u(-1) = e^{-1}$ and $u(1) = e$. The error is the norm of the difference between the computed solution and exact solution.

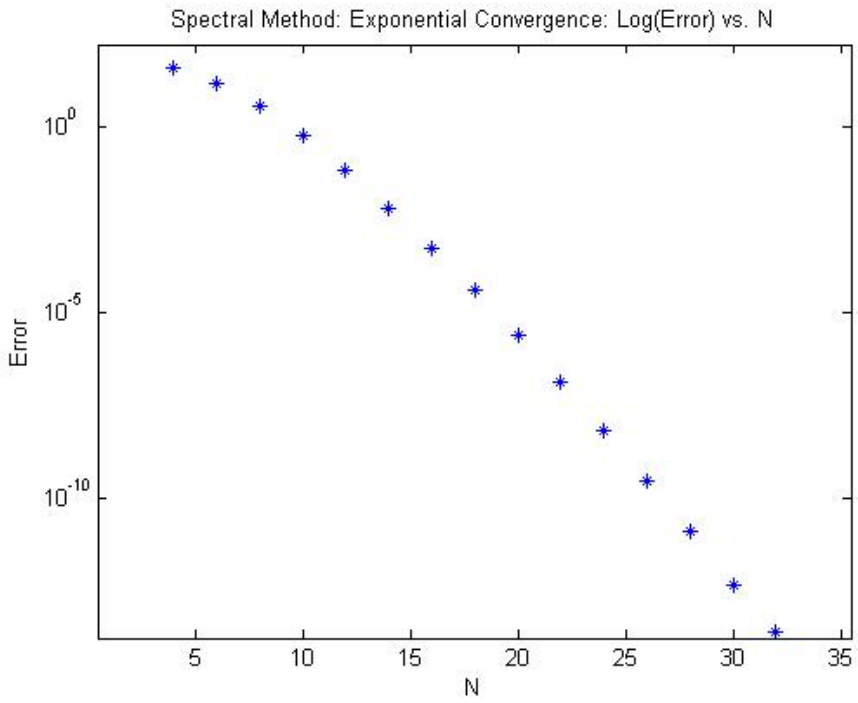

Figure B-3: Exponential convergence to the exact solution of the linear ODE, $u_{xx} + u_x + u = e^{\cos(x)}\left(1 - \sin(x) - \cos(x) + \sin^2(x)\right)$, with periodic boundary conditions on $[-\pi, \pi]$. The error is the norm of the difference between the computed solution and exact solution.

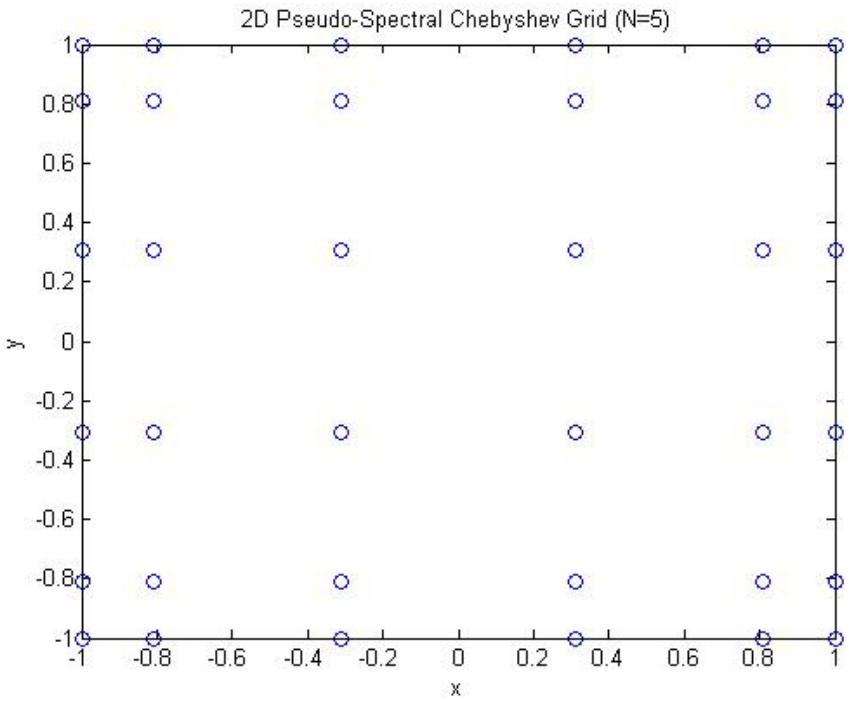

Figure B-4: An example computational domain constructed with the Chebyshev collocation points with $N_x = N_y = 6$.

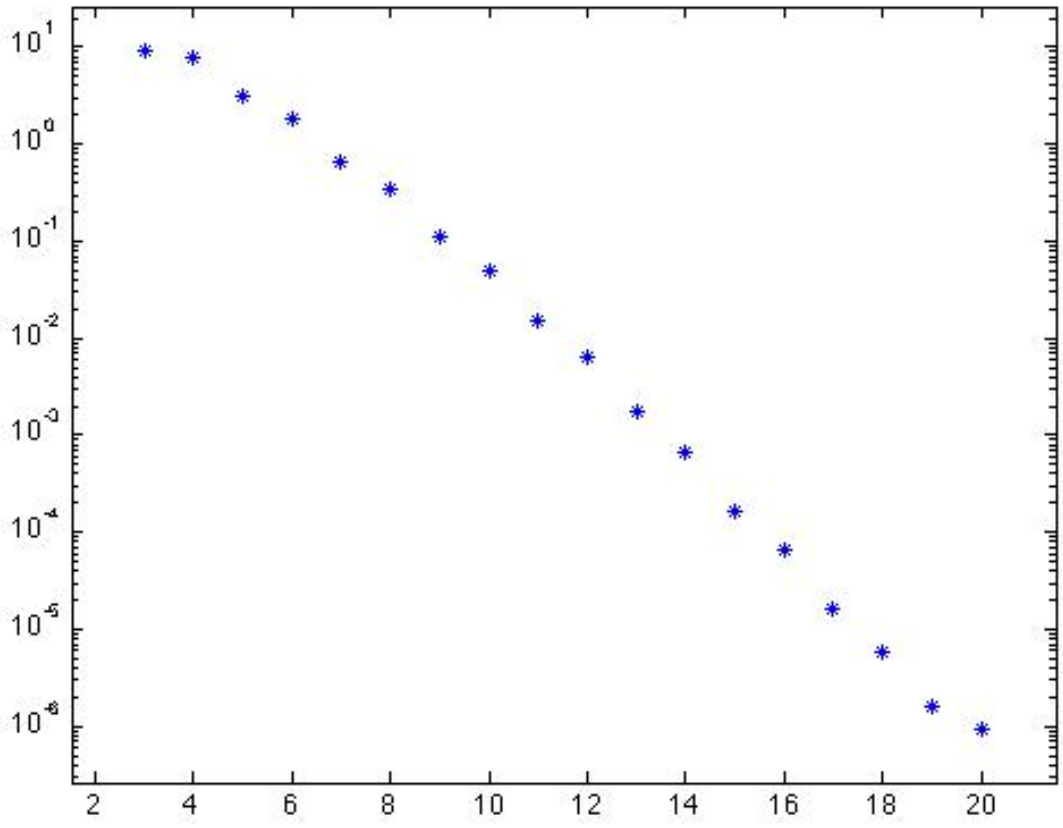

Figure B-5: Exponential convergence to the exact solution of the linear PDE, $u_{xx} + u_{yy} = -\pi^2 \sin(\pi y)\left[2\cos(\pi x) + 1\right]$. with Dirichlet boundary conditions on the domain [-1,1]×[-1,1]. The error is the norm of the difference between the computed solution and exact solution.

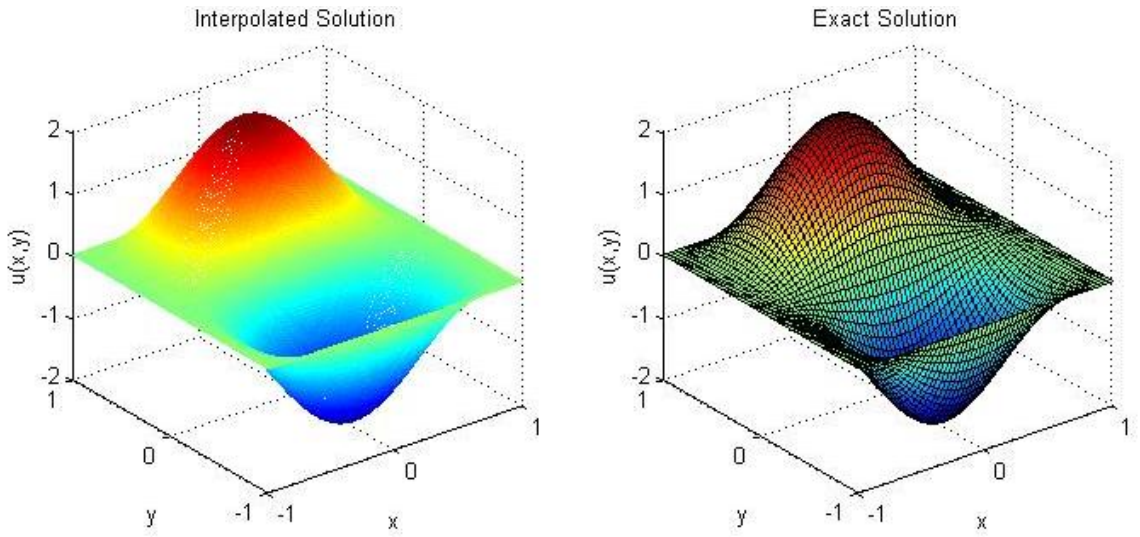

Figure B-6: Comparison of the computed solution (left) with the exact solution, $u(x, y) = \sin(\pi y)\,(\cos(\pi x) + 1)$, (right) for $N_x = N_y = 12$.

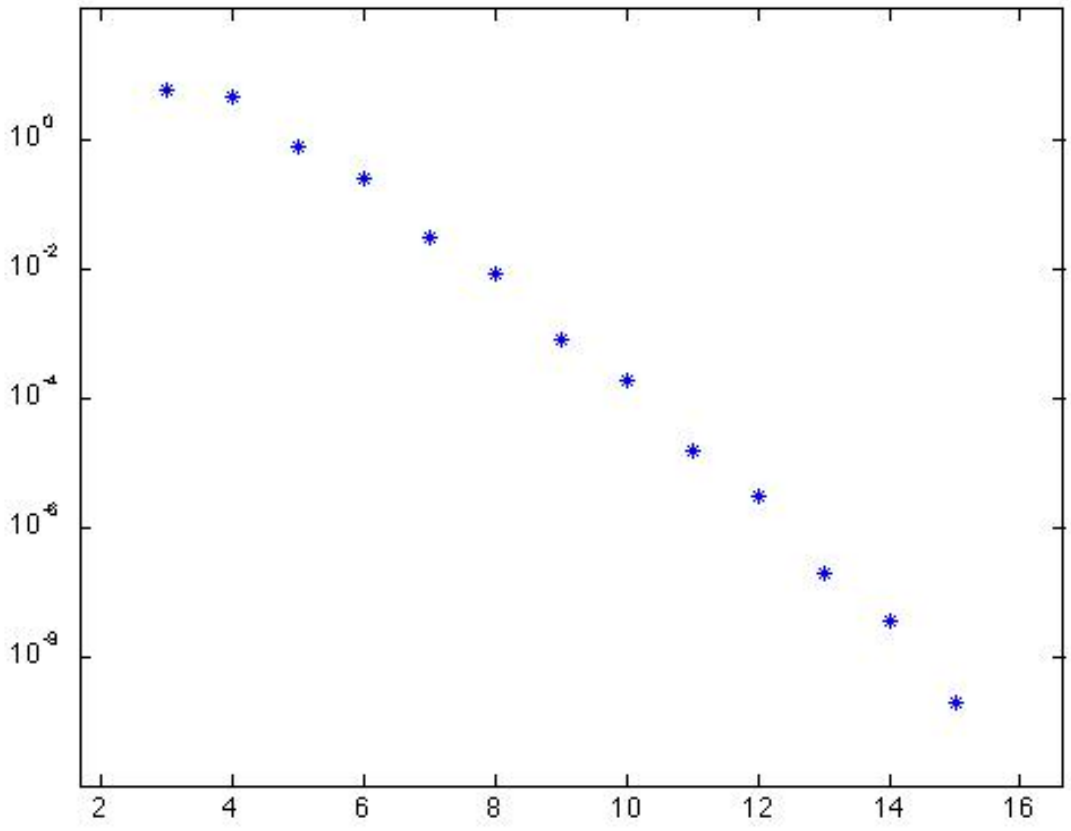

Figure B-7: Exponential convergence to the exact solution of the nonlinear PDE, $u_{xx} + u_{yy} + u^2 = -\pi^2 \sin(\pi y)\left[2\cos(\pi x) + 1\right] + \left(\sin(\pi y)\left(\cos(\pi x) + 1\right)\right)^2$ with Dirichlet boundary conditions on the domain [-1,1]×[-1,1]. The error is the norm of the difference between the computed solution and exact solution.

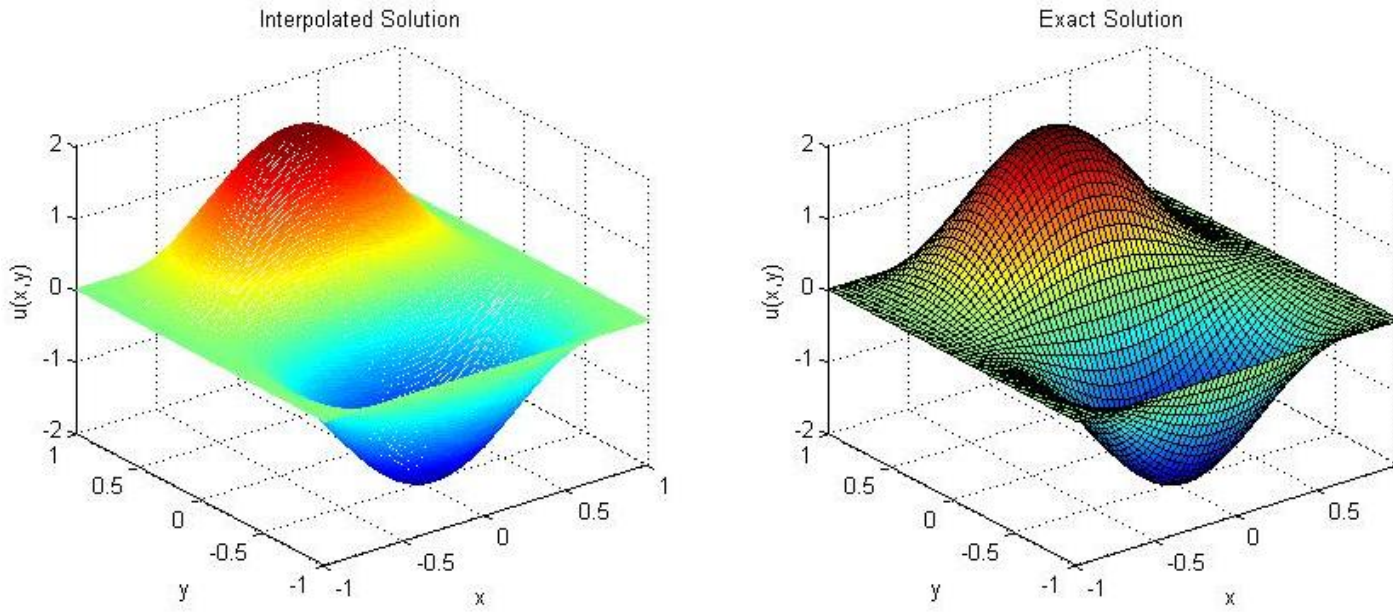

Figure B-8: Comparison of the computed solution (left) with the exact solution, $u(x, y) = \sin(\pi y)\,(\cos(\pi x) + 1)$, (right) for $N_x = N_y = 12$.

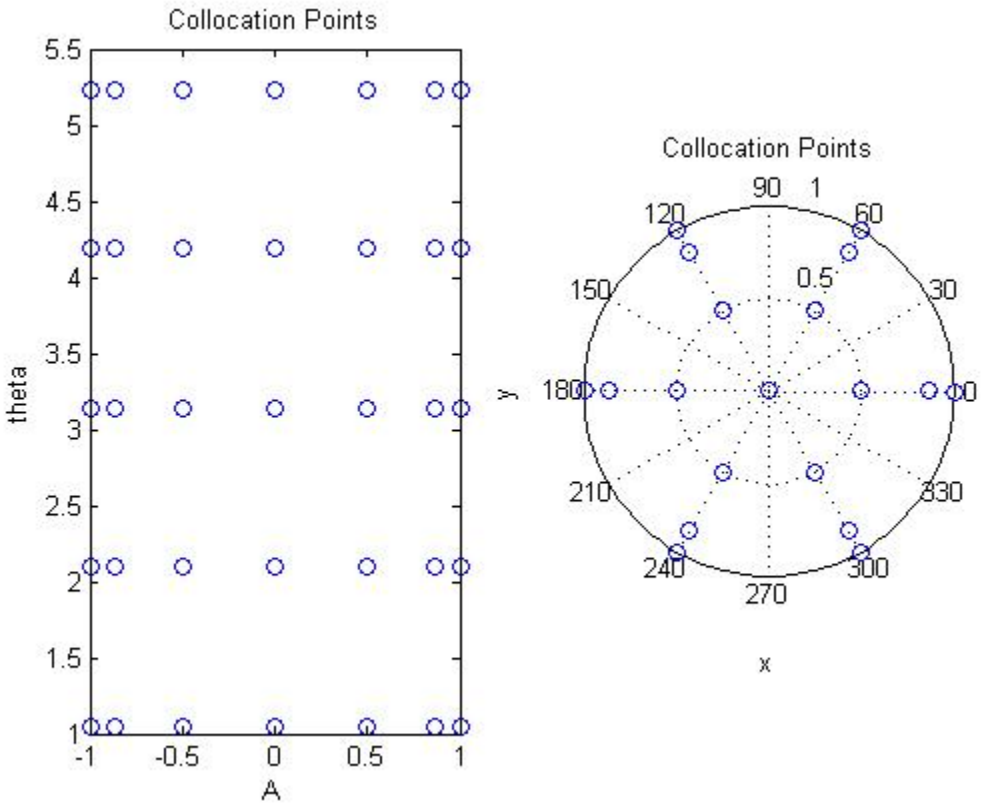

Figure B-9: An example computational domain constructed with the Chebyshev collocation points with $N_x = N_y = 6$.

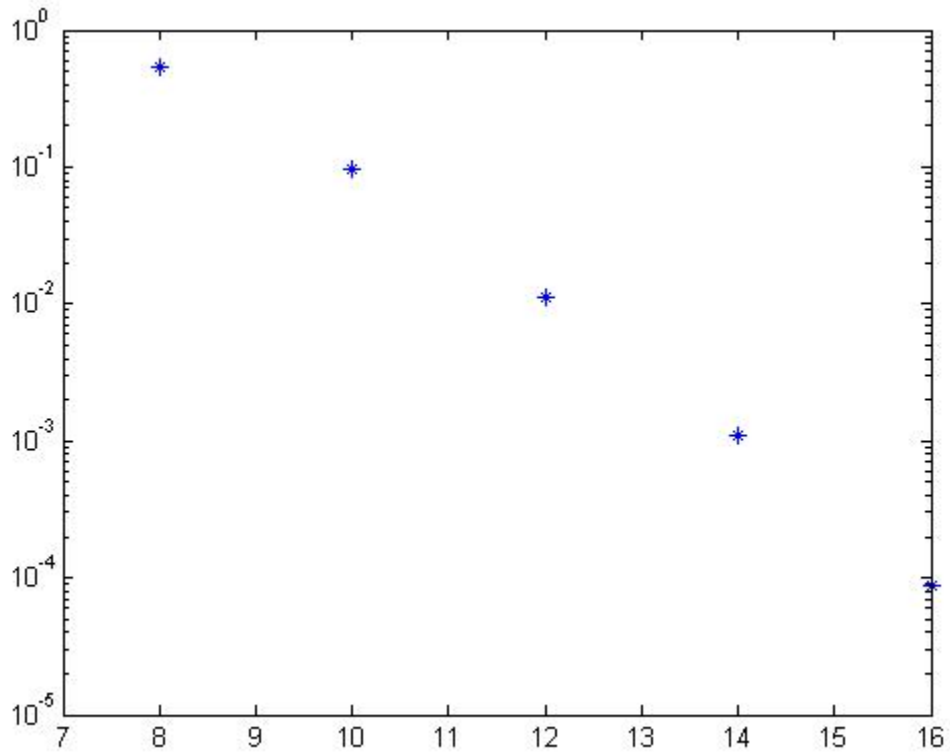

Figure B-10: Exponential convergence to the exact solution of the nonlinear PDE, $u_r + \frac{1}{r}u_r + \frac{1}{r^2}u_{\phi\phi} + u^2 = f$, where f is the inhomogeneous term corresponding to the exact solution $u(r,\phi) = [\cos[(2r-1)\pi + 1]]\, e^{\cos(\phi)}$ with Dirichlet boundary conditions on the boundary when $r = \{0, 1\}$ and periodicity in the ϕ coordinate. The error is the norm of the difference between the computed solution and exact solution.

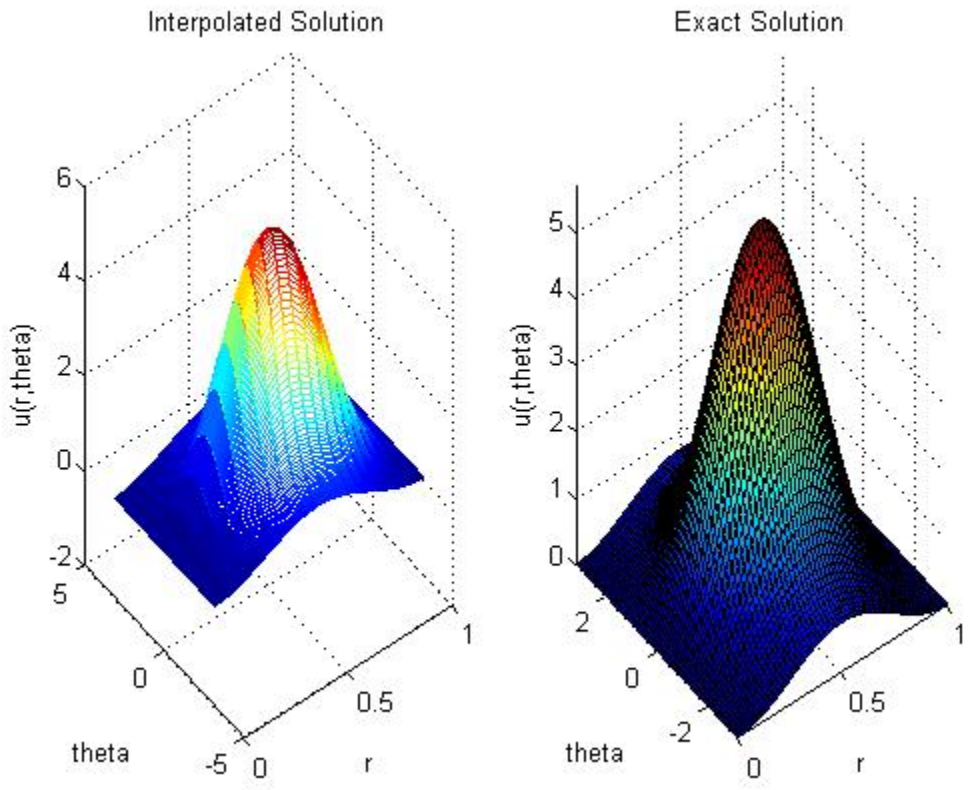

Figure B-11: Comparison of the computed solution (left) with the exact solution, $u(r, \phi) = [\cos[(2r-1)\pi + 1]]\, e^{\cos(\phi)}$, (right) for $N_r = N_\phi = 10$.

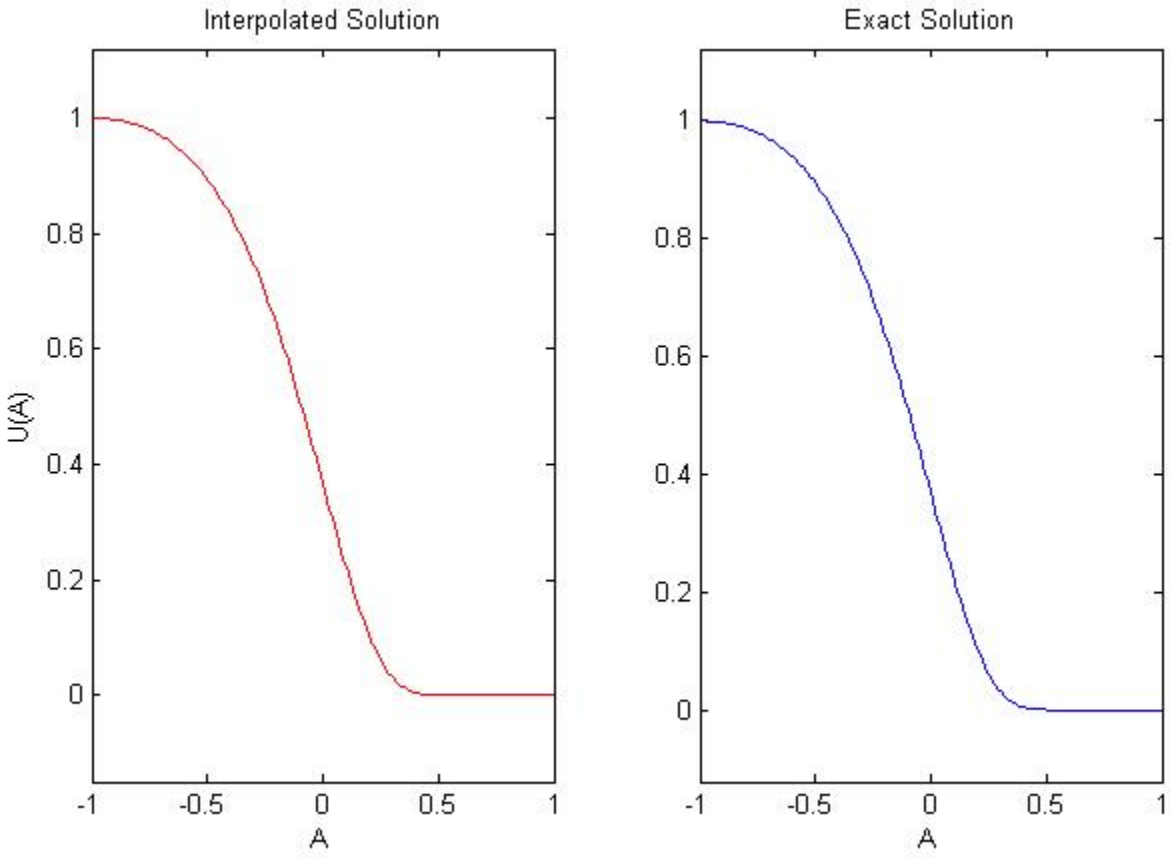

Figure B-12: Comparison of the computed solution (left) with the exact solution, $u(r) = e^{-r^2}$, (right) for $N_r = 10$.

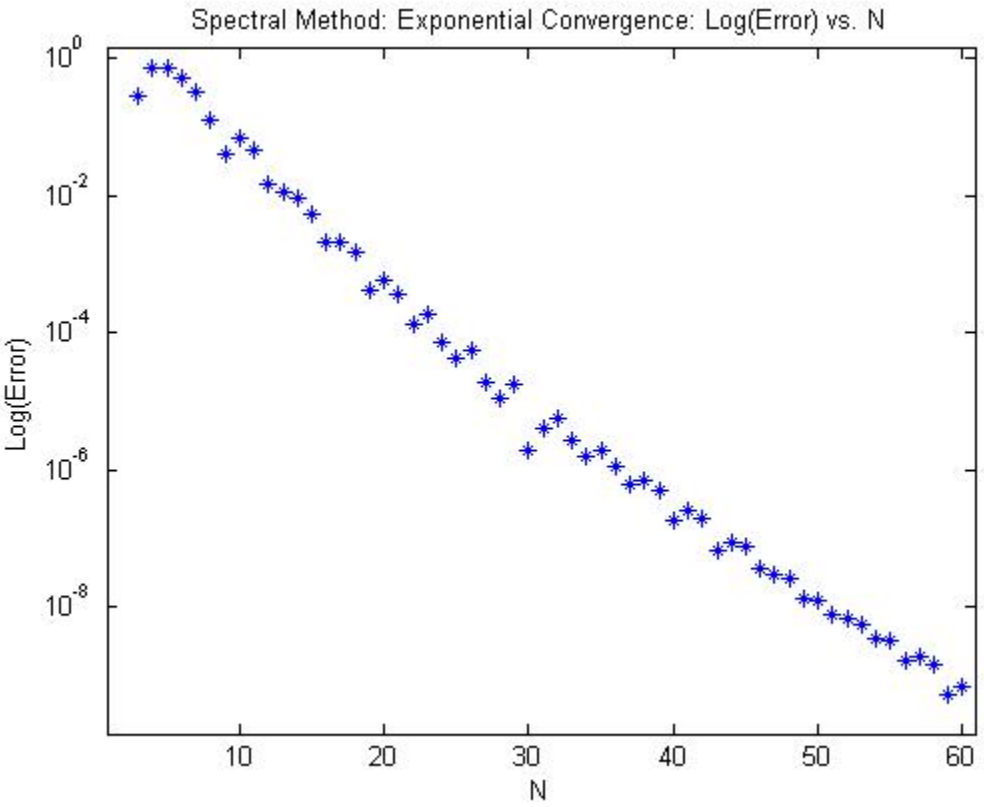

Figure B-13: Exponential convergence to the exact solution of the linear ODE, $u_{rr} + \frac{2}{r}u_r = (r^2 - 6)e^{-r^2}$, with homogeneous mixed boundary conditions. The error is the norm of the difference between the computed solution and exact solution.

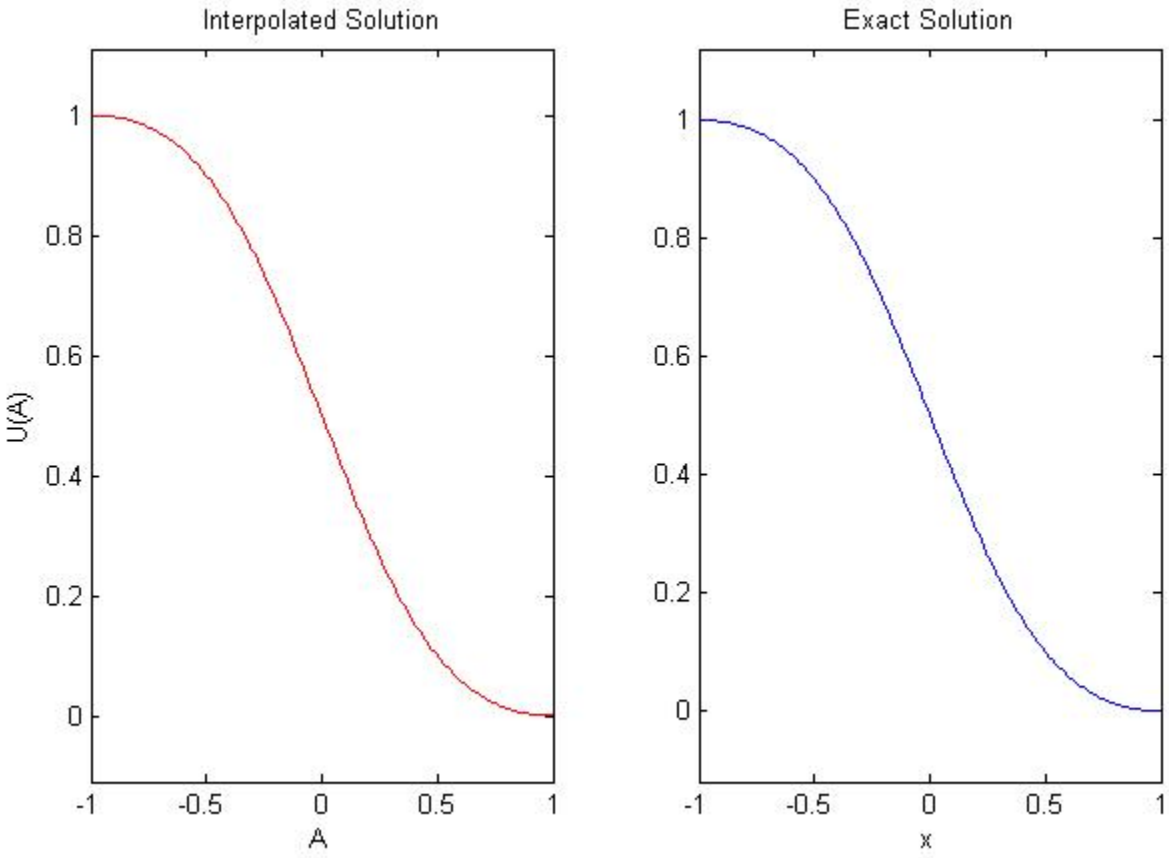

Figure B-14: Comparison of the computed solution (left) with the exact solution, $u(r) = \frac{1}{1+r^2}$, (right) for $N_r = 10$.

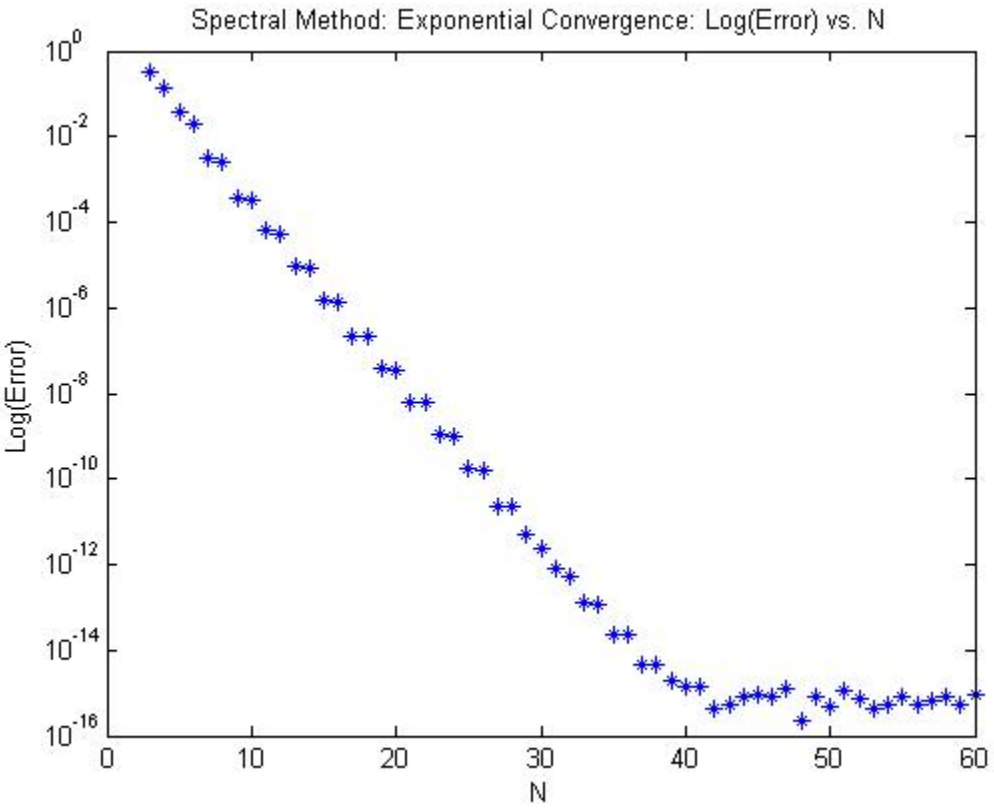

Figure B-15: Exponential convergence to the exact solution of the linear ODE, $u_{rr} + \frac{2}{r}u_r = \frac{8r^2}{(1+r^2)^3} - \frac{6}{(1+r^2)^2}$, with $u(0) = 1$ and $u(r \to \infty) = 0$. The error is the norm of the difference between the computed solution and exact solution.

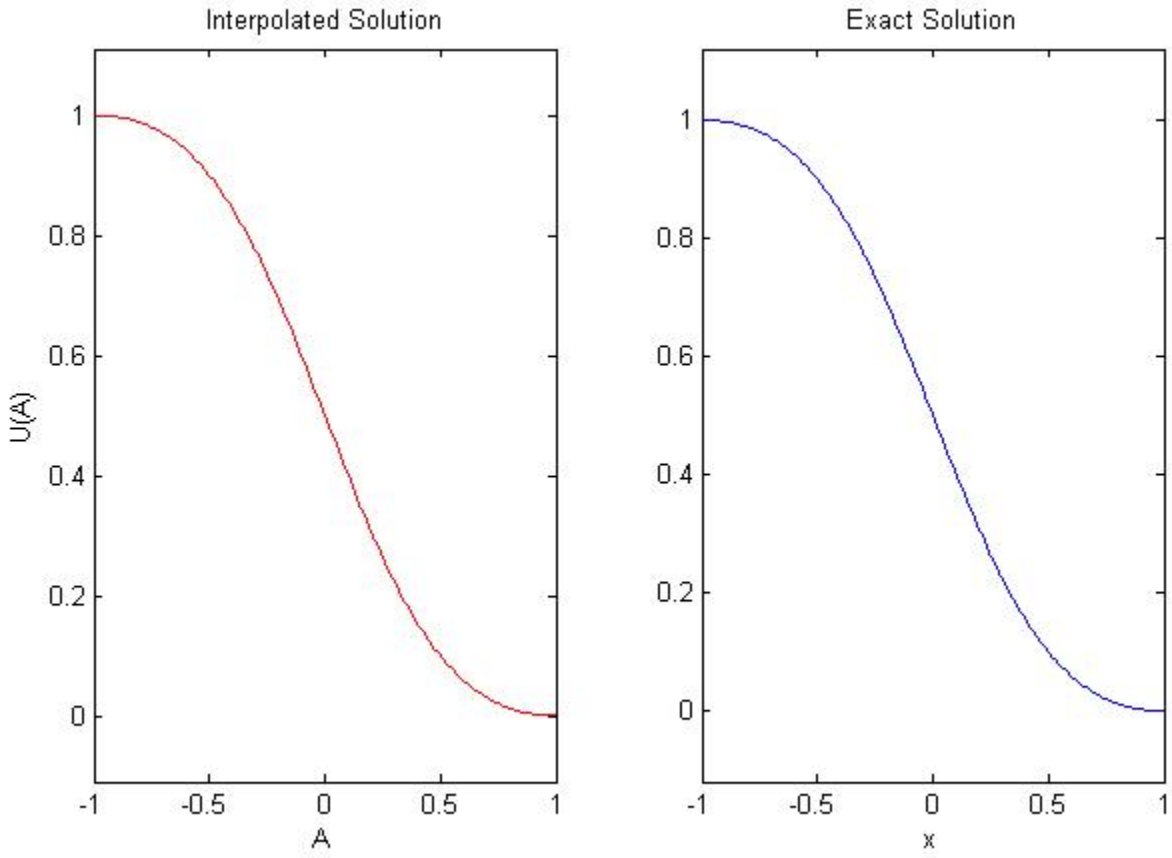

Figure B-16: Comparison of the computed solution (left) with the exact solution, $u(r) = \frac{1}{1+r^2}$, (right) for $N_r = 10$.

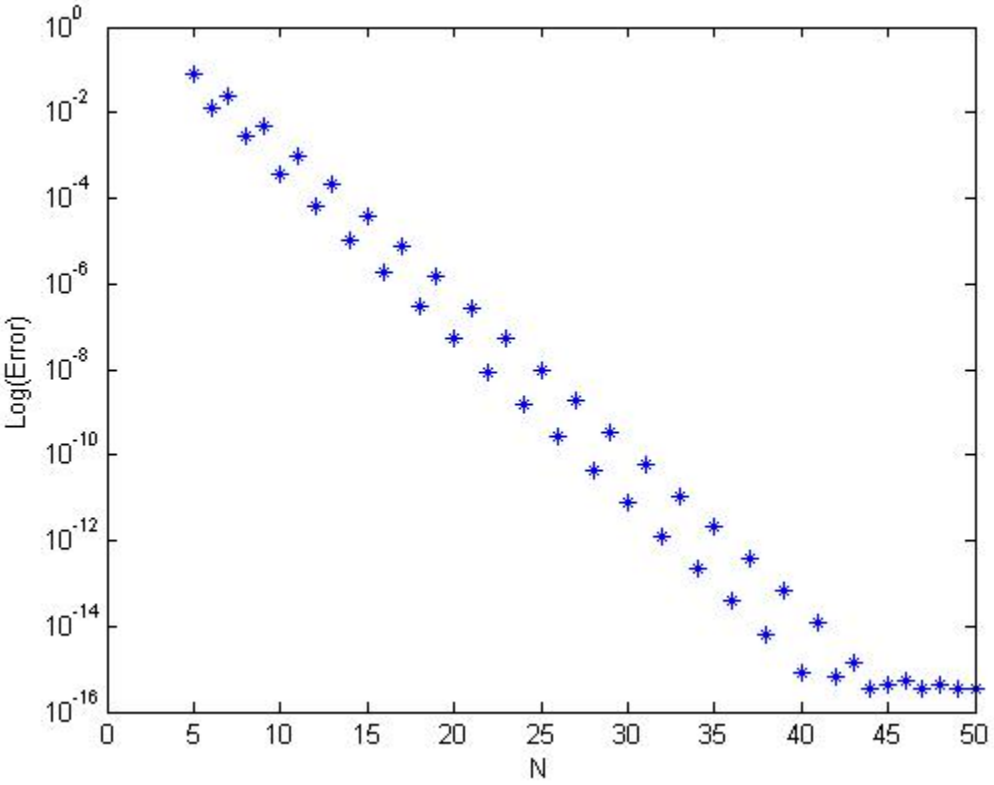

Figure B-17: Exponential convergence to the exact solution, $u(r) = \frac{1}{1+r^2}$, of the nonlinear ODE, $u_{rr} + \frac{2}{r}u_r + \frac{1}{1+u} = f$ with only the boundary condition of $u(r \rightarrow \infty) = 0$. The error is the norm of the difference between the computed solution and exact solution. Note the 2-cycle behavior in the convergence.

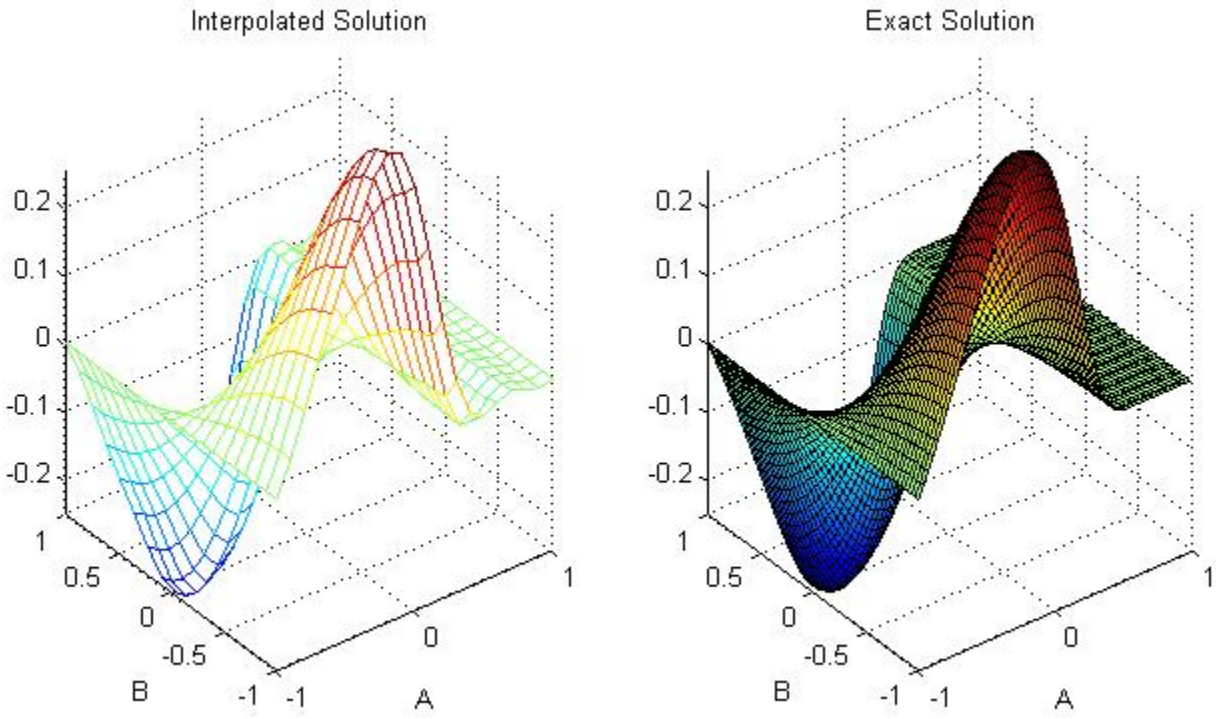

Figure B-18: Comparison of the computed solution (left) with the exact solution, $u(r, \theta) = r \cos\theta e^{-r^2}$,(right) for $N_r = N_\theta = 10$.

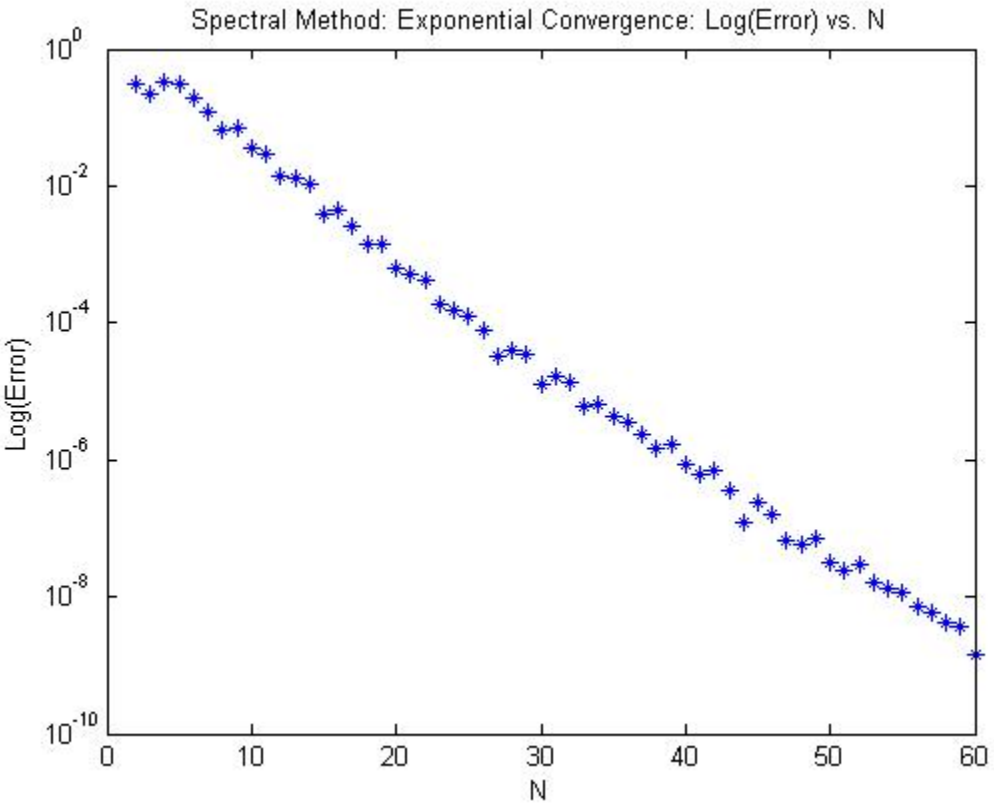

Figure B-19: Exponential convergence to the exact solution, $u(r,\theta) = r\cos\theta e^{-r^2}$, of the linear PDE, $u_{rr} + \frac{2}{r}u_r + \frac{1}{r^2}u_\theta + \frac{\cot\theta}{r^2}u_\theta = f(r,\theta)$, with $u(0,\theta) = u(r \to \infty, \theta = 0$, $u(r,0) = re^{-r^2}$, and $u(r,\pi) = -re^{-r^2}$. The error is the norm of the difference between the computed solution and exact solution.

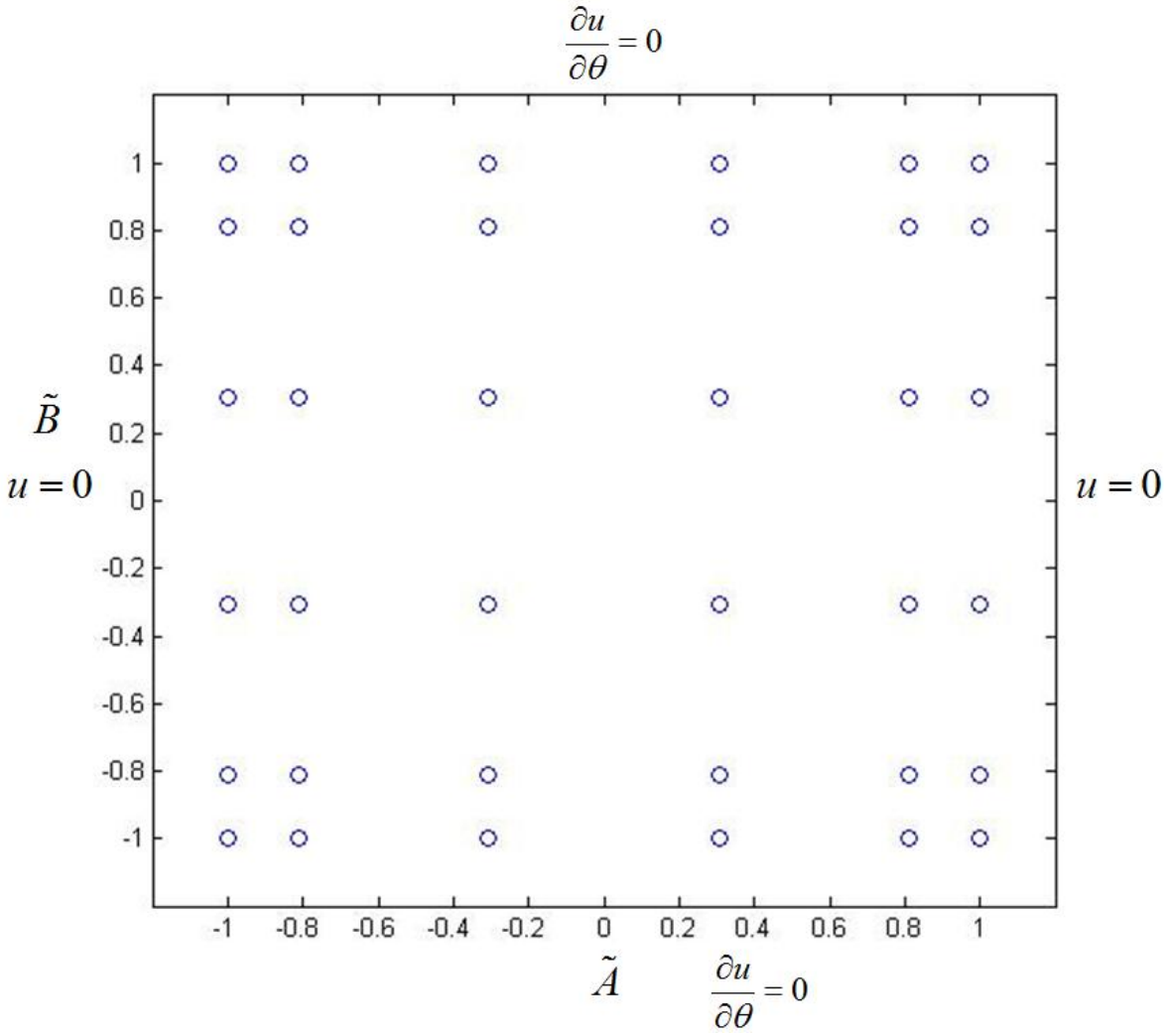

Figure B-20: An example computational domain constructed with the Chebyshev collocation points with $N_x = N_y = 6$. Note that we enforce Dirchlet homogeneous boundary conditions in the r-coordinate and Neumann homogeneous boundary conditions in the θ-coordinate.

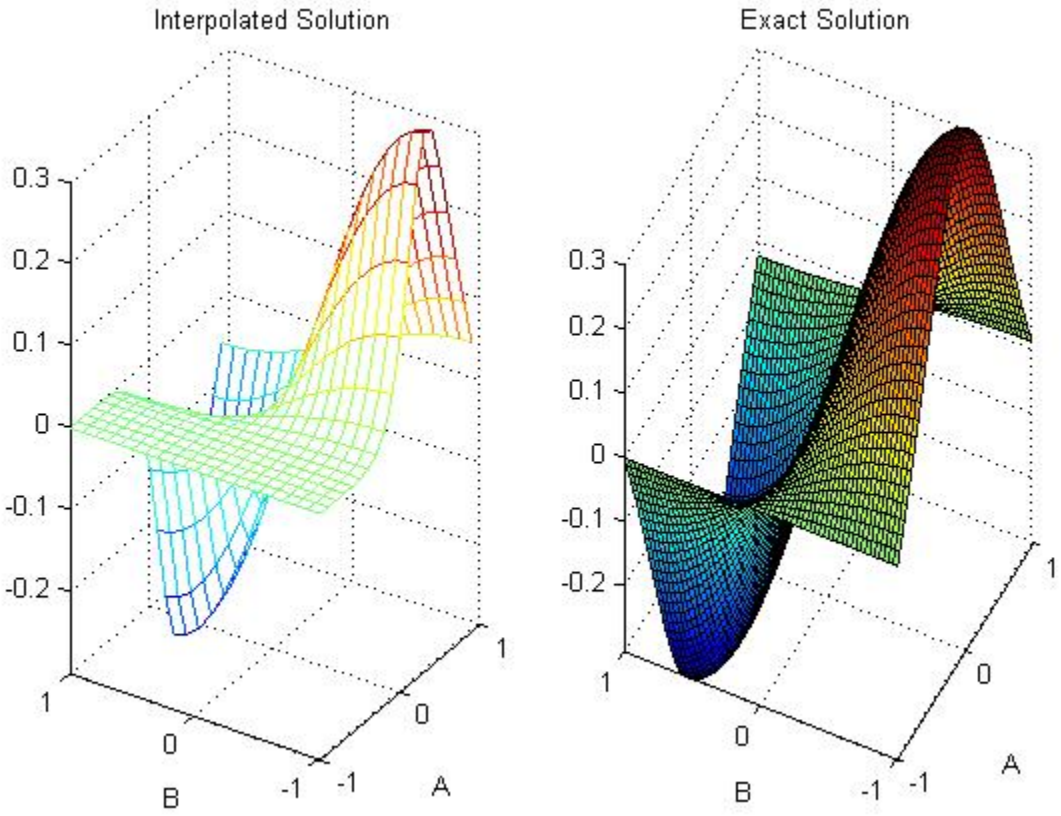

Figure B-21: Comparison of the computed solution (left) with the exact solution, $u(r,\theta) = \frac{r\cos\theta}{1+r^2}$,(right) for $N_r = N_\theta = 10$.

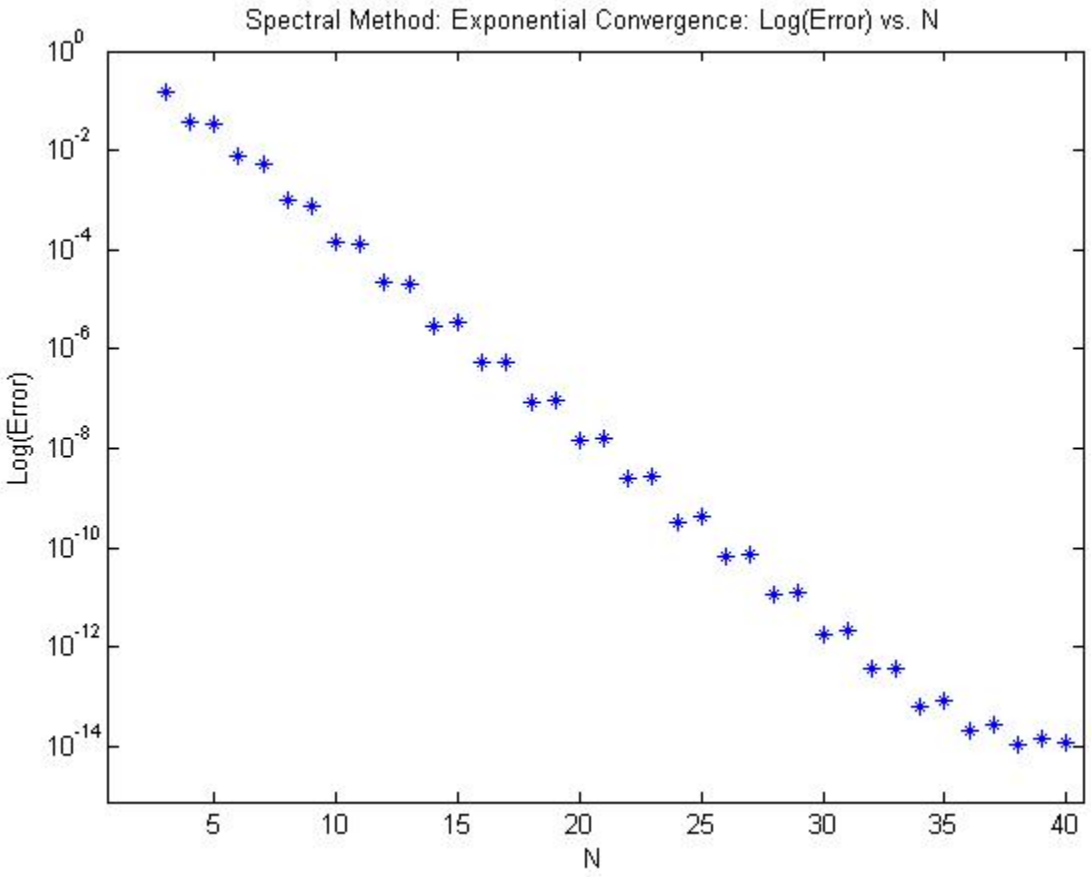

Figure B-22: Exponential convergence to the exact solution, $u(r,\theta) = \frac{r\cos\theta}{1+r^2}$, of the linear PDE, $u_{rr} + \frac{2}{r}u_r + \frac{1}{r^2}u_\theta + \frac{\cot\theta}{r^2}u_\theta = f(r,\theta)$, with $u(0,\theta) = u(r \to \infty, \theta = 0$, $\left.\frac{\partial u}{\partial \theta}\right|_{(r,0)} = 0$, and $\left.\frac{\partial u}{\partial \theta}\right|_{(r,\pi)} = 0$. The error is the norm of the difference between the computed solution and exact solution.

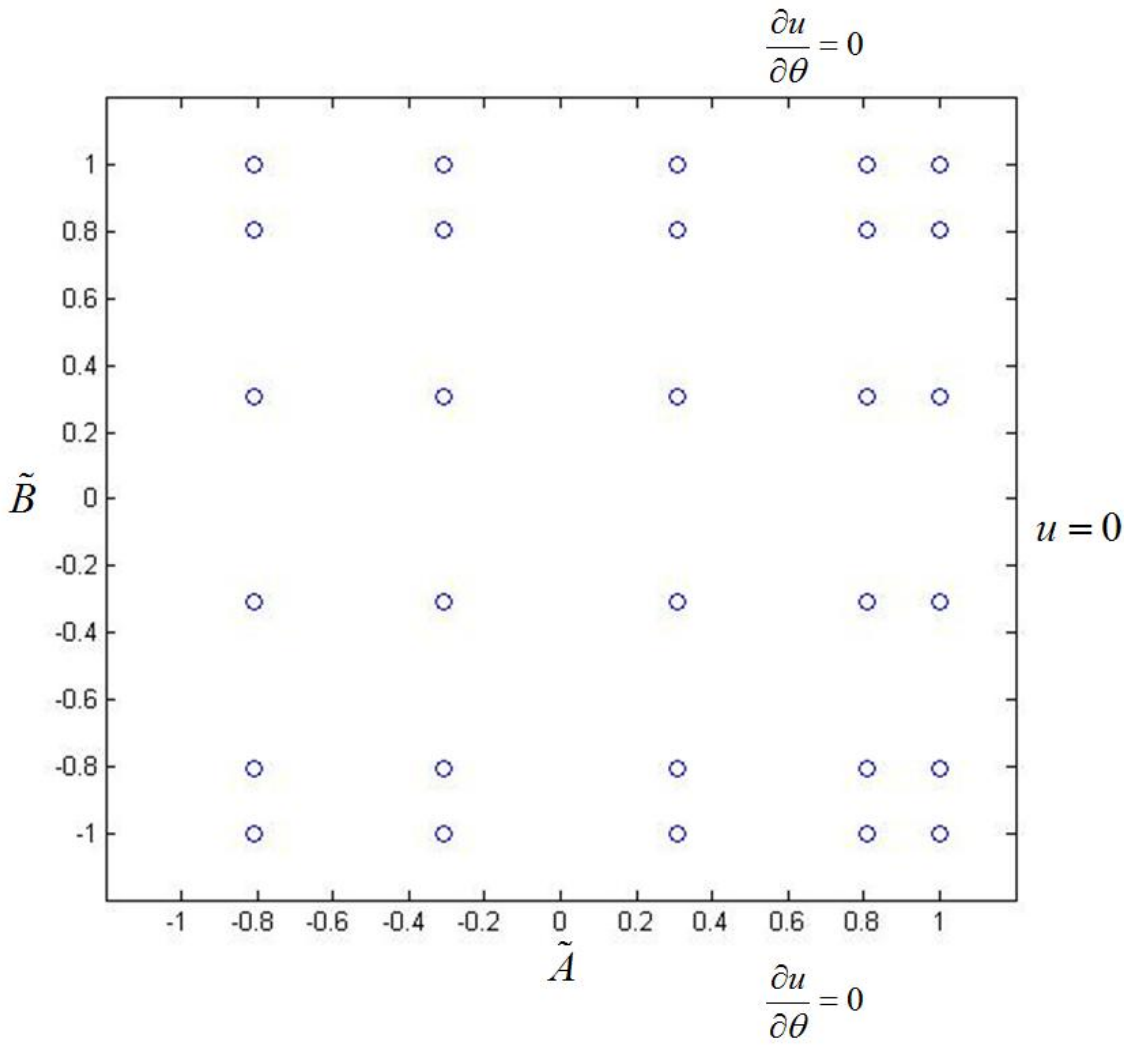

Figure B-23: An example computational domain constructed with the Chebyshev collocation points with $N_x = N_y = 6$. Note that we only enforce $u(r \to \infty, \theta) = 0$ in the r-coordinate and Neumann homogeneous boundary conditions in the θ-coordinate, so there is no explicit boundary condition at $r = 0$.

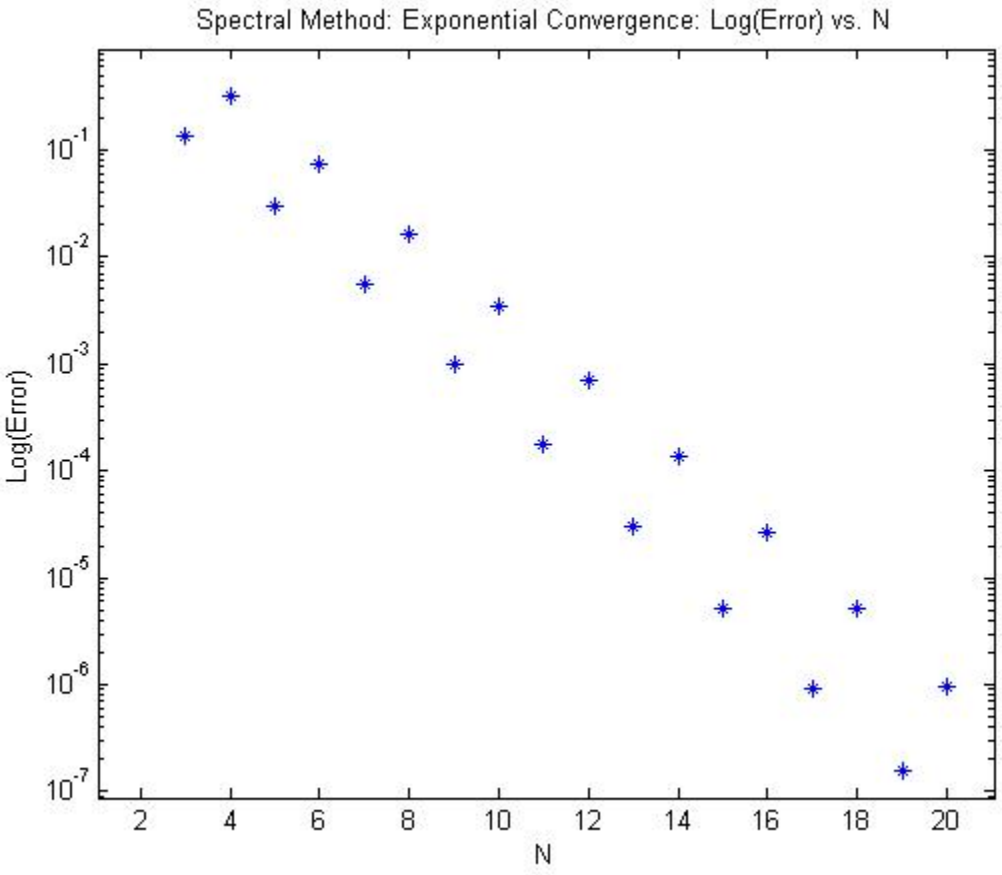

Figure B-24: Exponential convergence to the exact solution, $u(r,\theta) = \frac{r\cos\theta}{1+r^2}$, of the linear PDE, $u_{rr} + \frac{2}{r}u_r + \frac{1}{r^2}u_\theta + \frac{\cot\theta}{r^2}u_\theta = f(r,\theta)$, with $u(r \to \infty, \theta = 0$, $\left.\frac{\partial u}{\partial \theta}\right|_{(r,0)} = 0$, and $\left.\frac{\partial u}{\partial \theta}\right|_{(r,\pi)} = 0$. The error is the norm of the difference between the computed solution and exact solution.

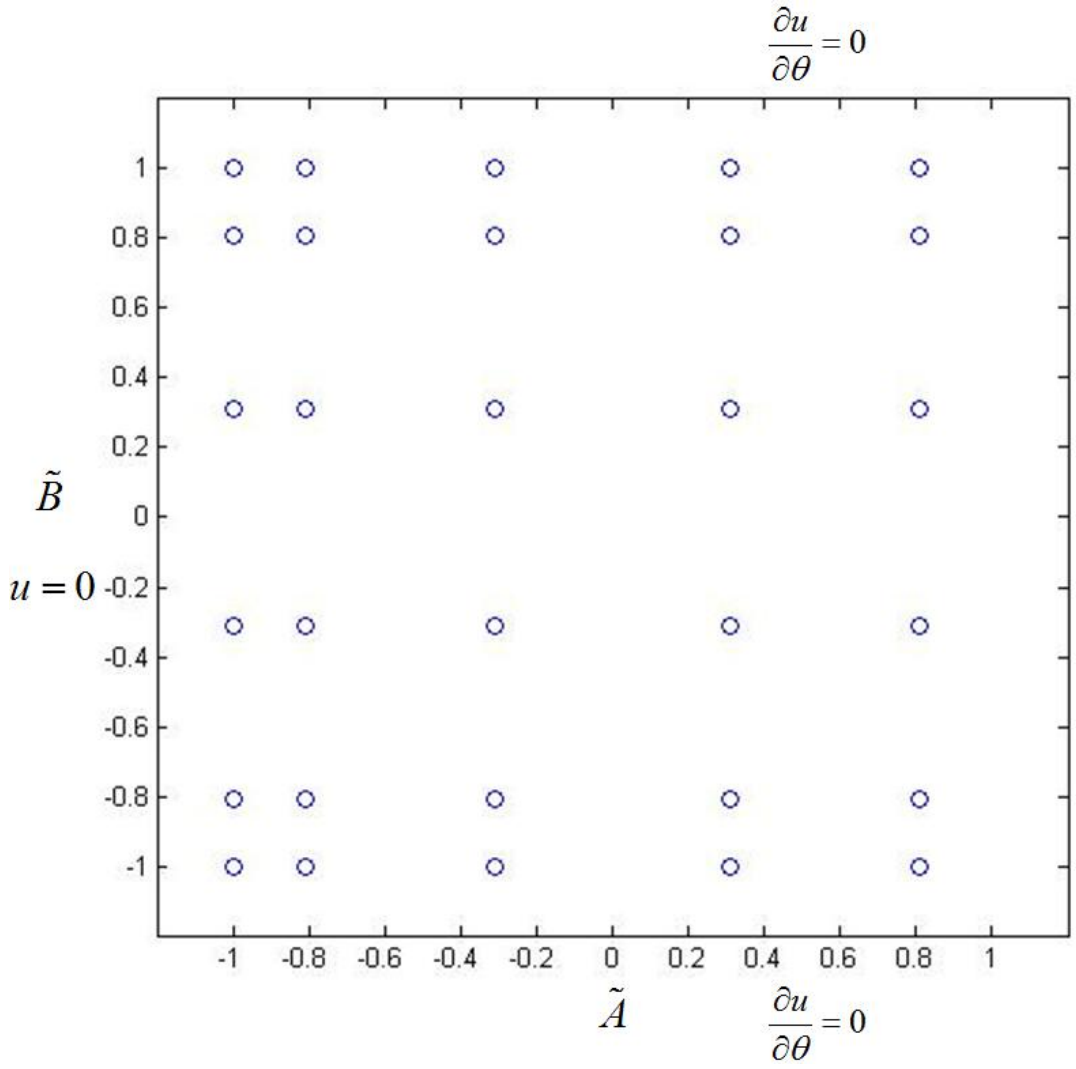

Figure B-25: An example computational domain constructed with the Chebyshev collocation points with $N_x = N_y = 6$. Note that we only enforce $u(0, \theta) = 0$ in the r-coordinate and Neumann homogeneous boundary conditions in the θ-coordinate, so there is no explicit boundary condition at $r \to \infty$.

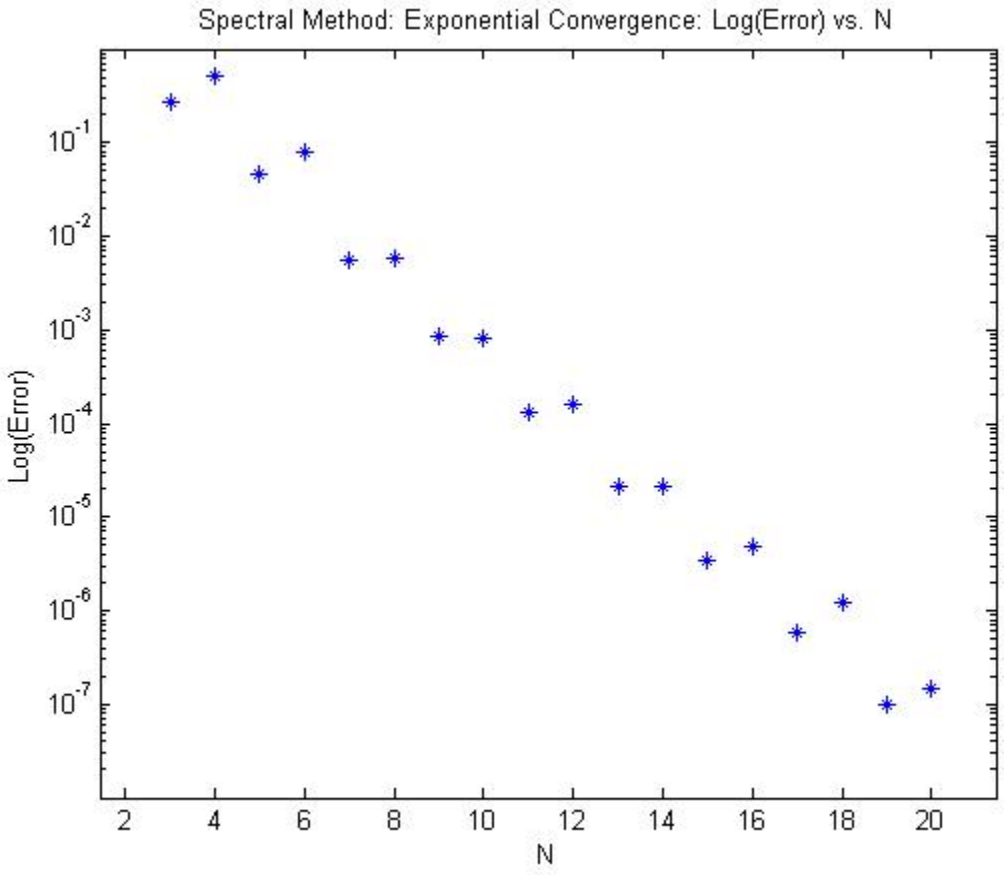

Figure B-26: Exponential convergence to the exact solution, $u(r,\theta) = \frac{r\cos\theta}{1+r^2}$, for the linear PDE, $u_{rr} + \frac{2}{r}u_r + \frac{1}{r^2}u_\theta + \frac{\cot\theta}{r^2}u_\theta = f(r,\theta)$, with $u(0,\theta = 0$, $\left.\frac{\partial u}{\partial\theta}\right|_{(r,0)} = 0$, and $\left.\frac{\partial u}{\partial\theta}\right|_{(r,\pi)} = 0$. The error is the norm of the difference between the computed solution and exact solution.

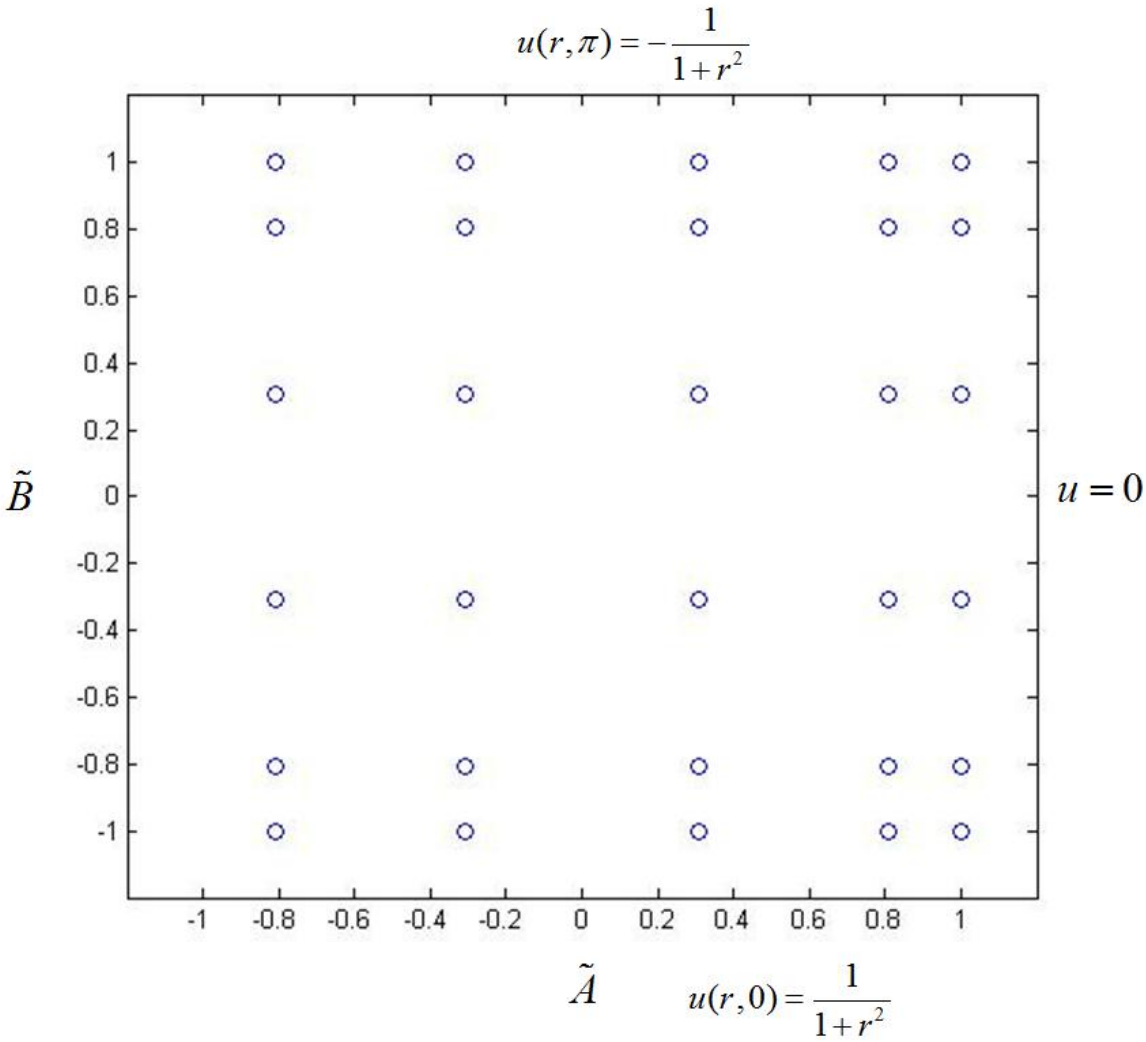

Figure B-27: An example computational domain constructed with the Chebyshev collocation points with $N_x = N_y = 6$. Note that we enforce $u(r \to \infty, \theta) = 0$, $u(r,0) = \frac{1}{1+r^2}$, and $u(r,\pi) = \frac{-1}{1+r^2}$.

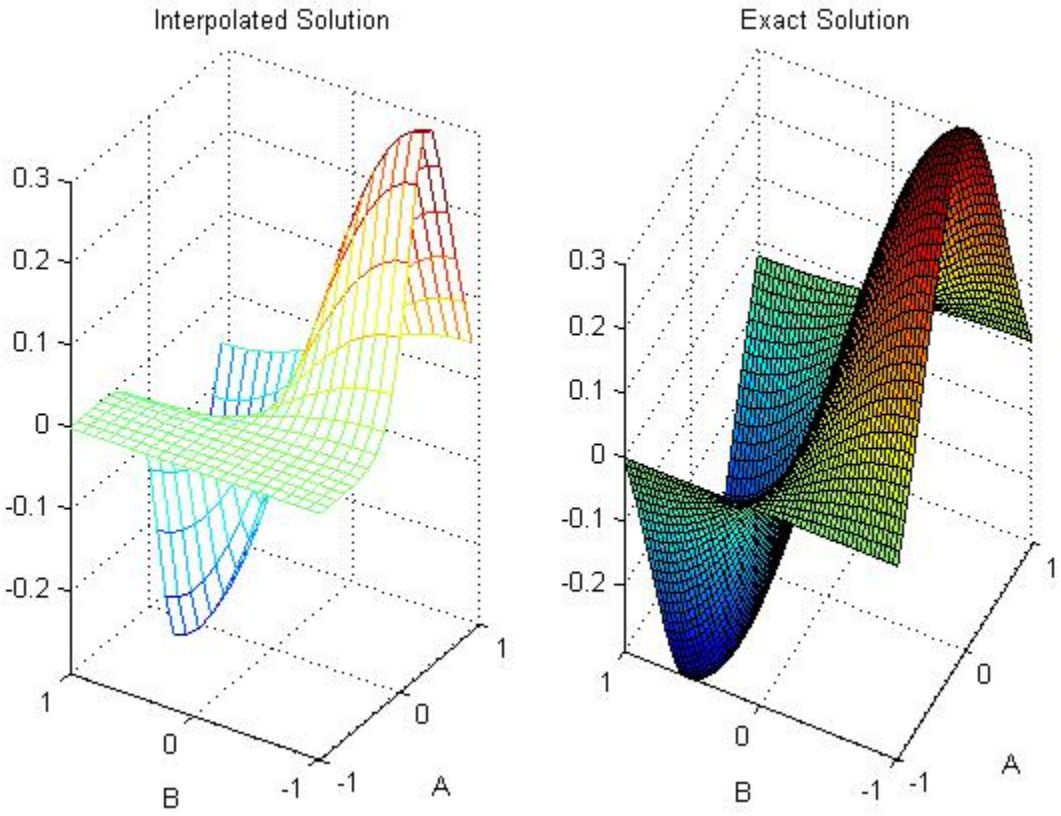

Figure B-28: Comparison of the computed solution (left) with the exact solution, $u(r,\theta) = \frac{r\cos\theta}{1+r^2}$,(right) for $N_r = N_\theta = 10$.

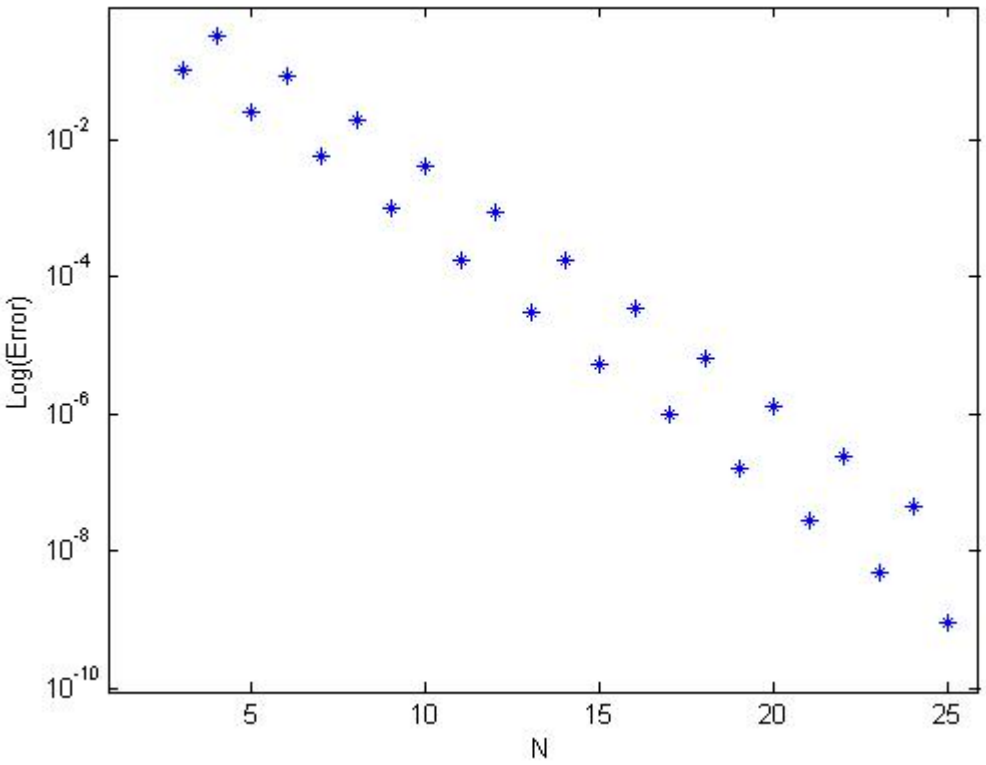

Figure B-29: Exponential convergence to the exact solution, $u(r,\theta) = \frac{r\cos\theta}{1+r^2}$, of the linear PDE, $u_{rr} + \frac{2}{r}u_r + \frac{1}{r^2}u_\theta + \frac{\cot\theta}{r^2}u_\theta = f(r,\theta)$, with $u(r \to \infty, \theta) = 0$, $u(r,0) = \frac{1}{1+r^2}$, and $u(r,\pi) = \frac{-1}{1+r^2}$. The error is the norm of the difference between the computed solution and exact solution.

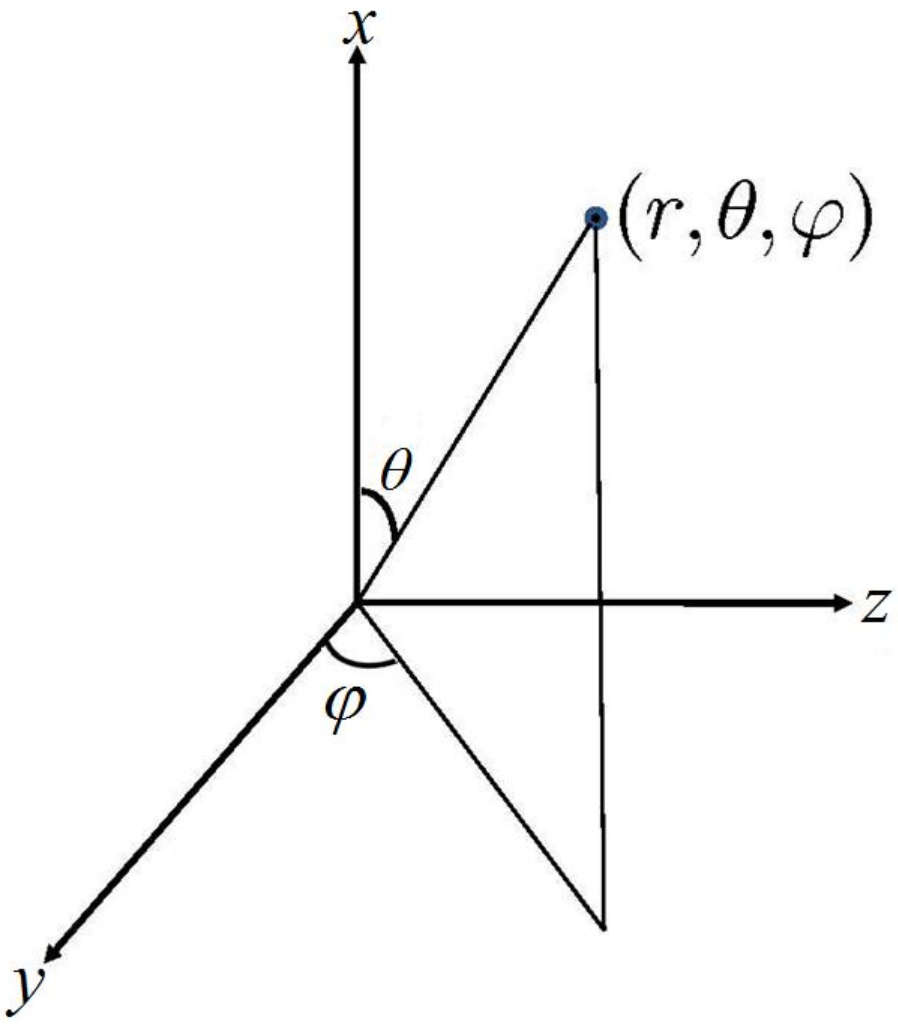

Figure B-30: Definition of spherical coordinates

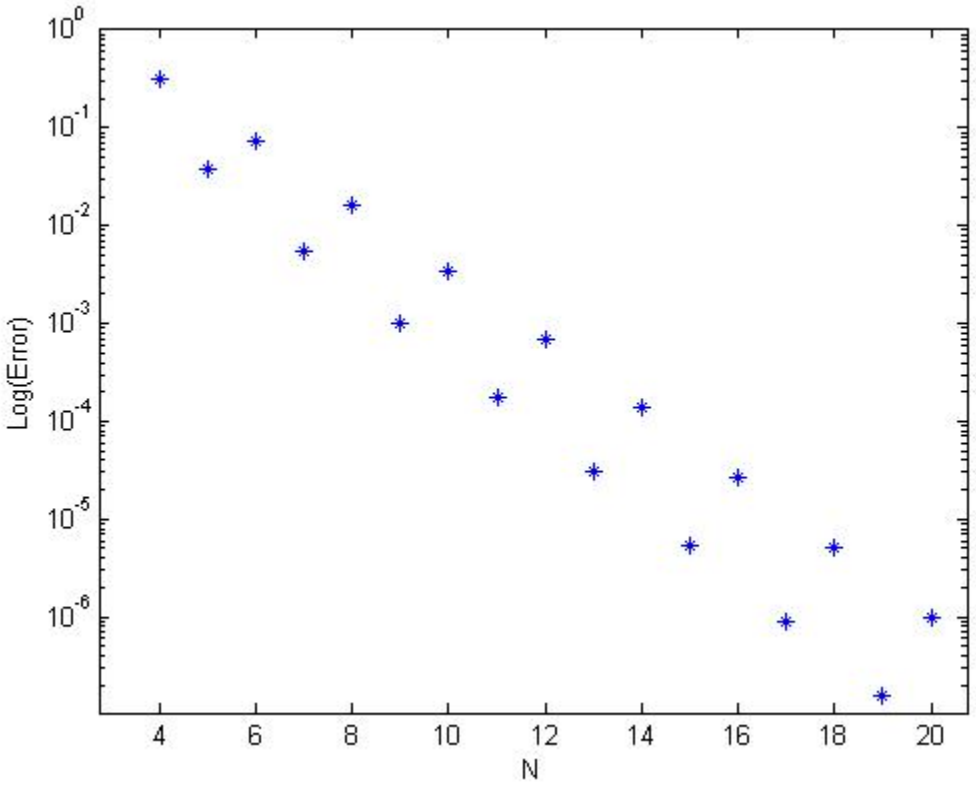

Figure B-31: Exponential convergence to the exact solution, $u(r,\theta) = \frac{r\cos\theta\sin phi}{1+r^2}$, of the nonlinear PDE, $\Delta u + \frac{9}{16r^6}\frac{\sin^2\theta}{\left(1+\frac{1}{r}+u\right)^7} = f(r,\theta,\phi)$, with $u(r\to\infty,\theta,\phi) = 0$, and periodicity in the ϕ-coordinate. The error is the norm of the difference between the computed solution and exact solution.

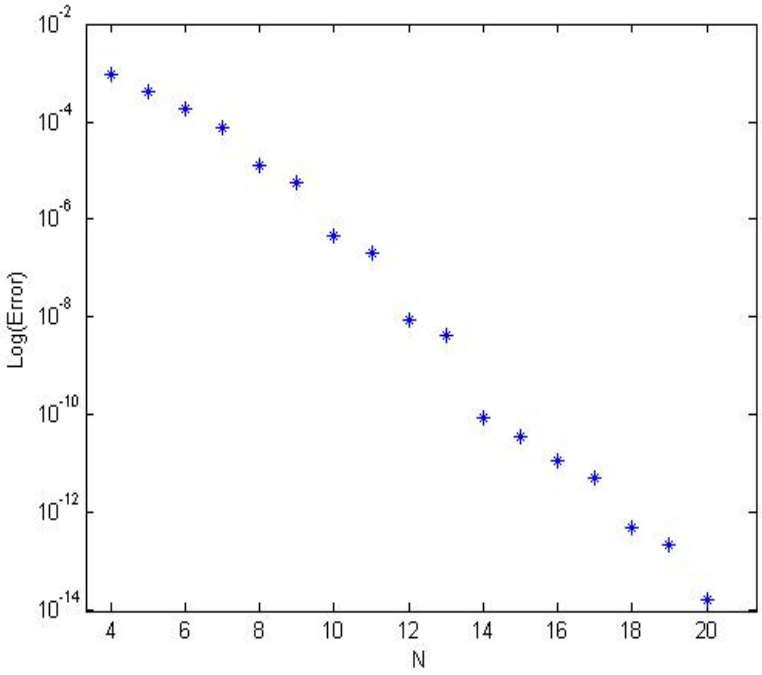

Figure B-32: Exponential convergence to the solution of the single puncture with spin nonlinear, elliptic PDE, $\Delta u = -\frac{9}{16r^6}\frac{\sin^2\theta}{\left(1+\frac{m}{2r}+u\right)^7}$, with $u(r \to \infty, \theta, \phi) = 0$, and periodicity in the ϕ-coordinate. The error is the norm of the difference between the computed solution and solution with $N_{\tilde{A}} = N_{\tilde{B}} = 30$ and $N_\phi = 4$.

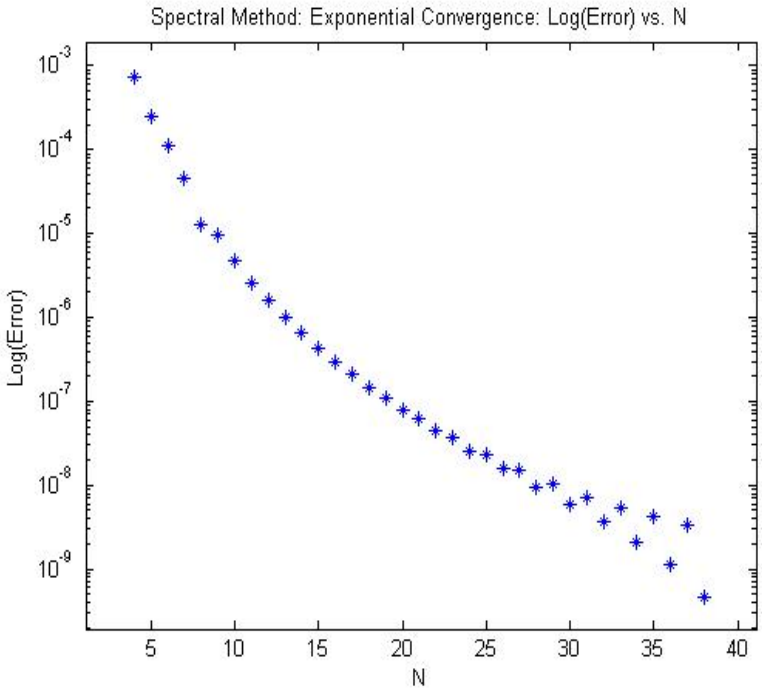

Figure B-33: Exponential convergence to the solution of the single puncture with linear momentum nonlinear, elliptic PDE, $\Delta u = -\frac{9}{4r^4}\frac{1+2\cos^2\theta}{\left(1+\frac{m}{2r}+u\right)^7}$, with $u(r \to \infty, \theta, \phi) = 0$, and periodicity in the ϕ-coordinate. The error is the norm of the difference between the computed solution and solution with $N_{\tilde{A}} = N_{\tilde{B}} = 40$ and $N_\phi = 4$.

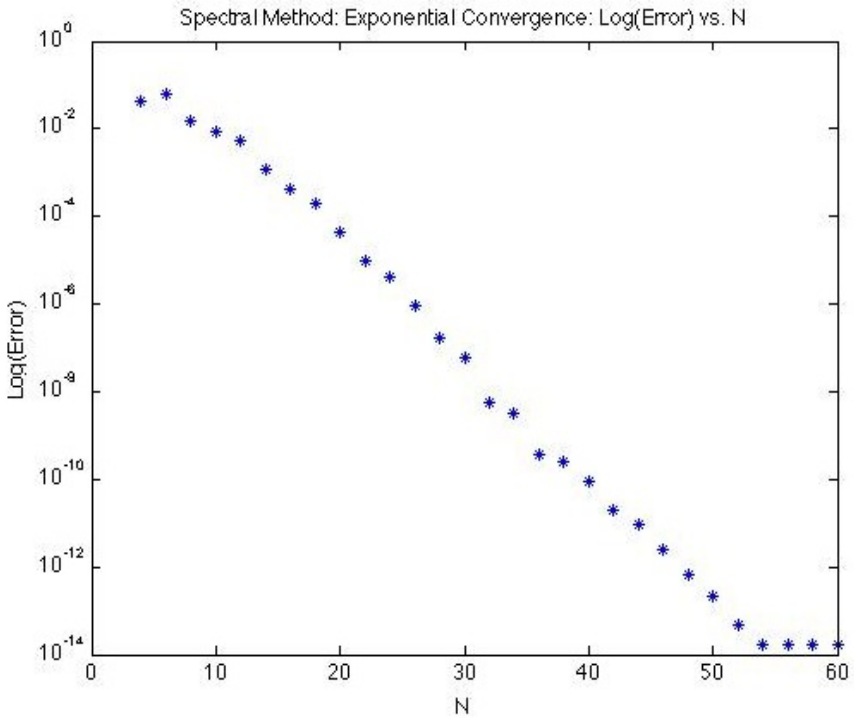

Figure B-34: Exponential convergence to the solution of the binary black hole case with spins of $S_{x_1} = S_{x_2} = 1$, by imposing only a single boundary condition at infinity, $u(r \to \infty, \theta, \phi) = 0$, and assuming periodicity in the ϕ-coordinate. The error is the norm of the difference between the computed solution and solution with $N_{\tilde{A}} = N_{\tilde{B}} = 60$ and $N_\phi = 4$.

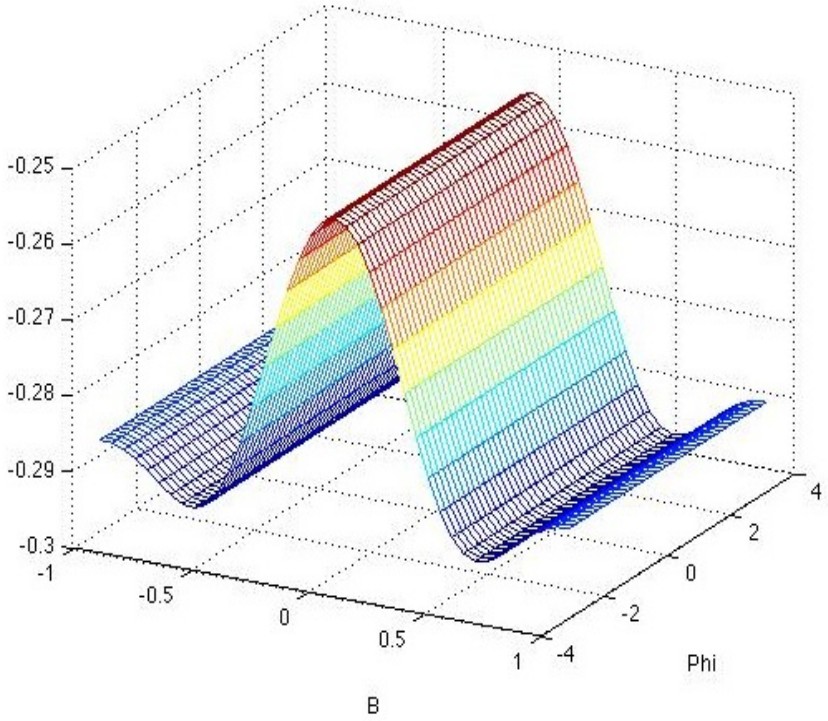

Figure B-35: Illustrating the solution in the binary black hole case with spins of $S_{x_1} = S_{x_2} = 1$ obeys the symmetry requirements of the compactification scheme on the $\tilde{A} = -1$ face, $u(-1, \tilde{B}, \phi) = u(-1, \tilde{B})$.

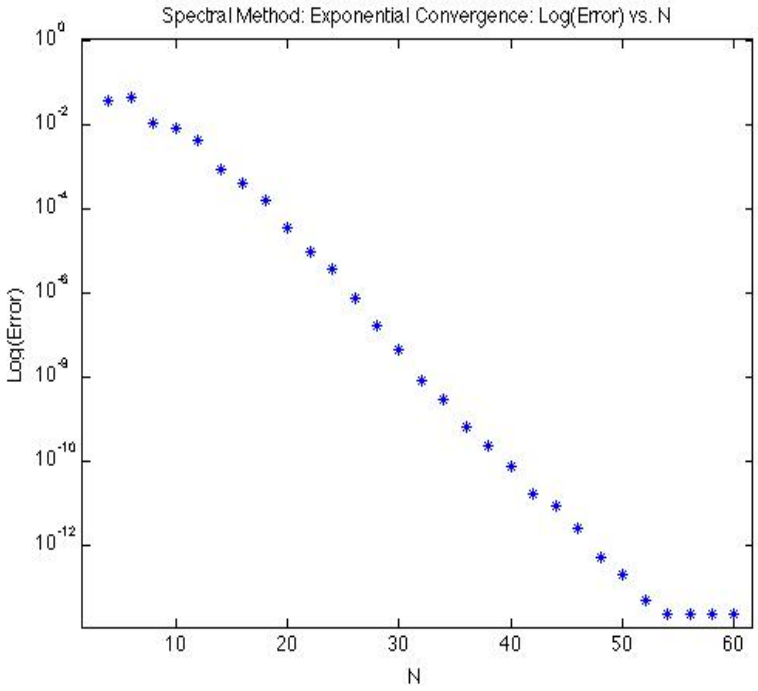

Figure B-36: Exponential convergence to the solution of the binary black hole case with spins of $S_{x_1} = S_{x_2} = 0.5$, by imposing only a single boundary condition at infinity, $u(r \to \infty, \theta, \phi) = 0$, and assuming periodicity in the ϕ-coordinate. The error is the norm of the difference between the computed solution and solution with $N_{\tilde{A}} = N_{\tilde{B}} = 60$ and $N_\phi = 4$.

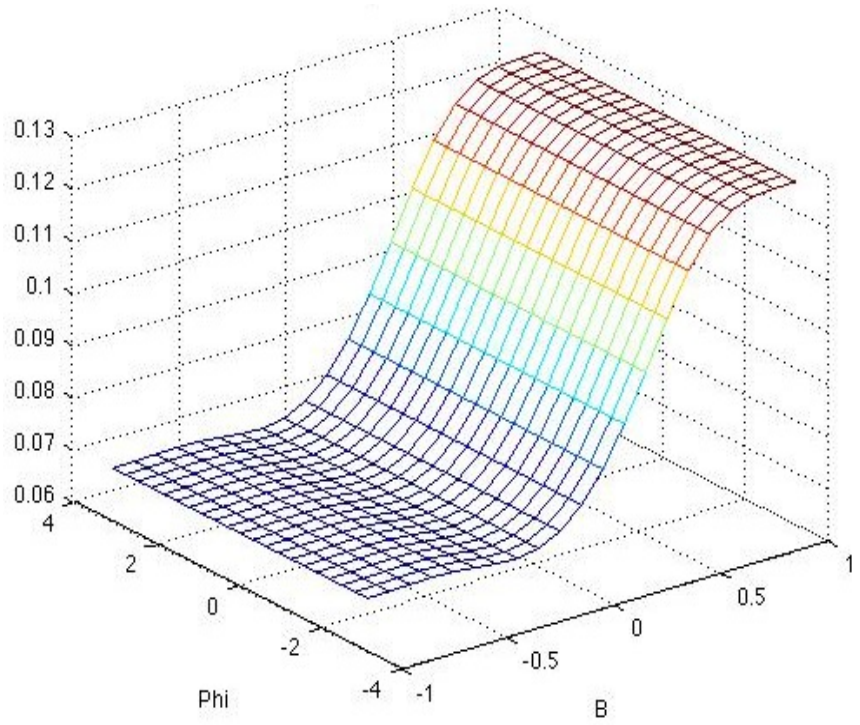

Figure B-37: Illustrating the solution in the binary black hole case with spins of $S_{x_1} = 1, S_{x_2} = 0.5$ obeys the symmetry requirements of the compactification scheme on the $\tilde{A} = -1$ face, $u(-1, \tilde{B}, \phi) = u(-1, \tilde{B})$.

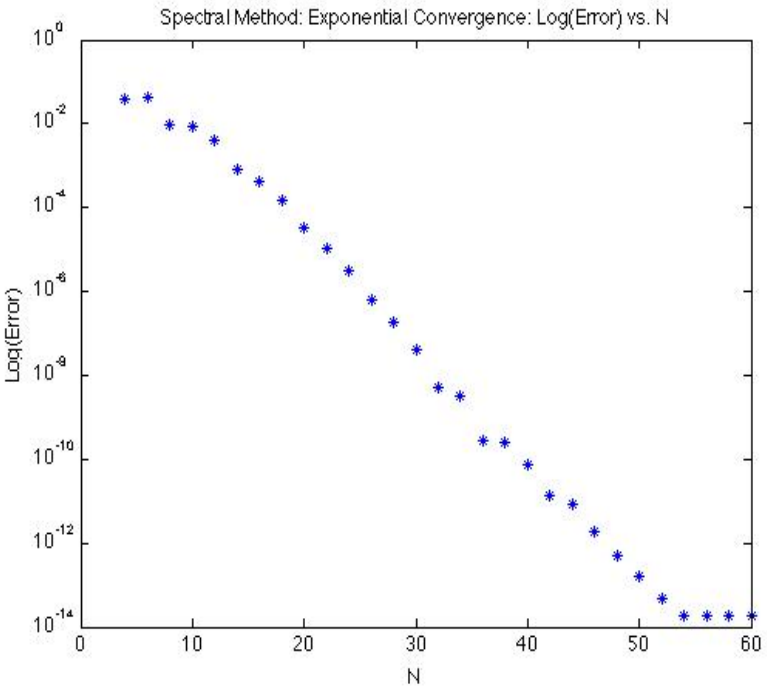

Figure B-38: Exponential convergence to the solution of the binary black hole case with spins of $S_{x_1} = S_{x_2} = 0.05$, by imposing only a single boundary condition at infinity, $u(r \to \infty, \theta, \phi) = 0$, and assuming periodicity in the ϕ-coordinate. The error is the norm of the difference between the computed solution and solution with $N_{\tilde{A}} = N_{\tilde{B}} = 60$ and $N_\phi = 4$.

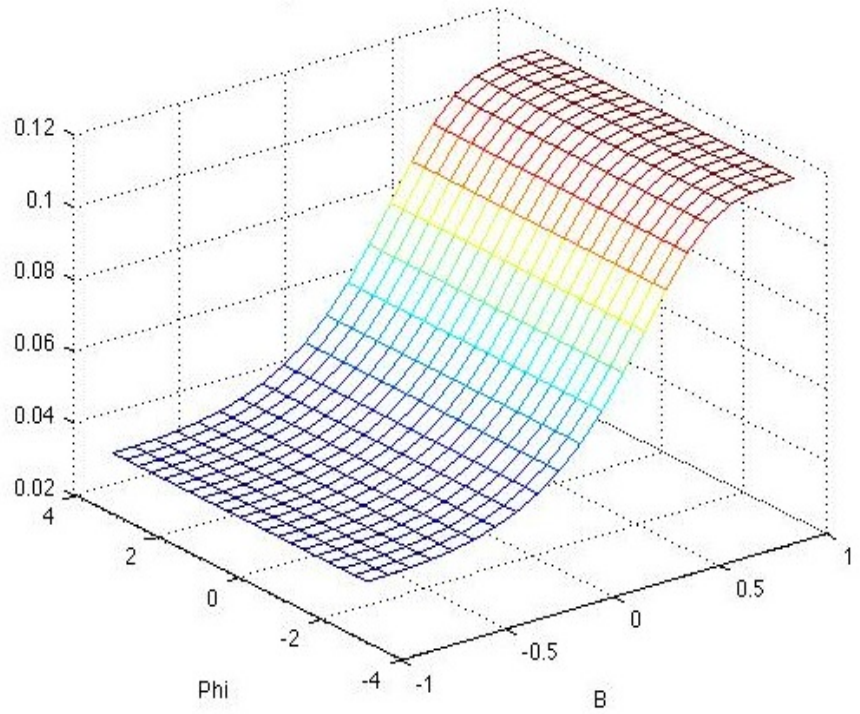

Figure B-39: Illustrating the solution in the binary black hole case with spins of $S_{x_1} = 1, S_{x_2} = 0.05$ obeys the symmetry requirements of the compactification scheme on the $\tilde{A} = -1$ face, $u(-1, \tilde{B}, \phi) = u(-1, \tilde{B})$.

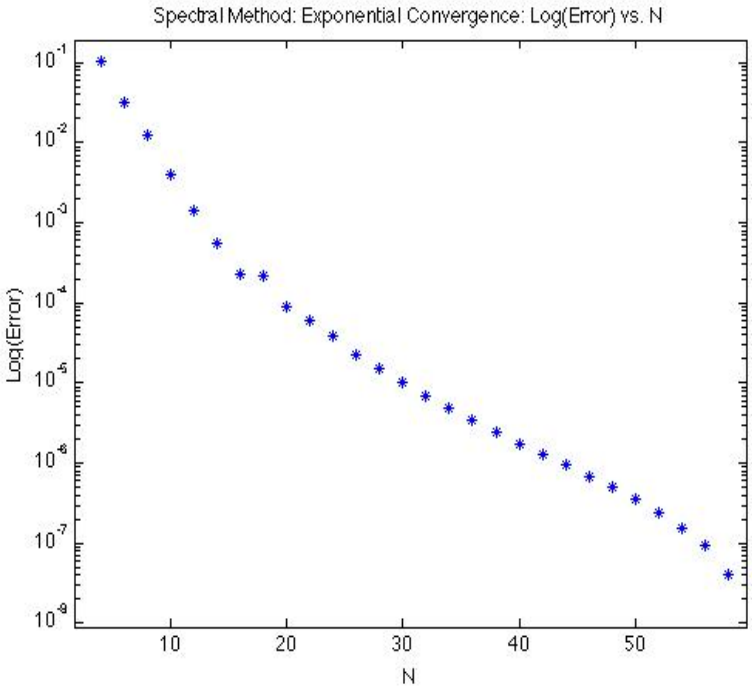

Figure B-40: Exponential convergence to the solution of the binary black hole case with linear momentum of $P_{x_1} = P_{x_2} = 1$, by imposing only a single boundary condition at infinity, $u(r \to \infty, \theta, \phi) = 0$, and assuming periodicity in the ϕ-coordinate. The error is the norm of the difference between the computed solution and solution with $N_{\tilde{A}} = N_{\tilde{B}} = 60$ and $N_\phi = 4$.

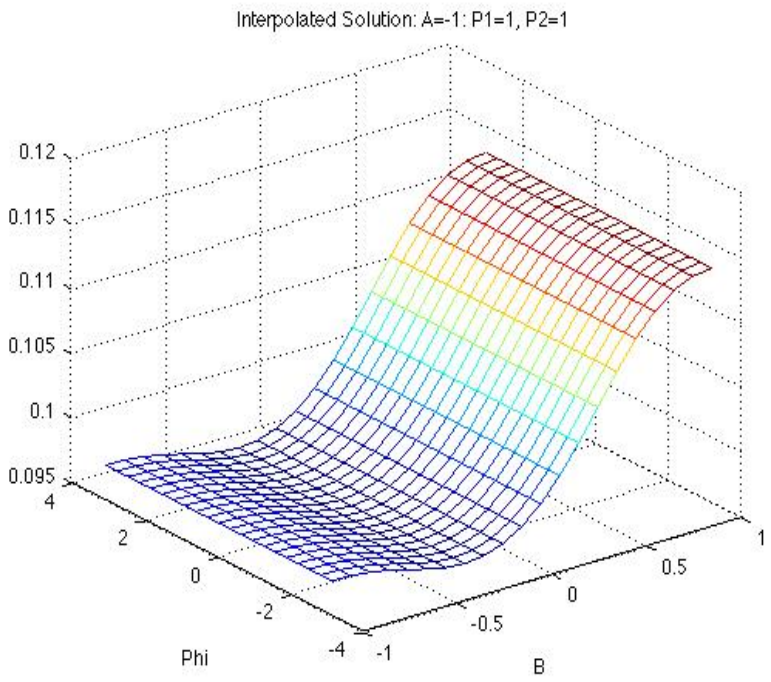

Figure B-41: Illustrating the solution in the binary black hole case with linear momenta of $P_{x_1} = P_{x_2} = 1$ obeys the symmetry requirements of the compactification scheme on the $\tilde{A} = -1$ face, $u(-1, \tilde{B}, \phi) = u(-1, \tilde{B})$.

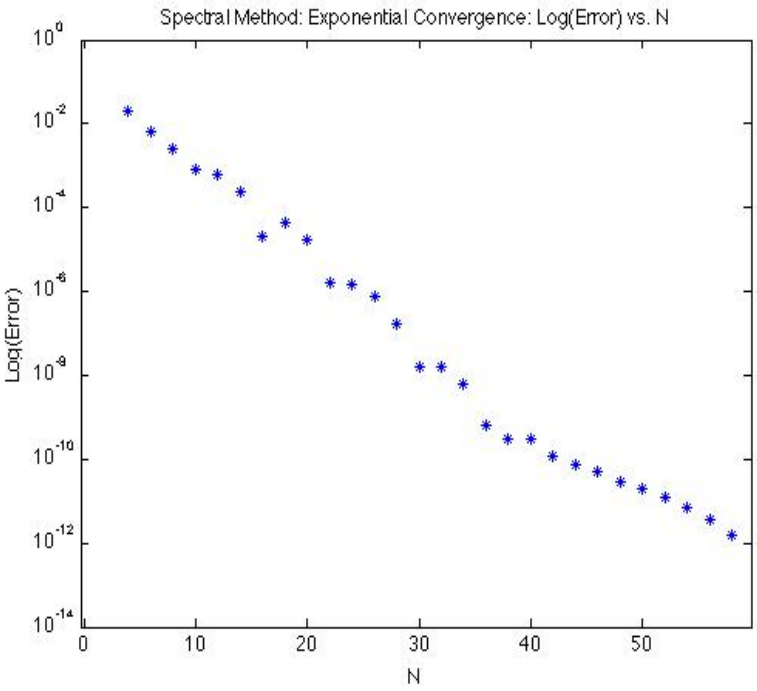

Figure B-42: Exponential convergence to the solution of the binary black hole case with linear momentum of $P_{x_1} = 1, P_{x_2} = -1$, by imposing only a single boundary condition at infinity, $u(r \to \infty, \theta, \phi) = 0$, and assuming periodicity in the ϕ-coordinate. The error is the norm of the difference between the computed solution and solution with $N_{\tilde{A}} = N_{\tilde{B}} = 60$ and $N_\phi = 4$.

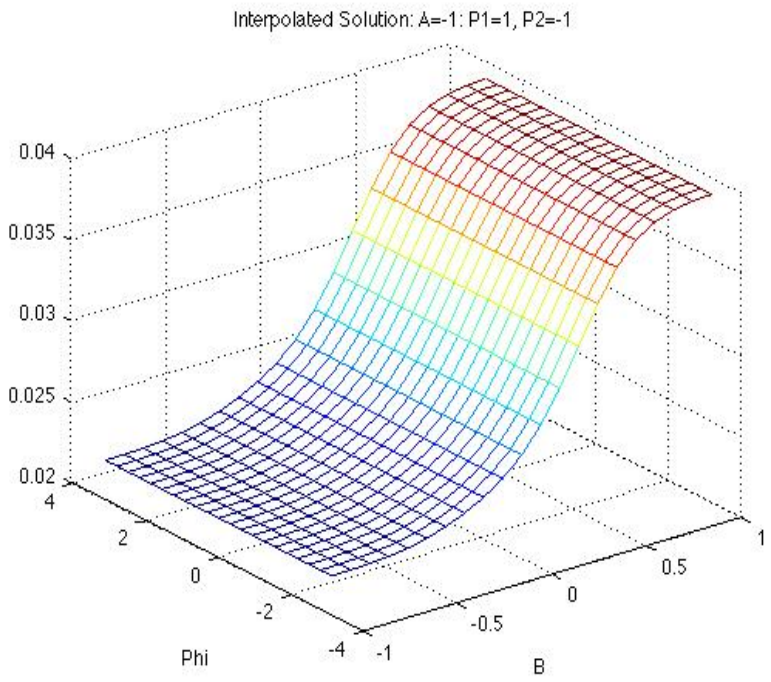

Figure B-43: Illustrating the solution in the binary black hole case with linear momenta of $P_{x_1} = 1, P_{x_2} = -1$ obeys the symmetry requirements of the compactification scheme on the $\tilde{A} = -1$ face, $u(-1, \tilde{B}, \phi) = u(-1, \tilde{B})$.

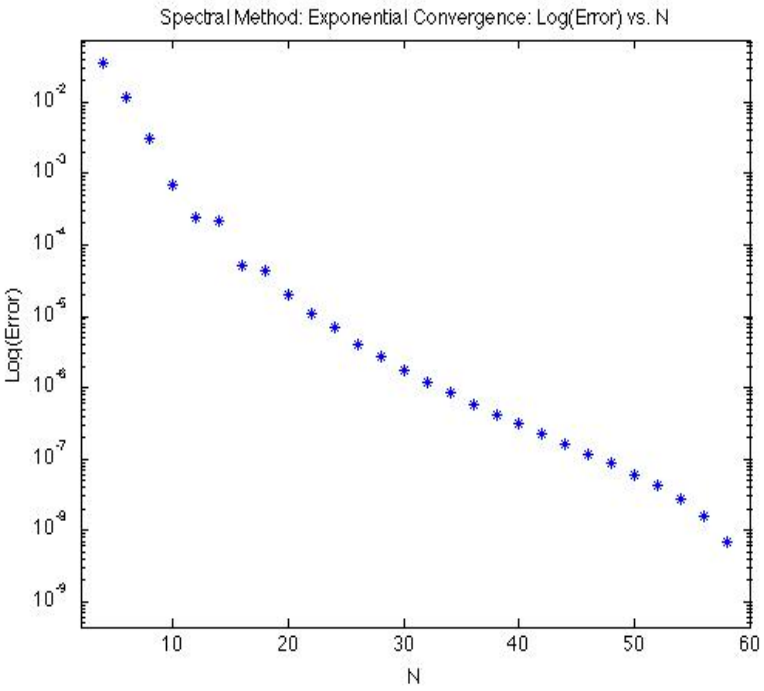

Figure B-44: Exponential convergence to the solution of the binary black hole case with linear momentum of $P_{x_1} = 0.05, P_{x_2} = -1$, by imposing only a single boundary condition at infinity, $u(r \to \infty, \theta, \phi) = 0$, and assuming periodicity in the ϕ-coordinate. The error is the norm of the difference between the computed solution and solution with $N_{\tilde{A}} = N_{\tilde{B}} = 60$ and $N_\phi = 4$.

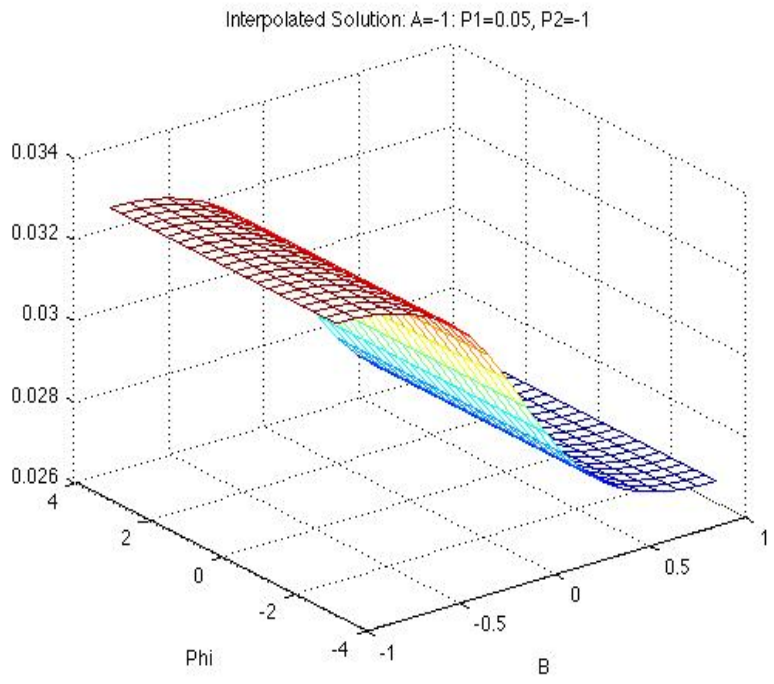

Figure B-45: Illustrating the solution in the binary black hole case with linear momenta of $P_{x_1} = 0.05, P_{x_2} = -1$ obeys the symmetry requirements of the compactification scheme on the $\tilde{A} = -1$ face, $u(-1, \tilde{B}, \phi) = u(-1, \tilde{B})$.

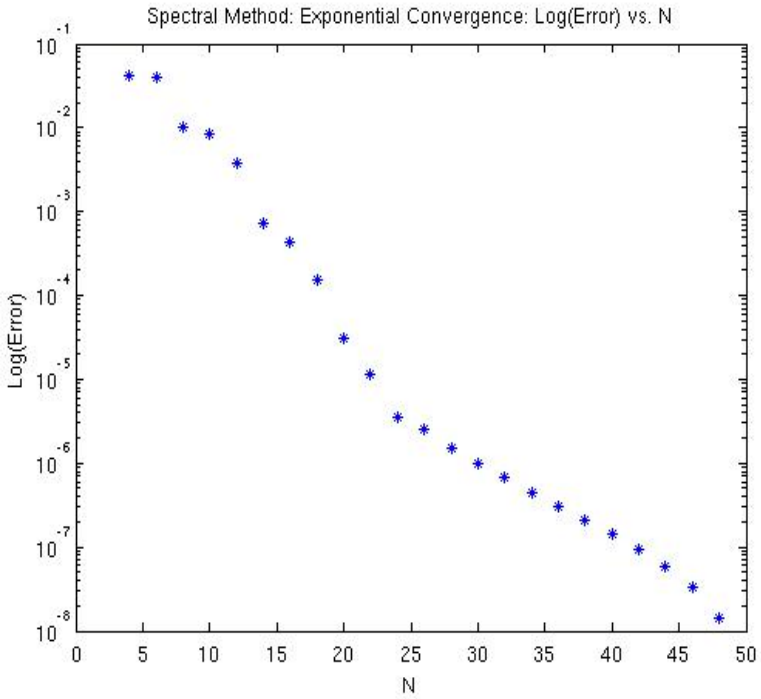

Figure B-46: Exponential convergence to the solution of the binary black hole case with $S_{x_1} = P_{z_2} = 1$, by imposing only a single boundary condition at infinity, $u(r \to \infty, \theta, \phi) = 0$, and assuming periodicity in the ϕ-coordinate. The error is the norm of the difference between the computed solution and solution with $N_{\tilde{A}} = N_{\tilde{B}} = 50$ and $N_\phi = 10$.

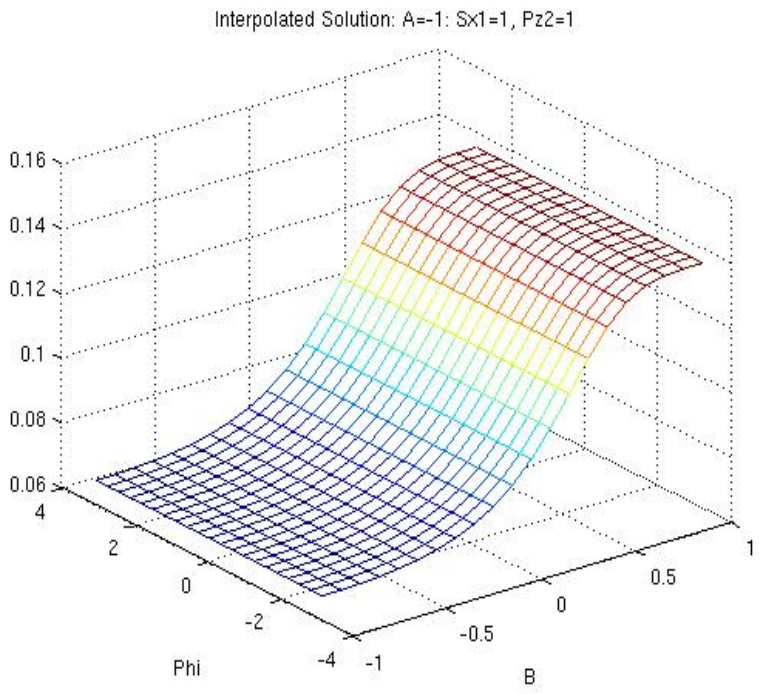

Figure B-47: Illustrating the solution in the binary black hole case with $S_{x_1} = P_{z_2} = 1$ obeys the symmetry requirements of the compactification scheme on the $\tilde{A} = -1$ face, $u(-1, \tilde{B}, \phi) = u(-1, \tilde{B})$.

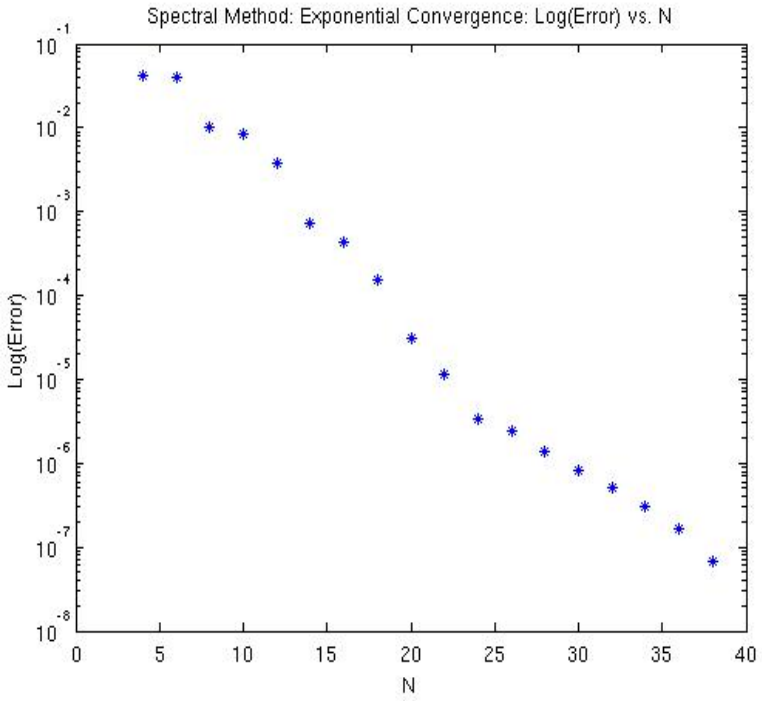

Figure B-48: Exponential convergence to the solution of the binary black hole case with $S_{x_1} = P_{z_2} = 1$, by imposing only a single boundary condition at infinity, $u(r \to \infty, \theta, \phi) = 0$, and assuming periodicity in the ϕ-coordinate. The error is the norm of the difference between the computed solution and solution with $N_{\tilde{A}} = N_{\tilde{B}} = 50$ and $N_\phi = 10$.

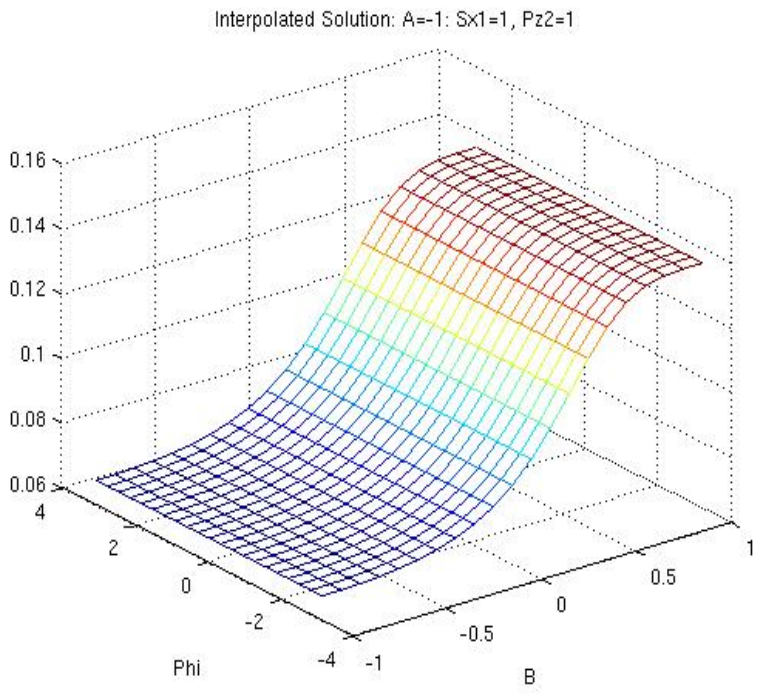

Figure B-49: Illustrating the solution in the binary black hole case with $S_{x_1} = P_{z_2} = 1$ obeys the symmetry requirements of the compactification scheme on the $\tilde{A} = -1$ face, $u(-1, \tilde{B}, \phi) = u(-1, \tilde{B})$.

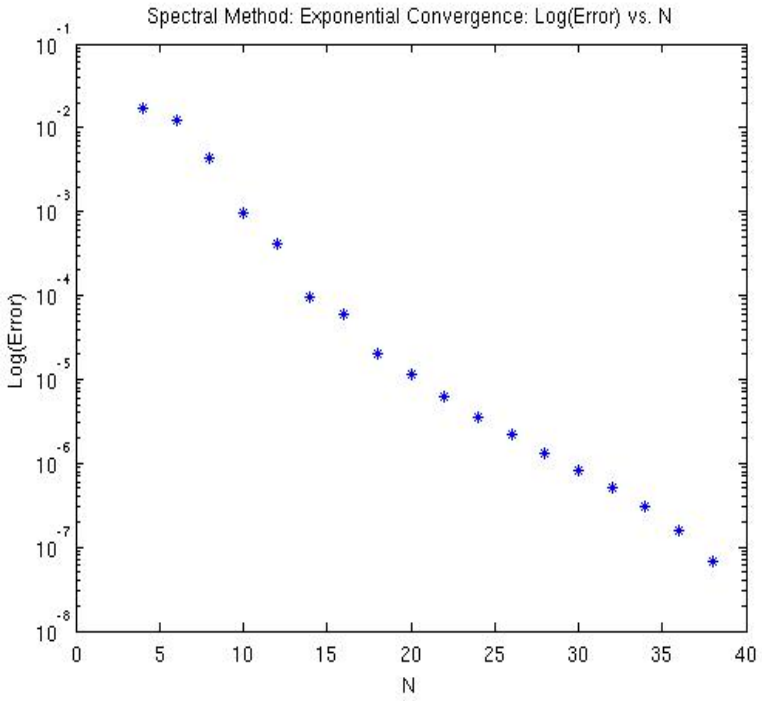

Figure B-50: Exponential convergence to the solution of the binary black hole case with $S_{x_1} = 0.05, P_{z_2} = 1$, by imposing only a single boundary condition at infinity, $u(r \to \infty, \theta, \phi) = 0$, and assuming periodicity in the ϕ-coordinate. The error is the norm of the difference between the computed solution and solution with $N_{\tilde{A}} = N_{\tilde{B}} = 40$ and $N_\phi = 10$.

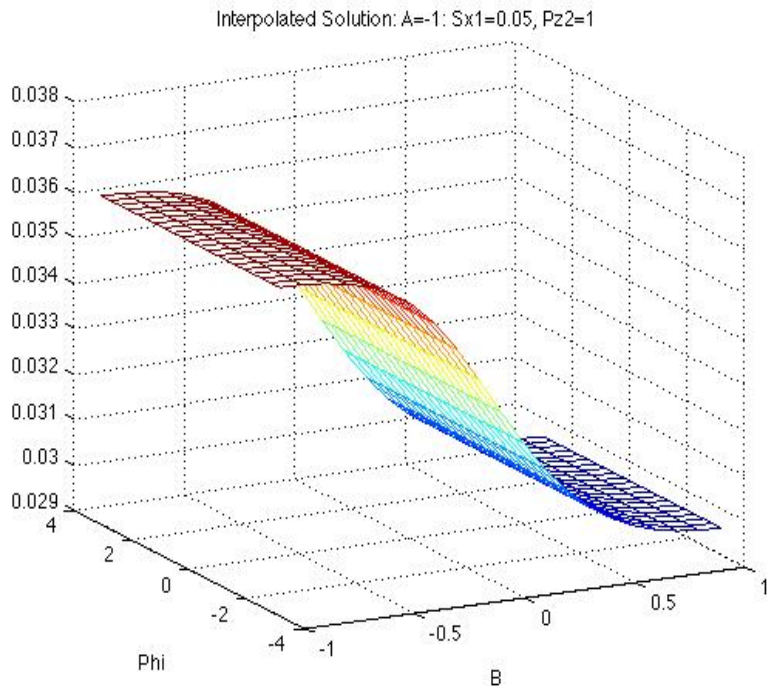

Figure B-51: Illustrating the solution in the binary black hole case with $S_{x_1} = 0.05, P_{z_2} = 1$ obeys the symmetry requirements of the compactification scheme on the $\tilde{A} = -1$ face, $u(-1, \tilde{B}, \phi) = u(-1, \tilde{B})$.

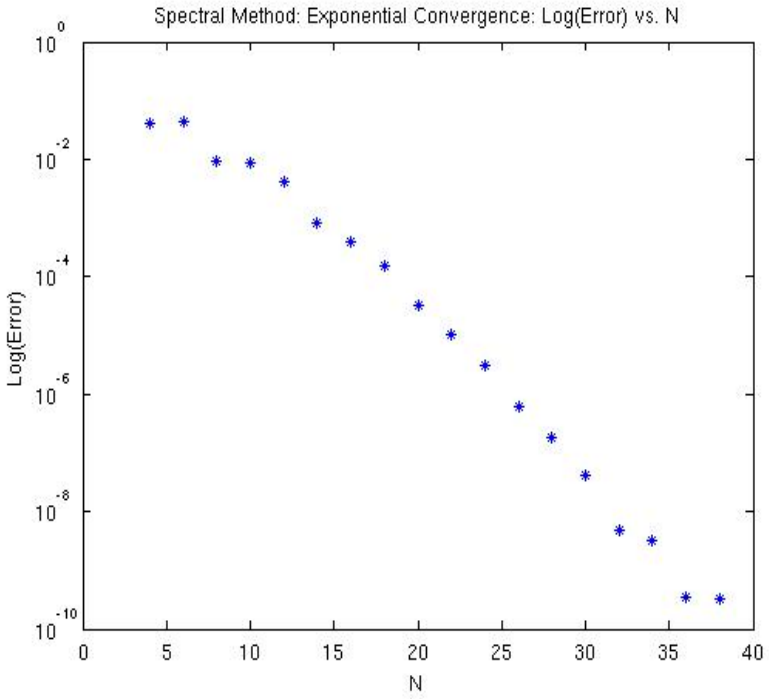

Figure B-52: Exponential convergence to the solution of the binary black hole case with $S_{x_1} = 1, P_{z_2} = 0.05$, by imposing only a single boundary condition at infinity, $u(r \to \infty, \theta, \phi) = 0$, and assuming periodicity in the ϕ-coordinate. The error is the norm of the difference between the computed solution and solution with $N_{\tilde{A}} = N_{\tilde{B}} = 40$ and $N_\phi = 10$.

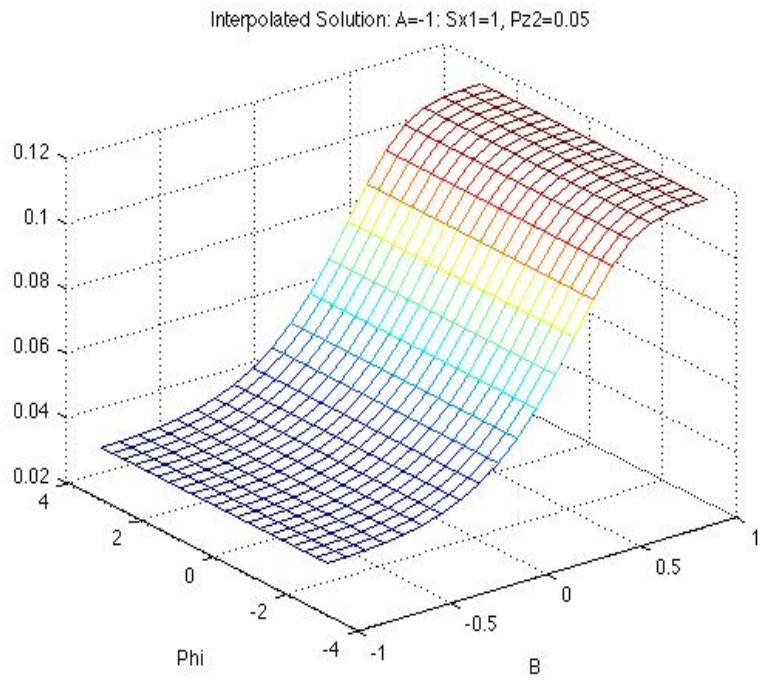

Figure B-53: Illustrating the solution in the binary black hole case with $S_{x_1} = 1, P_{z_2} = 0.05$ obeys the symmetry requirements of the compactification scheme on the $\tilde{A} = -1$ face, $u(-1, \tilde{B}, \phi) = u(-1, \tilde{B})$.

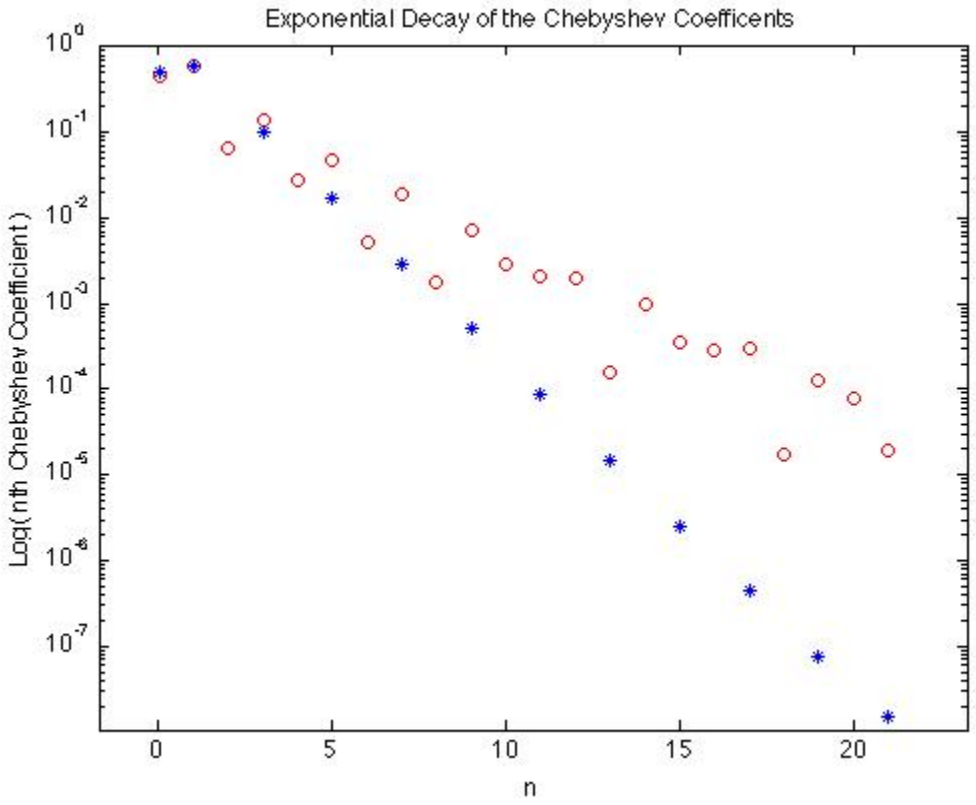

Figure B-54: Comparing the decay rate of Chebyshev coefficients for the function $f(x) = \frac{1}{1+x^2}$, which goes to zero algebraically, and $g(x) = e^{-x^2}$, which goes to zero exponentially for $0 \leq x \leq \infty$. We see that Chebyshev polynomials are better for approximating functions that decay algebraically than those that goes to zero exponentially.